Physical layer security in cellular networks

Babaei, Ayda

Awarding institution:
King's College London

Physical Layer Security in Cellular Networks

Ayda Babaei

A dissertation submitted in partial fulfillment
of the requirements for the degree of
Doctor of Philosophy

Department of Informatics
King's College London

April 2020

I, Ayda Babaei, confirm that the work presented in this thesis is my own. Where information has been derived from other sources, I confirm that this has been indicated in the work.

Abstract

In this work, we provide a theoretical study of physical layer security (PHYLS) performance in full-duplex (FD) small-cell networks. Here, the base stations (BSs) and user equipments (UEs) follow from the homogeneous Poisson point process (PPP)-based abstraction model.

First we consider the network where BSs serve a single user in one resource block where PHYLS in both scenarios of HD and FD UEs are analysed and compared. We derive the ergodic secrecy rate in both downlink (DL) and uplink (UL) in presence of a field of passive eavesdroppers (EDs). To facilitate FD communications, we take into account (i) successive interference cancellation (SIC) capability at the UE side via guard regions of arbitrary radii, and (ii) residual self-interference (SI) at the BS side using Rician fading distribution with arbitrary statistics. We study the affect of density of BSs and EDs in the FD mode and compare it to its HD counterpart.

Next, we consider the case where BSs serve several HD single-antenna users at the same time and frequency with assistance of multiple antennas. We investigate the small-cell network PHYLS performance in the presence of a Poisson field of EDs, under the different scenarios of passive and colluding eavesdropping. Considering linear zero-forcing (ZF) beam-forming in the multiple-input multiple-output (MIMO) scenario, we characterize the UL and DL ergodic secrecy rates and derive closed-form expressions for the different useful and interference signals statistics. Moreover, we look into the impact of SIC and SI capabilities in the UE and BS side, respectively.

Thereafter, we derive explicit expressions of the key performance indicators

using tools from machine learning. In particular, for certain special cases of interest, we apply supervised learning-based non-linear curve-fitting techniques to large sets of (exact) theoretical data in order to obtain closed-form approximations for the different ergodic rates and ergodic secrecy rates under consideration.

Our findings, obtained from theoretical analysis and system-level simulations, indicate that the FD functionality, in addition to enhancing the spectral efficiency (SE), can significantly improve the PHYLS performance, especially with the aid of multi-antenna communications and interference cancellation schemes. Finally, we highlight several promising future research directions in relation to the outcomes of this work, including the application of physical layer security and full-duplex operation in the context of 5G networks and beyond.

Acknowledgements

Firstly, I wish to express my deepest gratitude to my supervisor, Professor Hamid Aghvami, for his guidance, motivation and immense knowledge during my PhD study. For that and the encouragement during my PhD, I will be forever indebted to him.

Besides my supervisor, I'd like to thank my advisor, Dr Arman Shojaeifard who I have been fortunate to have known. Among everything, specifically I would like to thank him for his continuous support and believing in me.

My special thanks goes to my examiners, Dr Emad Alsusa and Professor Muhammad Imran, whom comments were essential towards improving the quality and scope of this work.

Last but not least, I would like to thank my brother Arta, for his insightful guidance, my father, Hassan, for his strong support of my studies and my mother, Shadan, for helping me to overcome the sleepless nights and hard days of my PhD. Without the help of my supportive family, I would not be here today.

Contents

List of Figures

List of Abbreviations

PHYLS Physical Layer Security

FD Full-Duplex

BS Base Station

HD Half-Duplex

UE User Equipment

PPP Possion Point Process

SIC Successive Interference Cancellation

SI Self-Interference

ED Eavesdropper

ZF Zero-Forcing

DL Downlink

UL Uplink

SE Spectral Efficiency

TDD Time-Division Duplex

FDD Frequency-Division Duplex

MI Mutual Interference

PDF Probability Density Function

HCN Heterogeneous Cellular Networks

OSI Open System Interconnection

KM Kuhn-Munkres

D2D Device-to-Device

QoS Quality of Service

MIMO Multiple-input and Multiple-output

AN Artificial Noise

SINR Signal-to-Interference-plus-Noise-Ratio

MC Monte Carlo

AWGN Additive White Gaussian Noise

NLOS Non-Light-Of-Sight

PGFL Probability Generating Functional

LT Laplace Transform

CSI Channel State Information

RMSE Root Mean Square Error

5G Fifth Generation

SIMO Single-Input and Multiple-Output

MISO Multiple-Input and Single-Output

List of Symbols

$\boldsymbol{X}$	Matrix X
$\boldsymbol{x}$	Vector X
T	Transpose
$\dagger$	Hermitian
$+$	Pseudo-Inverse
$\mathbb{E}_x[.]$	Expectation
$\Pr[.]$	Probability
$\mathscr{F}_x[.]$	Cumulative Distribution Function (CDF)
$\mathscr{P}_x[.]$	Probability Density Function (PDF)
$\mathscr{L}_x[.]$	Laplace Transform (LT) Function
$\lvert x\rvert$	Modulus
$\lVert\boldsymbol{x}\rVert$	Euclidean Norm
$[x]^+ = \max(x,0)$	Ramp Function
$\mathbf{I}_{(.)}$	Identity Matrix
$\mathscr{CN}(\mu,\nu^2)$	Circularly-Symmetric Complex Gaussian Distribution with Mean μ and Variance ν^2
$\Gamma(.)$	Gamma Function
$\Gamma(.,.)$	Incomplete (upper) Gamma Function
$\mathscr{G}(\kappa,\theta)$	Gamma Distribution with Shape Parameter κ and Scale Parameter θ
${}_2F_1(.,.;.;.)$	Gauss Hypergeometric Function

λ	Spatial Density
ϕ	Poisson Point Process
p	Transmit Power
$g_{x,y}$	Downlink Channel Gain
$h_{x,y}$	Uplink Channel Gain
α	Path Loss Exponent
γ	SINR
C	Ergodic Rate
ε	Guard Region Radius
exp	Exponential Function
N	Number of Antennas
K	Number of Served Users per Resource Block
$\boldsymbol{V}$	Linear Zero-Forcing Preceding Matrix
$\boldsymbol{W}$	Linear Zero-Forcing Post-coding Matrix
I	Interference
σ^2	Noise Variance

List of Publications

1. A. Babaei, A. H. Aghvami, A. Shojaeifard, K.-K. Wong, "Full-Duplex Small-Cell Networks: A Physical-Layer Security Perspective," *IEEE Trans. Commun.*, vol. 66, no. 7, pp. 3006-3021, July 2018.

2. A. Babaei, A. H. Aghvami, A. Shojaeifard, K.-K. Wong, "Full-Duplex MIMO Small-Cells: Secrecy Capacity Analysis," *IEEE Veh. Technol. Conf. (VTC-Spring)*, 2018.

3. A. Babaei, A. H. Aghvami, A. Shojaeifard, K.-K. Wong, "Physical Layer Security in Full-Duplex Cellular Networks," *IEEE Int. Symp. Personal Indoor Mobile Radio Commun. (PIMRC)*, 2017.

4. F. Hu, A. Babaei, A. H. Aghvami, "Physical Layer Security in Cellular Network in the Presence of Terrains," *International Conference on Telecommunications. (ICT)*, Accepted 2019.

Chapter 1

Introduction

1.1 Background

1.1.1 Cellular Networks

Based on statistics, the mobile data traffic is expected to increase 49 exabytes per month by 2021, equivalent to $\times 7$ grow by 2016 [1]. In order to account for this, Telecommunication is now evolving to the next generation of cellular networks (fifth generation (5G)) [2]. As one of the main features of 5G technology, the concept of small-cell has emerged as a mean for increasing throughput as well as decreasing power consumption [3, 4]. Therefore reducing cell-size has emerged as one of the key approaches for spectrum reuse which has already contributed to more than $\times 1600$ wider spectrum [2].

Figure 1.1: Cisco forecast of mobile data traffic by 2021.

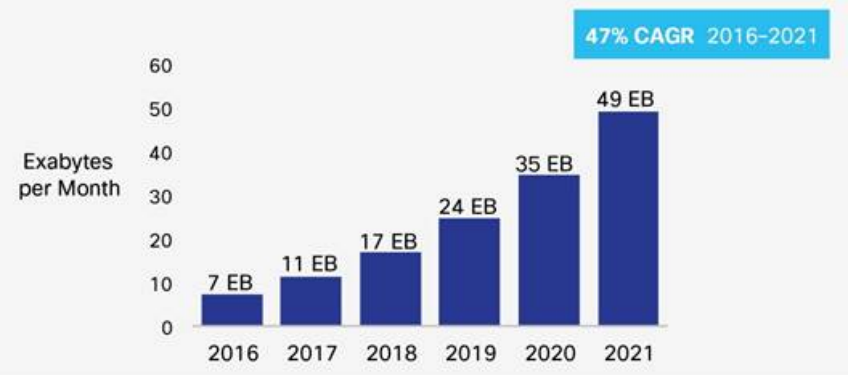

1.1.2 Full Duplex Operation

Legacy cellular networks have been designed and dimensioned according to a complete separation of the transmit and receive functionalities (what is known as half-duplex (HD) operation). Specifically, the transceiving of wireless signals, from the base stations (BSs) to the user equipments (UEs) in the downlink (DL), and from the UE to the BS in the uplink (UL), are either separated orthogonally in time or frequency domain; two prominent examples include time-division duplex (TDD) and frequency-division duplex (FDD) systems. A major motivation behind this design and dimensioning approach has been to bypass the extra interference which arises from the bi-directional wireless functionality, namely, residual self-interference (SI) at each full-duplex (FD) transceiver, and mutual interference (MI) between the DL and the UL modes of communications [5].

However, HD system has proved its inefficiently in supporting the rapid growth rate of data. Therefore the concept of FD gained significant attention to further improve or even double the spectral efficiency (SE). In a FD communication, the wireless terminals may transmit and receive at the same time and frequency band [6]. Therefore the performance of FD strongly depends on the interference cancellation capability of transceivers [7]. There are three main interference sources introduced by a FD communication. First, the SI from the transmit antenna to receive antenna in a transceiver [5]. Second, the inter-cell or inter-user interference caused by the simultaneous transmission of the UL mobile terminals in the same cell [8]. And finally, the interference coming from neighbouring cell also known as called cross-mode interference [9]. Recently, there have been major advances in the family of techniques used to combat SI directly in FD mode, including any combination of analog, digital, and spatial domain cancellation [10–12]. In addition, the MI, a main limiting factor in large-scale adoption of FD functionality, can be effectively tackled through applying interference management techniques such as successive interference cancellation (SIC) [13], [14]. With the aid of advanced techniques for tackling SI and MI, it has been shown that significant FD versus HD spectral efficiency (SE) gains can be achieved in cellular networks [7, 15–17]. The adoption of FD function-

ality is considered particularly attractive for dense small-cell BS deployment in the fifth generation (5G) cellular networks and beyond [18]. Follwoing above, small cell wireless communications are proved to be particularly useful due to their low transmit power, short transmission distances and low mobility of their UEs [19].

1.1.3 MIMO

One of the main technologies to account for the rapid growth of data traffic is introduction of multiple-input multiple-output (MIMO) systems. The concept of MIMO has emerged in the late 90s and was introduced to WiFi systems about 2006 [20] [21] and to the cellular networks shortly after [22]. In MIMO technology, BSs are equipped with multiple antennas and therefore, are able to communicate with multiple UEs simultaneously [23]. Unlike the traditional model where BSs served users by orthogonalising the channel, MIMO enables them to achieve higher rates and therefore increasing SE by serving more users in the same time and frequency resource [24]. Therefore, the more antennas a BS has, the more degrees of freedom it can provide and consequently a higher SE will be achieved [25].

Multiple works have investigated PHYLS in MIMO wiretap including [26–28] where the transmitter, receiver and EDs are equipped with more than one antennas. Moreover, beamforming with artificial noise (AN) in MIMO was addressed in [29] to compensate for imperfect channel state information (CSI). In [30] the affect of power allocation between the transmitted information and AN on PHYLS for multiple-input single-output (MISO) communication has been analysed. In [31] a regularized channel inversion precoding for a network with multiple-antenna BS and single-antenna UE system is proposed to maximise secrecy rate. In addition, [32] has looked into the importance of fading channels on secrecy performance from an information theoretic point of view where average secrecy rate and secrecy outage probability is introduced as performance metrics. Following this, [33] has investigated the secrecy outage probability in a single-input multiple-output (SIMO) with maximal ratio combining in a Rayleigh fading environment.

1.1.4 Channel Fading Models

In our work we apply the most commonly used channels in literature to model various channels. A brief description of each of these channels is given below.

Nakagami-*m* Fading: Nakagami-*m* distribution provides a flexible approach for matching the empirical data. This channel also includes Rayleigh fading as a special case [34]. In addition, Nakagami-*m* has been shown to be a very good fit for modelling mobile radio channels in reality [35].

Rayleigh Fading: As mentioned above, small-scale fading or Rayleigh fading is a special case of Nakagami-*m* fading. In the scenario where a large number of multiple reflective paths exist and there is no line-of-sight signal component, the envelope of the received signal can be statistically represented by a Rayleigh probability density function (PDF). Therefore in our work, we consider a great proportion of our channels to follow Rayleigh distribution.

Rician Fading: The Rician fading is a good model for capturing the small-scale fading when there exists a dominant stationary (non-fading) signal component such as a line-of-sight propagation path. In this case, a random multipath component arrives at different angles and superimpose on a stationary dominent signal. Considering above, in this work, the residual SI channels are considered to follow Rician distributed with arbitrary statistics.

1.2 Physical Layer Security

The mobile terminals are in nature more prone to interception in compare with their fixed counterpart [29]. Conventionally, the security was addressed in higher layers such as application layer in the Open System Interconnection (OSI) model [36]. This included the widely adopted security protocols based on cryptographic primitives which required generating and managing of secret keys bringing a costly and difficult challenge for large-scale network [37]. Therefore the PHYLS reappeared as an effective additional method to ensure secure transmission in a simple and inexpensive manner [38]. Today PHYLS is a de facto requirement for the safeguarding of wireless systems [39]. It is quantified by the difference in the useful

and eavesdropping channel capacities, what is known as secrecy rate [40]. This topic has received a great deal of attention in recent years, including the study of PHYLS in the context of relays [41–43], cognitive radios [44, 45], heterogeneous networks [46], wireless information and power transfer [47], and cloud radio access networks [48].

In [49] the PHYLS for DL using regularised channel inversion pre-coding has been studied. The importance of cellular association and location information of mobile terminals have been investigated in [50].

In addition, the Kuhn-Munkres (KM) algorithm has been implemented to find optimal solution for overall secrecy capacity in cellular and device-to-device (D2D) networks [51] while in [52] the interference generated by the D2D network is shown to improve secrecy of cellular transmission.

Different aspects of security performance in large scale networks have been studied in the past years including capacity [53, 54], coverage [55], connectivity [56,57] and percolation theory (where the secrecy of network under different system parameters is studied) [58,59]. Moreover, the rate of secrecy capacity as a function of node's density (scaling law) is investigated in [53, 60]. On the other hand, multiple recent works have investigated the area SE of the successful transmission of confidential messaging while imposing certain constraints of Quality of Service (QoS) [61, 62]. Therefore, while the scaling laws may explain the asymptotic behaviour of the network, the capacity analysis of security performance provides us insights into the affect of different system parameters. Given that the locations of the EDs are in most cases not known to the network, they can be modelled using stochastic processes. There already exists a very rich literature on the design, modelling, and analysis of large-scale wireless systems with random ED locations, see, e.g., [62–65]. More recently, the impact of randomly-located cooperating (a.k.a., colluding) EDs has been investigated in [66]. Moreover, various techniques for improving the channel of legitimate receiver and/or degrading the ED's channel have been proposed and investigated [67, 68]. For example, in [69] the ergodic secrecy rate and secrecy outage in a multi-cell massive MIMO was investigated where the

channel of ED was deteriorated with the help of AN while maintaining the channel condition for legitimate users. Interference alignment as another approach was explored in [70]. In a later work, another popular technique as cooperative jamming was investigated in [71] where a relay and the source transmit the jamming and intended signal simultaneously to confuse the ED.

The concept of PHYLS was first studied by Wyner in 1970s [72]. In this scenario, instead of protecting the data from decoding, the aim is to blind the ED from extracting information. The classic model consists of three entities which is illustrated in Fig. 1.2

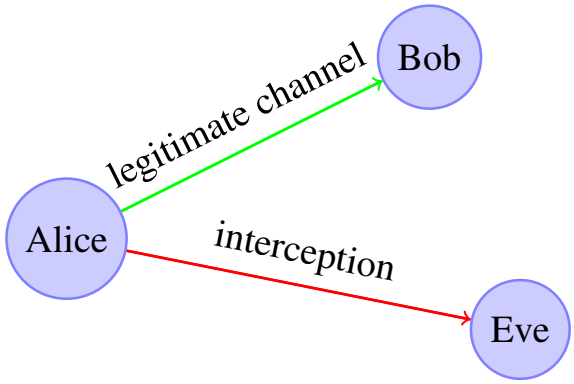

Figure 1.2: An illustration of physical layer security where the legitimate transmitter, Alice, is sending sending signals to legitimate receiver, Bob, while Eavesdropper Eve is attempting to overhear the source.

where the legitimate transmitter Alice is communicating over the main channel to a legitimate receiver Bob while the ED Eve is able to intercept the signal from the EDs' channels [73]. Wyner has shown that if the ED's channel (C_E) is degraded, then Alice can transmit the confidential information (C_B) with a positive secrecy rate of (S_B) [74]:

$$S_B = [C_B - C_E]^+. \tag{1.1}$$

In the following chapters, we use the above formula to calculate the average rate for our receiver to receive the data securely.

1.3 Tools and Techniques

1.3.1 Stochastic Geometry

Conventionally, The deterministic grid-based model, also known as hexagonal model, was used to simulate the large-scale cellular networks. However, in practice, the grid model is an optimistic measure of network performance, as the location of BSs do not follow this framework in reality [75]. In this model, some of the important characteristics of the network including nodes density and mobility are ignored. Recently, Stochastic geometry has been introduced as a useful tool for capturing these network's behaviour and therefore has been taking over the traditional grid-based model. Gilbert's paper in 1961 could be considered as the pioneer work where the connectivity of large scale wireless network has been analysed by tools of stochastic geometry [76]. However the increasing trends of studies on the subject has started only by 2000. For example, the recent works in [77–79] have shown that stochastic geometry may well represent the deployment of heterogeneous cellular networks (HCNs) which allows us to derive analytical results on important problems [80].

In simple words, as the network's behaviours varies at each moment, stochastic geometry observes the snapshots of different realizations of the network, and gives a probabilistic analysis of its performance metrics. If the considered random model is ergodic, one can calculate the spatial averages in order to capture the underlying dependencies of network's elements such as connectivity and stability. (The "spatial average" refers to the mean taken over a large sample of nodes that follow a certain distribution [81]).

As a part of this powerful tool, it is common to model the uncertainty of locations of nodes according to a point process and in particular, a Poisson point process (PPP) [82–84] which is described as follows.

Poisson Point Process (PPP): A point process framework which helps to overcome the limits of Wyner's model when addressing topological randomness. In this approach, the network is modelled as a collection of nodes representing transmitters and receivers in a two-dimensional space. Depending on the network, these

nodes may denote BSs, mobile terminals or access points of a WiFi mesh and so on. Moreover, the location of these nodes are not deterministic but subject to a certain randomness [85]. It is important to note that, unlike mobile users, it may seem less reasonable to model the location of BSs as a point process due to their fixed nature. However, the recent studies have shown that results derived by the point process are extremely close to the real deployment of 4G cellular network [86] and in particular, large scale networks. Furthermore, implementing point process enables us with more tractability in analytical results compared with the traditional models.

If a PPP is homogeneous, it implies that the density of points is constant as well as stationary. This feature brings useful computational advantages which we will use in the next chapters.

Slivnyak's Theorem: If the distribution of our points follow a PPP, this implies that we may carry out the analysis for any of the points in our data set and their characteristics would remain unchanged. This phenomenon is known as Slivnyak's theorem [84, 85, 87]. In the following chapter we consider this node to be the origin in order to simplify the analysis.

Probability Generation Functional (PGFL): PGFL for finite point processes was initially introduced by Moyal in 1962 [88]. This theorem which is described below, enbales us to simplify expectation of a product to an exponential function. Let ϕ be a PPP with density λ and $f(x) : R^2 \rightarrow [0,1]$ be a real value function. Then:

$$\mathbb{E}\{\prod_{x\in\phi} f(x)\} = \exp\left(-\lambda \int_{R^2} (1 - f(x)dx)\right) \tag{1.2}$$

1.3.2 Supervised Learning

Supervised learning is the machine learning task of creating a dependency between the actual data and training data [89]. Given a set of labelled (known) data set, supervised learning technique attempts to find a function such that it captures the dependency of data as well as minimising the errors in predicting new data. Consid-

ering above, one of the popular methods of supervised learning is the curve-fitting technique which we leverage in our work in order to find closed-form expressions in certain cases of interests.

Curve Fitting: Curve fitting is a supervised learning technique, where we utilise large sets of (empirical) data in order to obtain explicit analytical expressions. This is particularly useful for drawing insights into the performance of a cellular network, where in general, closed-form expressions do not exist. In this technique, a linear or non-linear curve is placed through the scatter points in the most fitted approach. The fitness of this curve can be measured through different variables including the logarithmic form where root-mean-square-error (the square root of the arithmetic mean of squared values) (RMSE) and variance (the expectation of the squared deviation of a random variable from its mean) as two metrics for error measurements are calculated and minimised.

1.4 Thesis Overview

Considering the evolving application of wireless networks and the great importance of PHYLS, the main focus of our research is on analysing and improving PHYLS in the wireless cellular networks which is structured as follows.

1. As described in Chapter 2 we begin by investigating the PHYLS performance in a large-scale FD cellular network in presence of a field of EDs whose locations are not known to the network. In this chapter, the BSs are operating in FD mode with one transmitting and one receiving antenna and therefore, serving one user in each resource block. In addition, EDs are equipped with single antenna and not cooperating with each other. Considering this model, we study the PHYLS performance of both HD and FD UEs with and without SIC capability. We also consider the case where BSs and UEs apply SI cancellation techniques to mitigate the affect of interference. Using stochastic geometry tools, we mathematically model the network including: interference, channels and the received signal-to-interference-plus-noise ratio (SINR) at the receiver. Accordingly, we derive the average secrecy rate for

various cases as a measure of PHYLS performance. In the end, we simulate and confirm our mathematical results for our receivers in both cases of HD and FD UEs where we explore the impact of density of EDs as well as BSs on the security performance.

2. In chapter 3 we expand our analysis to the case where BSs are equipped with multiple antennas. Benefiting from MIMO technology and applying beamforming techniques, BSs are able to serve up to a certain number of UEs simultaneously. Here, due to the limited power of UEs, they are considered to operate in HD only. Next, we look into both cases of colluding and non-colluding EDs with single antennas. In the passive scenario, we derive explicit expressions for the average secrecy rate at UEs and BSs. However in the colluding case, we derive this measure as a bounded expression. Next we investigate the impact of different parameters of the network on the secrecy rate including: 1) the number of receive and transmit antennas at the BSs 2) the number of serving UEs per resource block in UL and DL and 3) density of UEs. Further investigation and its result is also given in the appendix.

3. In the final chapter of our analysis we apply curve-fitting techniques in order to derive closed-form expressions in special cases. For the sake of simplifying the non-linear curve-fitting process, we consider the case where each BS serves a single user only – whilst we elaborate on the possible extension to multi-user MIMO. Moreover, we introduce two parameters of R-squared and Variance for measuring the goodness of fit for our approximations. We assess the performance of these explicit closed-form approximations for the key performance indicators against empirical data for all cases under consideration.

Chapter 2

Baseline SISO System Secrecy Performance under Passive Eavesdropping

2.1 Introduction

Recently, many works have analyzed the PHYLS performance in different wireless networks, such as the study of the achievable secrecy rate in the presence of artificial noise [90], relay wiretap channel [91], and with colluding EDs [92], [93]. Most works in the literature, however, study conventional HD systems. With increasing number of users and data rate demands, FD communications, has become a topic of interest [7]. In FD systems, DL and UL occur over the same RF resources; hence, the spectral efficiency can be improved depending on the severity of the added interference [5], [94].

Motivated by the above, in this chapter, we provide a unified theoretical framework for the study of the ergodic secrecy rate performance in FD small-cell networks where the location of EDs are not known to the network. We study the PHYLS performance of a large-scale single-user cellular networks under the homogeneous PPP-based abstraction model of BSs and UEs.

We first consider the general case where the HD UEs may be capable of performing SIC through imposing guard regions of arbitrary radii when modelling the

UE-UE interference. Moreover, the EDs are assumed to be non-colluding and their locations to follow PPP model. Then we consider the FD case for UEs as well as BSs which are equipped with SI cancellation capability. By leveraging on the tools from stochastic geometry theory, we model the received signal, interference channels and SINR at the destination using Shannon capacity theorem. Accordingly, we derive explicit expressions for the DL and UL ergodic secrecy rates, with the statistics of the different useful and interference signals given in closed-form.

Through our mathematical results and Monte Carlo (MC) simulation, we study the impact of density of EDs with respect to the FD base stations in both scenarios of FD and HD UEs. We also investigate the affect of implementing SIC and SI cancellation schemes on the secrecy rate performance. Using our results, we build the fundamentals for our next chapter where we expand our system model to a more complex scenario of multi-antenna FD BSs with MIMO technology.

2.2 System Description

2.2.1 Network Topology

Here, we consider a large-scale FD cellular network where the BSs and mobile UEs are deployed according to independent stationary PPPs ϕ_d and ϕ_u with spatial densities λ_d and λ_u, respectively. The locations of the EDs are not known to the network, therefore in this work, they are modelled according to a homogeneous PPP ϕ_e with spatial density λ_e [48,62]. Moreover, the EDs are considered to operate independently which means they do not exchange their observations [92, 95].

2.2.2 Cellular Association

By invoking the Slivnyak's theorem [85], we perform the DL analysis for a typical FD UE o considered to be located at the centre. Let $l \in \phi_d$, $k \in \phi_u$, and $e \in \phi_e$ denote the locations of the BS l, UL UE k, and ED e, respectively. We consider the cellular association strategy based on the maximum received SINR [96]. For single-tier deployments, this is equivalent to cellular association based on the closest transmitter-receiver distances [83]. Mathematically, the tagged BS of the reference DL UE o satisfies $b = \arg\min(r_{l,o}), l \in \phi_d$, where $r_{l,o} = \|l - o\|$ denotes the

Euclidean distance. The UL analysis, on the other hand, is carried out at the tagged BS b with respect to the signal of an arbitrary UL UE i. It should be noted that due to the cellular association procedure, the scheduled UEs locations are inherently correlated [97]. Here, conditioning on the spatial constraints, we assume that the set of scheduled UEs follows from a stationary PPP [98, 99]. Further, we consider the most malicious EDs in the DL and UL, respectively denoted with v and c, which receive the strongest SINRs [41].

2.2.3 Fading Channel Model

Let p_d and p_u denote the BS and UE transmit powers, respectively. The DL channel gains from the BS l at the UE k and ED e are $g_{l,k}$ and $g_{l,e}$, respectively. Further, we denote the UL channel gains from the UE k at the BS l and ED e using $h_{k,l}$ and $h_{k,e}$, respectively. The cross-mode channel gains from the BS l at the BS b, and from the UE k at the UE o are represented using $h_{l,b}$ and $g_{k,o}$, respectively. In addition, the residual SI channel gain at the BS b is denoted with $h_{b,b}$. Similarly, the residual SI channel gain at the UE o is denoted with $g_{o,o}$. The residual SI channels are Rician distributed with independent and identically distributed (i.i.d.) $\mathscr{CN}(\mu, v^2)$ coefficients. Accordingly, the channel power gain parameters can also be approximated using Gamma (κ, θ) where [100]:

$$\kappa \triangleq \frac{(\mu^2 + v^2)^2}{(2\mu^2 + v^2)v^2} \tag{2.1}$$

and

$$\theta \triangleq \frac{(2\mu^2 + v^2)v^2}{(\mu^2 + v^2)^2}. \tag{2.2}$$

All other channels are considered to be Rayleigh distributed with i.i.d. elements drawn from $\mathscr{CN}(0,1)$. In addition, the additive white Gaussian noise (AWGN) with variance σ^2 is considered at all receivers and we utilise the unbounded path-loss model with exponent $\alpha > 2$.

2.2.4 SINR Formulation

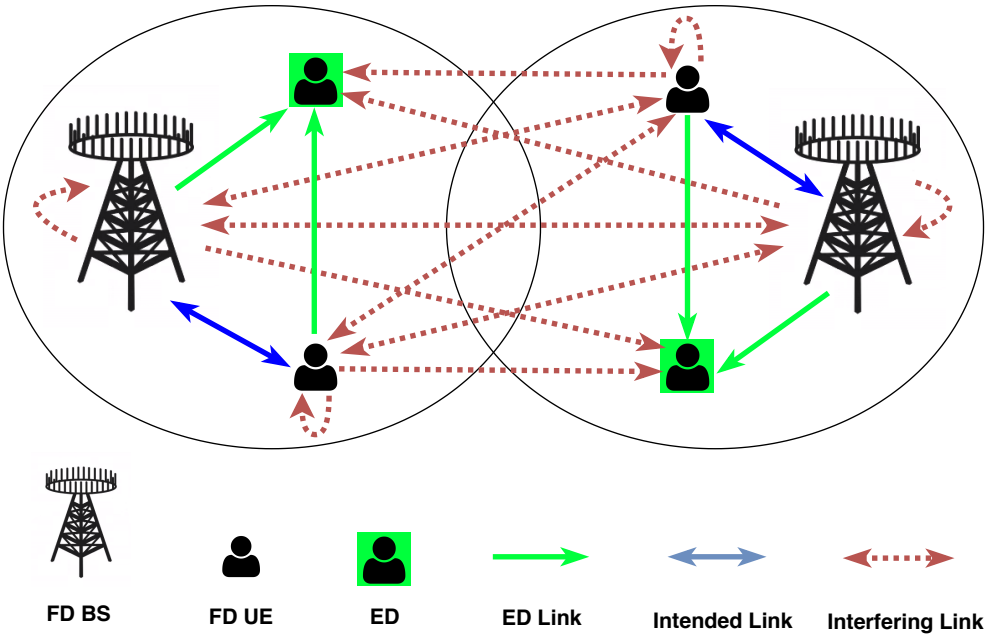

Figure 2.1: Illustrative example of a two-cell full-duplex setup where in each a BS and UE communicate in FD mode in the presence of an ED. The intended, interfering, and eavesdropping links are captured in the diagram.

Before proceeding with the characterisations of the SINRs, we provide a sample diagram of the system under consideration for illustration purposes in Fig. 2.1. Here, we have two cells where in each a BS and UE communicate in full-duplex mode in the presence of an ED. As it can be seen from the diagram, there are intended, interfering, and eavesdropping links that need to be taken into account when formulating the SINRs.

The SINR in the DL at the UE o can accordingly be written as

$$\gamma_o^{\mathrm{FD}} = \frac{X_o}{I_o^{d,d} + I_o^{u,d} + I_o^{o,o} + \sigma_o^2} \tag{2.3}$$

where $X_o = p_d g_{b,o} r_{b,o}^{-\alpha}$ is the intended received signal power (from the serving BS), $I_o^{d,d} = \sum_{l \in \phi_d \setminus \{b\}} p_d g_{l,o} r_{l,o}^{-\alpha}$ is the inter-cell interference (from the transmitting BSs), $I_o^{u,d} = \sum_{k \in \phi_u} p_u h_{k,o} r_{k,o}^{-\alpha}$ is the cross-mode interference (from the transmitting UEs), $I_o^o = p_u g_o^o$ is the residual SI (from the bi-directional operation) and σ_o^2 is the noise

variance.

The received SINR in the UL at the BS b with respect to the signal from an arbitrary UL UE i is given by

$$\gamma_i^{\mathrm{FD}} = \frac{X_i}{I_i^{u,u} + I_i^{d,u} + I_i^{i} + \sigma_i^2} \tag{2.4}$$

where $X_i = p_u h_{i,b} r_{i,b}^{-\alpha}$ is the intended received signal power (from the reference UE), $I_i^{u,u} = \sum_{k \in \hat{\phi}_u} p_u h_{k,b} r_{k,b}^{-\alpha}$, with $\hat{\phi}_u$ denoting the set of outer-cell scheduled UL UEs, is the inter-cell interference (from the transmitting UEs), $I_i^{d,u} = \sum_{l \in \phi_d \setminus \{b\}} p_d g_{l,b} r_{l,b}^{-\alpha}$ is the cross-mode interference (from the transmitting BSs), $I_i^{i} = p_b g_{b,b}$ is the residual SI (from the bi-directional operation), and σ_i^2 is the noise variance.

The received SINR in the DL at the most malicious passive ED v is given by

$$\gamma_v^{\mathrm{FD}} = \max_{e \in \phi_e} \left(\frac{X_e}{I_e^{d,d} + I_e^{u,d} + \sigma_e^2} \right) \tag{2.5}$$

where $X_e = p_d g_{b,e} r_{b,e}^{-\alpha}$ is the intended received signal (from the serving BS), $I_e^{d,d} = \sum_{l \in \phi_d} p_d g_{l,e} r_{l,e}^{-\alpha}$ is the inter-cell interference (from the transmitting BSs), $I_e^{u,d} = \sum_{k \in \phi_u} p_u \; h_{k,e} r_{k,e}^{-\alpha}$ is the cross-mode interference (from the transmitting UEs), and σ_e^2 is the noise variance.

The received SINR in the UL at the most malicious passive ED is given by

$$\gamma_c^{\mathrm{FD}} = \max_{e \in \phi_e} \left(\frac{X_e}{I_e^{u,u} + I_e^{d,u} + \sigma_e^2} \right) \tag{2.6}$$

where $X_e = p_u h_{o,e} r_{o,e}^{-\alpha}$ is the intended received signal (from the reference UE), $I_e^{u,u} = \sum_{k \in \phi_u} p_u h_{k,e} r_{k,e}^{-\alpha}$ is the inter-cell interference (from the transmitting UEs), $I_e^{d,u} = \sum_{l \in \phi_d} p_d \; g_{l,e} r_{l,e}^{-\alpha}$ is the cross-mode interference (from the transmitting BSs), and σ_e^2 is the noise variance.

Note that the EDs' SINR expressions in this work correspond to the case where the EDs have no information regarding the codebook of UEs and BSs. However, the analysis can be modified to capture other scenarios (e.g., by removing certain

interference terms from the EDs' SINRs) [101].

2.3 Analysis

In this section, we study the PHYLS performance in FD small-cell networks under with a field of passive EDs. Note that the ergodic rates (in b/s/Hz) of the reference DL and UL UEs, o and i, over two resource blocks, are given by $C_o^{\mathrm{FD}} = 2\mathbb{E}[\log_2(1+\gamma_o^{\mathrm{FD}})]$ and $C_i^{\mathrm{FD}} = 2\mathbb{E}[\log_2(1+\gamma_i^{\mathrm{FD}})]$ in FD mode, and $C_o^{\mathrm{HD}} = \mathbb{E}[\log_2(1+\gamma_o^{\mathrm{HD}})]$ and $C_i^{\mathrm{HD}} = \mathbb{E}[\log_2(1+\gamma_i^{\mathrm{HD}})]$ in HD mode, respectively. Similarly, the ergodic rates (in b/s/Hz) of the most malicious DL and UL EDs, v and c, over two resource blocks, are given by $C_v^{\mathrm{FD}} = 2\mathbb{E}[\log_2(1+\gamma_v^{\mathrm{FD}})]$ and $C_c^{\mathrm{FD}} = 2\mathbb{E}[\log_2(1+\gamma_c^{\mathrm{FD}})]$ in FD mode, and $C_v^{\mathrm{HD}} = \mathbb{E}[\log_2(1+\gamma_v^{\mathrm{HD}})]$ and $C_c^{\mathrm{HD}} = \mathbb{E}[\log_2(1+\gamma_c^{\mathrm{HD}})]$ in HD mode, respectively.

Remark 1. According to Jensen's inequality, $\mathbb{E}[\max(X,Y)\} \geq \max\{\mathbb{E}\{X\},\mathbb{E}\{Y\}]$ the bounded DL and UL ergodic secrecy rates (considering FD BSs) are respectively given by $S_o^{\mathrm{FD}} = [C_o^{\mathrm{FD}} - C_v^{\mathrm{FD}}]^+$ and $S_i^{\mathrm{FD}} = [C_i^{\mathrm{FD}} - C_c^{\mathrm{FD}}]^+$. Similarly, in the case of HD operation, the bounded DL and UL ergodic secrecy rates are respectively given by $S_o^{\mathrm{HD}} = [C_o^{\mathrm{HD}} - C_v^{\mathrm{HD}}]^+$ and $S_i^{\mathrm{HD}} = [C_i^{\mathrm{HD}} - C_c^{\mathrm{HD}}]^+$.

2.3.1 User Equipments

We proceed by deriving explicit expressions for the DL and UL UEs ergodic rates. Note that the DL MI is characterized considering the UEs may be capable of performing SIC. In order to capture performance for general cases, we consider an exclusion region of radius ε when modeling the UE-UE interference [102].

Theorem 1. The DL ergodic rates (in b/s/Hz) of the useful UE o in the FD and HD small-cell networks over two resource blocks are given by

$$C_o^{\mathrm{FD}} = \frac{4\pi\lambda_d}{\ln(2)} \int_0^{\infty}\int_0^{\infty} \frac{1}{1+\gamma} \left(\left\{ \exp\left(-s\sigma_o^2\right) \mathscr{L}_{I_o^{d,d}}[s] \mathscr{L}_{I_o^{u,d}}[s] \mathscr{L}_{I_o^{o}}[s] \right\}_{s=\frac{\gamma r^{\alpha}}{P_d}} \right) \mathrm{d}\gamma \cdot r \exp\left(-\pi\lambda_d r^2\right) \mathrm{d}r \tag{2.7}$$

and

$$C_o^{\mathrm{HD}} = \frac{2\pi\lambda_d}{\ln(2)} \int_0^{\infty} \int_0^{\infty} \frac{1}{1+\gamma} \left(\left\{ \exp\left(-s\sigma_o^2\right) \mathscr{L}_{I_o^{d,d}}[s] \right\}_{s=\frac{\gamma r^{\alpha}}{p_d}} \right) \\ . \, \mathrm{d}\gamma r \exp\left(-\pi\lambda_d r^2\right) \mathrm{d}r \tag{2.8}$$

where

$$\mathscr{L}_{I_o^{d,d}}[s] = \exp\left(-\pi\lambda_d r^2 \left({}_2F_1\left(1, -\frac{2}{\alpha}; 1-\frac{2}{\alpha}; -\frac{sp_d}{r^{\alpha}}\right) - 1 \right) \right) \tag{2.9}$$

and

$$\mathscr{L}_{I_o^{u,d}}[s] = \exp\left(-\pi\lambda_d \varepsilon^2 \left({}_2F_1\left(1, -\frac{2}{\alpha}; 1-\frac{2}{\alpha}; -\frac{sp_u}{\varepsilon^{\alpha}}\right) - 1 \right) \right) \tag{2.10}$$

and

$$\mathscr{L}_{I_i^{o,o}}(s) = \left(1 + sp_u\theta\right)^{-\kappa}. \tag{2.11}$$

Proof: See Appendix A.

Remark 2. The guard region radius ε in the MI expression in (2.10) can be set by design or through measurements based on the SIC capability at the UE side. In particular, $\varepsilon = 0$ corresponds to the worst-case without SIC capability.

Theorem 2. The UL ergodic rates (in b/s/Hz) of the useful UE i in the FD and HD small-cell networks over two resource blocks are given by

$$C_i^{\mathrm{FD}} = \frac{4\pi\lambda_d}{\ln(2)} \int_0^{\infty} \int_0^{\infty} \frac{1}{1+\gamma} \left\{ \exp\left(-s\sigma_i^2\right) \mathscr{L}_{I_i^{u,u}}[s] \mathscr{L}_{I_i^{d,u}}[s] \mathscr{L}_{I_i^{i}}[s] \right\}_{s=\frac{\gamma r^{\alpha}}{p_u}} \mathrm{d}\gamma \\ \cdot r \exp\left(-\pi\lambda_d r^2\right) \mathrm{d}r \tag{2.12}$$

and

$$C_i^{\mathrm{HD}} = \frac{2\pi\lambda_d}{\ln(2)} \int_0^{\infty} \int_0^{\infty} \frac{1}{1+\gamma} \left\{ \exp\left(-s\sigma_i^2\right) \mathscr{L}_{I_i^{u,u}}[s] \right\}_{s=\frac{\gamma r^{\alpha}}{p_u}} \\ . \, \mathrm{d}\gamma r \exp\left(-\pi\lambda_d r^2\right) \mathrm{d}r \tag{2.13}$$

where

$$\mathscr{L}_{I_i^{u,u}}[s] = \exp\left(-\pi\lambda_d r^2 \left({}_2F_1\left(1, -\frac{2}{\alpha}; 1-\frac{2}{\alpha}; -\frac{sp_u}{r^\alpha}\right) - 1\right)\right) \tag{2.14}$$

and

$$\mathscr{L}_{I_i^{d,u}}[s] = \exp\left(-\pi\lambda_d \left(sp_d\right)^{\frac{2}{\alpha}} \frac{\Gamma\left(1-\frac{2}{\alpha}\right)\Gamma\left(1+\frac{2}{\alpha}\right)}{\Gamma(1)}\right) \tag{2.15}$$

and

$$\mathscr{L}_{I_i^i}[s] = (1+sp_d\theta)^{-\kappa}. \tag{2.16}$$

Proof: See Appendix B.

Remark 3. The Rician fading distribution parameters μ and ν in the residual SI expression in (2.15) can be tuned by design or measurements to capture the SI cancellation capability at the BS side. For example, $\nu = 0$ and $\mu = 0$ correspond to perfect SI removal and non line-of-sight (NLOS) SI, respectively.

2.3.2 Passive Eavesdroppers

Next, we derive explicit expressions for the ergodic rates of the most malicious passive EDs in the DL and UL. Note that in this case the EDs act independently (do not exchange information).

Theorem 3. The DL ergodic rates (in b/s/Hz) of the most malicious passive ED v in the FD and HD small-cell networks over two resource blocks are given by

$$C_v^{\mathrm{FD}} = \frac{2}{\ln(2)} \int_0^\infty \frac{1}{1+\gamma} \times \left(1 - \exp\left(-2\pi\lambda_e \int_0^\infty \left[\exp\left(-s\sigma_v^2\right) \mathscr{L}_{I_v^{d,d}}[s] \mathscr{L}_{I_v^{u,d}}[s]\right]_{s=\frac{\gamma r^\alpha}{p_d}} r \, \mathrm{d}r\right)\right) \mathrm{d}\gamma \tag{2.17}$$

and

$$C_v^{\mathrm{HD}} = \frac{1}{\ln(2)} \int_0^\infty \frac{1}{1+\gamma} \times$$

$$\left(1-\exp\left(-2\pi\lambda_e\int_0^{\infty}\left[\exp\left(-s\sigma_v^2\right)\mathscr{L}_{I_v^{d,d}}[s]\mathscr{L}_{I_v^{u,d}}[s]\right]_{s=\frac{\gamma r^{\alpha}}{p_d}} r\,\mathrm{d}r\right)\right)\mathrm{d}\gamma \quad (2.18)$$

where

$$\mathscr{L}_{I_v^{d,d}}[s]=\exp\left(-\pi\lambda_d\left(sp_d\right)^{\frac{2}{\alpha}}\frac{\Gamma\left(1-\frac{2}{\alpha}\right)\Gamma\left(1+\frac{2}{\alpha}\right)}{\Gamma(1)}\right) \quad (2.19)$$

and

$$\mathscr{L}_{I_v^{u,d}}[s]=\exp\left(-\pi\lambda_d\left(sp_u\right)^{\frac{2}{\alpha}}\Gamma\left(1-\frac{2}{\alpha}\right)\Gamma\left(1+\frac{2}{\alpha}\right)\right). \quad (2.20)$$

Proof: See Appendix C.

Theorem 4. The UL ergodic rates (in b/s/Hz) of the most malicious passive ED c in the FD and HD small-cell networks over two resource blocks are given by

$$C_c^{\mathrm{FD}}=\frac{2}{\ln(2)}\int_0^{\infty}\frac{1}{1+\gamma}\times \left(1-\exp\left(-2\pi\lambda_e\int_0^{\infty}\left\{\exp\left(-s\sigma_c^2\right)\mathscr{L}_{I_c^{u,u}}[s]\mathscr{L}_{I_c^{d,u}}[s]\right\}_{s=\frac{\gamma r^{\alpha}}{pu}} r\,\mathrm{d}r\right)\right)\mathrm{d}\gamma \quad (2.21)$$

and

$$C_c^{\mathrm{HD}}=\frac{1}{\ln(2)}\int_0^{\infty}\frac{1}{1+\gamma}\times \left(1-\exp\left(-2\pi\lambda_e\int_0^{\infty}\left\{\exp\left(-s\sigma_c^2\right)\mathscr{L}_{I_c^{u,u}}[s]\mathscr{L}_{I_c^{d,u}}[s]\right\}_{s=\frac{\gamma r^{\alpha}}{pu}} r\,\mathrm{d}r\right)\right)\mathrm{d}\gamma \quad (2.22)$$

where

$$\mathscr{L}_{I_c^{u,u}}[s]=\exp\left(-\pi\lambda_d\left(sp_u\right)^{\frac{2}{\alpha}}\Gamma\left(1-\frac{2}{\alpha}\right)\Gamma\left(1+\frac{2}{\alpha}\right)\right) \quad (2.23)$$

and

$$\mathscr{L}_{I_c^{d,u}}[s]=\exp\left(-\pi\lambda_d\left(sp_d\right)^{\frac{2}{\alpha}}\frac{\Gamma\left(1-\frac{2}{\alpha}\right)\Gamma\left(1+\frac{2}{\alpha}\right)}{\Gamma(1)}\right). \quad (2.24)$$

Proof: See Appendix D.

2.4 Numerical Results

We provide several numerical examples in order to assess the PHYLS performance of FD and HD small-cell networks in the presence of a Poisson field of EDs. The spatial density of the small-cell BSs is set to be $\lambda^{(d)} = \frac{4}{\pi}$ per km^2. The (per-user) BS and UE transmit powers are kept fixed at $p_d = 23$ dBm and $p_u = 20$ dBm, respectively. The noise spectral density at all receivers is -170 dBm/Hz and the total system bandwidth is $W = 10$ MHz. The MC simulations are obtained from 20 k trials in a circular region of radius 10 km. Note that all results correspond to the per-user ergodic secrecy performance over two resource blocks. In the FD small-cell network, the DL and UL run simultaneously, whereas in the HD small-cell network, the DL and UL occur over different resource blocks. Furthermore, in the FD system, we take into account different interference cancellation schemes. In particular, in the DL, we consider the cases with and without SIC capability at the UE side. Moreover, in the UL, we capture the performance under different perfect SI cancellation.

2.4.1 Impact of the Eavesdroppers' Density on HD UEs

Here, we study the impact of the EDs' spatial density on the small-cell network in case of DL and UL PHYLS performances under a PPP-based abstraction model of passive EDs. As illustrated in Fig. 2.2, the ergodic secrecy rate decreases with increasing the density of EDs in compare with BSs. In addition, the performance gain difference between FD and HD increases in a field with denser number of EDs. This is due to the fact that EDs in the FD suffer from a greater channel degradation caused by extra interference in small-cell netwroks than the HD counterpart. On the other hand the HD BS in the UL benefits from a higher security gain in compare with its FD counterpart. This is due to the extra SI caused on the BS side which is the reason for the difference to become negligible via SI cancellation capabilities. Note that the MC results confirm the validity of our proposed theoretical framework.

2.4.2 Impact of the Eavesdroppers' Density on FD UEs

Next, we proceed by investigating the affect of EDs' spatial density on both FD BSs and UEs in the small-cell network. As Fig. 2.3 illustrates, in this scenario the PHYLS in DL also benefits from a better gain in the FD mode than HD with a denser field of passive EDs. Similarly, employing SIC on the UE side improves the FD versus HD PHYLS performance. It is important to note that, changing the UEs operation mode from HD to FD, does not affect the ergodic secrecy rate in the UL. This is due to the fact that the latter case does not cause any extra interference on the BSs side and therefore the UL SINR remains unchanged. Similarly, the MC results confirm the validity of the proposed theoretical framework.

In general, FD operation at the UE side may be unrealistic, at least in the short term. Existing devices typically are battery-constrained, as a result having self-interference cancellation and successive interference cancellation may be challenging. The devices when at the cell-edge also may perform really poorly in the presence of mutual-interference from other FD UEs. The results presented in the figures in this section confirm this trend. Please note that given the interference-limited nature of emerging small-cell deployments, changing the SNR does not affect the underlying trends observed here (we have used state-of-the art parameters for the noise floor figure and transmit power of BSs and UEs throughout this thesis).

In this next chapter, we extend the results of this chapter to cases with MIMO communications and colluding eavesdroppers.

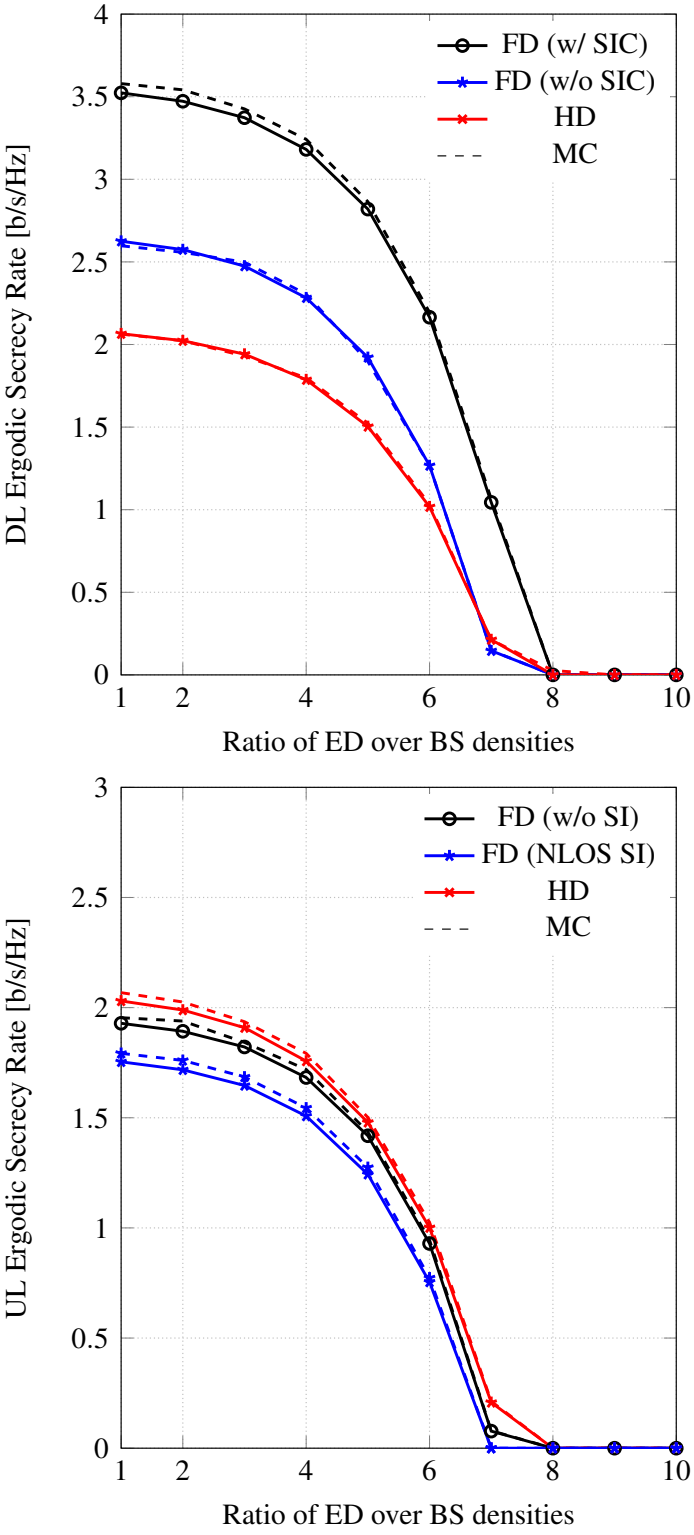

Figure 2.2: Impact of passive EDs' spatial densities on the small-cell network with FD BSs and HD UEs PHY-layer security performance. System parameters are: $\lambda_d = \frac{4}{\pi}$ km^{-2}, $\lambda_u = \lambda_d$ km^{-2}, $p_d = 23$ dBm, $p_u = 20$ dBm, $W = 10$ MHz, $\sigma_o^2 = \sigma_v^2 = \sigma_i^2 = \sigma_c^2 = -170$ dBm/Hz, $\alpha = 4$.

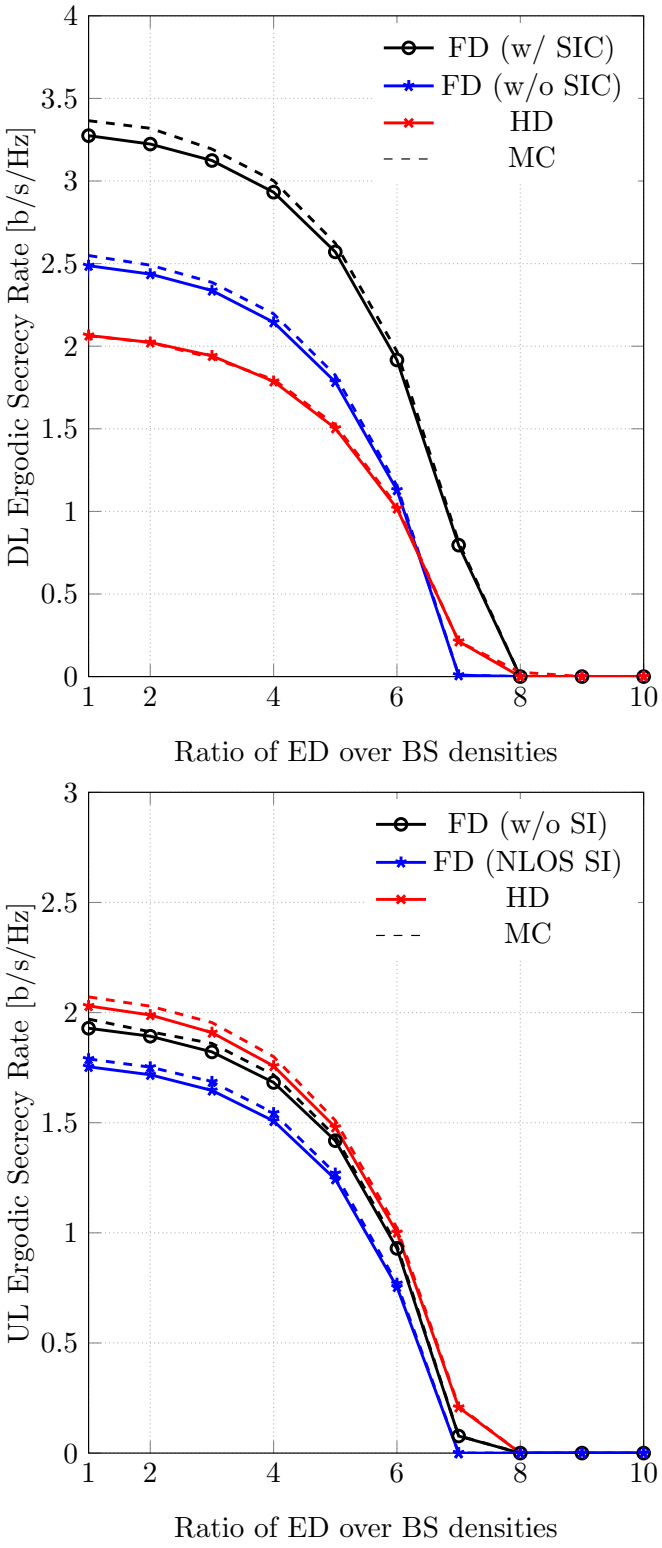

Figure 2.3: Impact of passive EDs' spatial densities on the small-cell network with FD BSs and FD UEs PHY-layer security performance. System parameters are: $\lambda_d = \frac{4}{\pi}$ km^{-2}, $\lambda_u = \lambda_d$ km^{-2}, $p_d = 23$ dBm, $p_u = 20$ dBm, $W = 10$ MHz, $\sigma_o^2 = \sigma_v^2 = \sigma_i^2 = \sigma_c^2 = -170$ dBm/Hz, $\alpha = 4$.

2.5 Conclusions

In this chapter, we studied the PHYLS performance in a FD cellular network with a field of passive EDs. The BSs, UEs, and EDs were modelled according to the PPP-based abstraction model. First, we investigated the basic scenario where the BSs operate in FD mode but UEs are equipped with single antennas and therefore transmitting and receiving in separate resource blocks. Next we expanded the case to the scenario where UEs operate in FD mode as well as the BSs. We derived explicit expressions for the secrecy rate in the DL and UL scenarios. Moreover, we explored the affect of SI cancellation scheme on the BS side as well as the SIC capability of UEs. The proposed framework was utilized to study the FD versus HD secrecy rate gain. Our findings indicated that the FD operation allows for significant improvements in the secrecy rate, particularly through adopting advanced interference cancellation schemes. In addition to above, it has been shown that the FD mode has negligible affect on the secrecy rate in the UE side. In the next chapter, we will extend our work to the multi antenna scenario, where BSs are capable of serving more than one user at the time by employing MIMO technology.

The findings of this chapter can also be extended in other ways. One promising approach is to look at full-duplex cell-free systems where many access points (typically with single-antennas) can be jointly utilised to serve many users at the same time with the aid of user-centric cellular association. The use of cooperation can significantly improve the physical layer security given the links will add a lot of robustness, increasing the ergodic secrecy rates.

Chapter 3

MIMO System Secrecy Performance under Passive and Colluding Eavesdropping

3.1 Introduction

The emergence of FD provides a new paradigm concerning all aspects of wireless system design, including PHYLS performance. This topic has been studied in the recent literature (see, e.g., [103] and the references therein). In [104], a new solution for improving the secrecy capacity using FD transceivers which perform joint reception and jamming was proposed. The work in [104], as well as other related papers such as [105], were based on a deterministic single-cell setup. On the other hand, the PHYLS performance in large-scale FD systems is not well understood.

As an extension of the previous chapter, we consider a large-scale small-cell network where the FD multi-antenna BSs benefit from MIMO technology to improve the received SINR at both sides. In this scenario, due to the limited power of UEs, we consider the single-antenna UEs to operate in HD mode only. Similar to the previous chapter, the FD BSs and HD UL UEs are deployed based on homogeneous PPPs ϕ_d and ϕ_u with spatial densities λ_d and λ_u, respectively.

In the UL, each FD small-cell BS, is equipped with N_d transmit and N_u receive antennas ($N_d + N_u$ radio-frequency chains in total), which is considered to simulta-

neously serve K_d DL and K_u UL HD single-antenna UEs per resource block. Note that the assumption of HD UEs is made due to the inherent restrictions of the legacy devices [106], otherwise, the framework can be readily extended to the case of FD UEs [107]. Similar to the previous chapter, the locations of the EDs are generally not known to the network, therefore they are modelled according to a homogeneous PPP ϕ_e with spatial density λ_e [48, 62]. Moreover, we consider the different scenarios where the (single-antenna) EDs are operating independently and cooperatively [66]. Note that with obvious adjustments, the HD system, where the DL and UL occur over different resource blocks, can be described. Applying stochastic geometry tools and considering linear zero-forcing (ZF) beamforming, we characterize the SINR distribution at the reference BS, UE, the most malicious ED and the total sum in the colluding case. Accordingly, we develop explicit expressions for the secrecy rates in both UL and DL of the FD cellular network.

3.1.1 Cellular Association

Following the same procedure and notations as chapter 2, we consider the cellular association according to the strongest SINR which in our system model is equivalent to cellular association based on the shortest transmitter-receiver distances [83]. Further to our previous assumptions, in the case of collusion, we consider the cooperative EDs are capable of optimally combining their eavesdropping signals [108, 109].

3.1.2 Beamfomring Design

In this work, we employ linear ZF beamforming for suppressing intra-cell interference in both DL and UL directions of communications [110]. Let $\boldsymbol{G}_l = [\boldsymbol{g}_{l,j}^T]_{1\leq j\leq K_d}^T \in \mathscr{C}^{K_d\cdot N_d}$ denote the collective DL channels from the BS l to its K_d DL UEs. At the BS l, the linear ZF precoding matrix $\boldsymbol{V}_l = [\boldsymbol{v}_{l,j}]_{1\leq j\leq K_d} \in \mathscr{C}^{N_d\cdot K_d}$, $\mathbb{E}[\|\boldsymbol{v}_{l,j}\|^2] = 1$, is selected equal to the normalized columns of $\boldsymbol{G}_l^+ = \boldsymbol{G}_l^\dagger(\boldsymbol{G}_l\boldsymbol{G}_l^\dagger)^{-1} \in \mathscr{C}^{N_d\cdot K_d}$. Moreover, let $\boldsymbol{H}_l = [\boldsymbol{h}_{j,l}]_{1\leq j\leq K_u} \in \mathscr{C}^{N_u\cdot K_u}$ represent the collective UL channels at the BS l from its K_u scheduled UL UEs. At the BS l, the linear postcoding ZF matrix $\boldsymbol{W}_l = [\boldsymbol{w}_{j,l}^T]_{1\leq j\leq K_u}^T \in \mathscr{C}^{K_u\cdot N_u}$, $\mathbb{E}[\|\boldsymbol{w}_{j,l}\|^2] = 1$, is selected equal to the normalized rows of $\boldsymbol{H}_l^+ = (\boldsymbol{H}_l^\dagger\boldsymbol{H}_l)^{-1}\boldsymbol{H}_l^\dagger \in \mathscr{C}^{K_u\cdot N_u}$.

3.1.3 SINR Formulation

The received SINR (considering FD BSs) in the DL at the UE o under linear ZF precoding is given by

$$\gamma_o^{\mathrm{FD}} = \frac{X_o}{I_o^{d,d} + I_o^{u,d} + \sigma_o^2} \tag{3.1}$$

where $X_o = p_d |\boldsymbol{g}_{b,o} \boldsymbol{v}_{b,o}|^2 r_{b,o}^{-\alpha}$ is the intended received signal power (from the serving BS), $I_o^{d,d} = \sum_{l \in \phi_d \setminus \{b\}} p_d \|\boldsymbol{g}_{l,o} \boldsymbol{V}_l\|^2 r_{l,o}^{-\alpha}$ is the inter-cell interference (from the transmitting BSs), $I_o^{u,d} = \sum_{k \in \phi_u} p_u |h_{k,o}|^2 r_{k,o}^{-\alpha}$ is the cross-mode interference (from the transmitting UEs), and σ_o^2 is the noise variance. The linear ZF precoding vector $\boldsymbol{v}_{b,o}$ is selected in the direction of the projection of $\boldsymbol{g}_{b,o}$ on the $(N_d - K_d + 1)$-dimensional nullspace spanned by the multi-user interference. Hence, the distribution of the intended channel power gain is given by $G_{b,o} = |\boldsymbol{g}_{b,o} \boldsymbol{v}_{b,o}|^2 \sim \mathscr{G}(N_d - K_d + 1, 1)$ [111, 112]. With the assumption that the other BSs precoding matrices have independent columns, the channel power gain from each interfering BS is interpreted as the aggregation of multiple separate beams from the projection of $\boldsymbol{g}_{l,o}$ onto the one-dimensional precoding vectors. Based on this assumption, the inter-cell interference channel power gain distribution is given by $G_{l,o} = \|\boldsymbol{g}_{l,o} \boldsymbol{V}_l\|^2 \sim \mathscr{G}(K_d, 1)$. Moreover, the cross-mode interference (from the single-antenna UEs) channel power gain distribution is given by $H_{k,o} = |h_{k,o}|^2 \sim \mathscr{G}(1,1)$.

The received SINR (considering FD BSs) in the UL at the BS b with respect to the signal from an arbitrary UL UE i under linear ZF postcoding is given by

$$\gamma_i^{\mathrm{FD}} = \frac{X_i}{I_i^{u,u} + I_i^{d,u} + I_i^{i} + \sigma_i^2} \tag{3.2}$$

where $X_i = p_u |\boldsymbol{w}_{i,b}^T \boldsymbol{h}_{i,b}|^2 r_{i,b}^{-\alpha}$ is the intended received signal power (from the reference UE), $I_i^{u,u} = \sum_{k \in \hat{\phi}_u} p_u |\boldsymbol{w}_{i,b}^T \boldsymbol{h}_{k,b}|^2 r_{k,b}^{-\alpha}$, with $\hat{\phi}_u$ denoting the set of outer-cell scheduled UL UEs, is the inter-cell interference (from the transmitting UEs), $I_i^{d,u} = \sum_{l \in \phi_d \setminus \{b\}} p_d \|\boldsymbol{w}_{i,b}^T \boldsymbol{G}_{l,b} \boldsymbol{V}_l\|^2 r_{l,b}^{-\alpha}$ is the cross-mode interference (from the transmitting BSs), $I_i^{i} = p_b \|\boldsymbol{w}_{i,b}^T \boldsymbol{G}_{b,b} \boldsymbol{V}_b\|^2$ is the residual SI (from the bi-directional operation), and σ_i^2 is the noise variance. Considering linear ZF postcoding, the intended

channel power gain distribution is given by $H_{i,b} = |\boldsymbol{w}_{i,b}^T \boldsymbol{h}_{i,b}|^2 \sim \mathscr{G}(N_u - K_u + 1, 1)$. Moreover, the inter-cell interference (from the single-antenna UEs) channel power gain distribution is given by $H_{k,b} = |\boldsymbol{w}_{i,b}^T \boldsymbol{h}_{k,b}|^2 \sim \mathscr{G}(1,1)$. By invoking the assumption of independent (column-wise) outer-cell precoding matrices, the cross-mode interference (from transmitting BSs) channel power gain distribution is given by $G_{l,b} = \|\boldsymbol{w}_{i,b}^T \boldsymbol{G}_{l,b} \boldsymbol{V}_l\|^2 \sim \mathscr{G}(K_d, 1)$. Furthermore [100], the residual SI channel power gain over the multi-user MIMO Rician fading channel can be approximated as $G_{b,b} = \|\boldsymbol{w}_{i,b}^T \boldsymbol{G}_{b,b} \boldsymbol{V}_b\|^2 \sim \mathscr{G}(\kappa, \theta)$ where

$$\kappa \triangleq \frac{K_d(N_u+1)(N_d-K_d+2)\left(\mu^2+\nu^2\right)^2}{\left(2N_uN_d+\frac{K_d(N_d-K_d+2)}{N_u+1}(N_uN_d-N_u-N_d-1)\right)\mu^4+(N_u+1)(N_d+1)\nu^2\left(2\mu^2+\nu^2\right)} \tag{3.3}$$

and

$$\theta \triangleq \frac{\left(2N_uN_d+\frac{K_d(N_d-K_d+2)}{(N_d+1)}(N_uN_d-N_u-N_d-1)\right)\mu^4+(N_u+1)(N_d+1)\nu^2\left(2\mu^2+\nu^2\right)}{(N_u+1)(N_d-K_d+2)\left(\mu^2+\nu^2\right)}. \tag{3.4}$$

The received SINR (considering FD BSs) in the DL at the most malicious passive and colluding ED v are respectively given by

$$\gamma_v^{\mathrm{FD}} = \max_{e \in \phi_e} \left(\frac{X_e}{I_e^{d,d} + I_e^{u,d} + \sigma_e^2} \right) \tag{3.5}$$

and

$$\gamma_v^{\mathrm{FD}} = \sum_{e \in \phi_e} \left(\frac{X_e}{I_e^{d,d} + I_e^{u,d} + \sigma_e^2} \right) \tag{3.6}$$

where $X_e = p_d \|\boldsymbol{g}_{b,e} \boldsymbol{v}_{b,e}\|^2 r_{b,e}^{-\alpha}$ is the intended received signal (from the serving BS), $I_e^{d,d} = \sum_{l \in \phi_d} p_d \|\boldsymbol{g}_{l,e} \boldsymbol{V}_l\|^2 r_{l,e}^{-\alpha}$ is the inter-cell interference (from the transmitting BSs), $I_e^{u,d} = \sum_{k \in \phi_u} p_u \ |h_{k,e}|^2 r_{k,e}^{-\alpha}$ is the cross-mode interference (from the transmitting UEs), and σ_e^2 is the noise variance. The channel power gain distributions are given by $G_{b,e} = \|\boldsymbol{g}_{b,e} \boldsymbol{v}_{b,e}\|^2 \sim \mathscr{G}(1,1)$, $G_{l,e} = \|\boldsymbol{g}_{l,e} \boldsymbol{V}_l\|^2 \sim \mathscr{G}(K_d, 1)$, and $H_{k,e} = |h_{k,e}|^2 \sim \mathscr{G}(1,1)$.

The received SINR (considering FD BSs) in the UL at the most malicious

passive and colluding ED c are respectively given by

$$\gamma_c^{\mathrm{FD}} = \max_{e \in \phi_e} \left(\frac{X_e}{I_e^{u,u} + I_e^{d,u} + \sigma_e^2} \right) \tag{3.7}$$

and

$$\gamma_c^{\mathrm{FD}} = \sum_{e \in \phi_e} \left(\frac{X_e}{I_e^{u,u} + I_e^{d,u} + \sigma_e^2} \right) \tag{3.8}$$

where $X_e = p_u |h_{o,e}|^2 r_{o,e}^{-\alpha}$ is the intended received signal (from the reference UE), $I_e^{u,u} = \sum_{k \in \phi_u} p_u |h_{k,e}|^2 r_{k,e}^{-\alpha}$ is the inter-cell interference (from the transmitting UEs), $I_e^{d,u} = \sum_{l \in \phi_d} p_d \ \|\boldsymbol{g}_{l,e} \boldsymbol{V}_l\|^2 r_{l,e}^{-\alpha}$ is the cross-mode interference (from the transmitting BSs), and σ_e^2 is the noise variance. The channel power gain distributions are given by $H_{o,e} = |h_{o,e}|^2 \sim \mathscr{G}(1,1)$, $H_{k,e} = |h_{k,e}|^2 \sim \mathscr{G}(1,1)$, and $G_{l,e} = \|\boldsymbol{g}_{l,e} \boldsymbol{V}_l\|^2 \sim \mathscr{G}(K_d, 1)$.

Note that the EDs' SINR expressions in this work correspond to the case where the EDs have no information regarding the codebook of UEs and BSs. However, the analysis can be modified to capture other scenarios (e.g., by removing certain interference terms from the EDs' SINRs) [101].

3.2 Analysis

In this section, we study the PHYLS performance in FD small-cell networks under both scenarios of passive and colluding eavesdropping. Note that the ergodic rates (in b/s/Hz) of the reference DL and UL UEs, o and i, over two resource blocks, are given by $C_o^{\mathrm{FD}} = 2\mathbb{E}[\log_2(1+\gamma_o^{\mathrm{FD}})]$ and $C_i^{\mathrm{FD}} = 2\mathbb{E}[\log_2(1+\gamma_i^{\mathrm{FD}})]$ in FD mode, and $C_o^{\mathrm{HD}} = \mathbb{E}[\log_2(1+\gamma_o^{\mathrm{HD}})]$ and $C_i^{\mathrm{HD}} = \mathbb{E}[\log_2(1+\gamma_i^{\mathrm{HD}})]$ in HD mode, respectively. Similarly, the ergodic rates (in b/s/Hz) of the most malicious DL and UL EDs, v and c, over two resource blocks, are given by $C_v^{\mathrm{FD}} = 2\mathbb{E}[\log_2(1+\gamma_v^{\mathrm{FD}})]$ and $C_c^{\mathrm{FD}} = 2\mathbb{E}[\log_2(1+\gamma_c^{\mathrm{FD}})]$ in FD mode, and $C_v^{\mathrm{HD}} = \mathbb{E}[\log_2(1+\gamma_v^{\mathrm{HD}})]$ and $C_c^{\mathrm{HD}} = \mathbb{E}[\log_2(1+\gamma_c^{\mathrm{HD}})]$ in HD mode, respectively.

Remark 1. Note that through invoking the Jensen's inequality, $\mathbb{E}[\max(X,Y)\} \geq \max\{\mathbb{E}\{X\}, \mathbb{E}\{Y\}]$, the bounded DL and UL ergodic secrecy rates (considering FD

BSs) are respectively given by $S_o^{\mathrm{FD}} = [C_o^{\mathrm{FD}} - C_v^{\mathrm{FD}}]^+$ and $S_i^{\mathrm{FD}} = [C_i^{\mathrm{FD}} - C_c^{\mathrm{FD}}]^+$. Similarly, in the case of HD operation, the bounded DL and UL ergodic secrecy rates are respectively given by $S_o^{\mathrm{HD}} = [C_o^{\mathrm{HD}} - C_v^{\mathrm{HD}}]^+$ and $S_i^{\mathrm{HD}} = [C_i^{\mathrm{HD}} - C_c^{\mathrm{HD}}]^+$.

3.2.1 User Equipments

We proceed by deriving explicit expressions for the DL and UL UEs ergodic rates under linear ZF beamforming. Note that the DL MI is characterized considering the UEs may be capable of performing SIC. In order to capture performance for general cases, we consider an exclusion region of radius ε when modelling the UE-UE interference [102].

Theorem 1. The DL ergodic rates (in b/s/Hz) of the useful UE o in the FD and HD small-cell networks over two resource blocks are given by

$$C_o^{\mathrm{FD}} = \frac{4\pi\lambda_d}{\ln(2)} \int_0^{\infty} \int_0^{\infty} \frac{1}{1+\gamma} \left(\sum_{n=0}^{N_d-K_d} \left\{ \frac{(-s)^n}{n!} \frac{\mathrm{d}^n}{\mathrm{d}s^n} \exp\left(-s\sigma_o^2\right) \mathscr{L}_{I_o^{d,d}}[s] \mathscr{L}_{I_o^{u,d}}[s] \right\}_{s=\frac{\gamma r^\alpha}{p_d}} \right) \cdot \mathrm{d}\gamma r \exp\left(-\pi\lambda_d r^2\right) \mathrm{d}r \tag{3.9}$$

and

$$C_o^{\mathrm{HD}} = \frac{2\pi\lambda_d}{\ln(2)} \int_0^{\infty} \int_0^{\infty} \frac{1}{1+\gamma} \left(\sum_{n=0}^{N_d-K_d} \left\{ \frac{(-s)^n}{n!} \frac{\mathrm{d}^n}{\mathrm{d}s^n} \exp\left(-s\sigma_o^2\right) \mathscr{L}_{I_o^{d,d}}[s] \right\}_{s=\frac{\gamma r^\alpha}{p_d}} \right) \cdot \mathrm{d}\gamma r \exp\left(-\pi\lambda_d r^2\right) \mathrm{d}r \tag{3.10}$$

where

$$\mathscr{L}_{I_o^{d,d}}[s] = \exp\left(-\pi\lambda_d r^2 \left({}_2F_1\left(K_d, -\frac{2}{\alpha}; 1-\frac{2}{\alpha}; -\frac{sp_d}{r^\alpha} \right) - 1 \right) \right) \tag{3.11}$$

and

$$\mathscr{L}_{I_o^{u,d}}[s] = \exp\left(-\pi K_u \lambda_d \varepsilon^2 \left({}_2F_1\left(1, -\frac{2}{\alpha}; 1-\frac{2}{\alpha}; -\frac{sp_u}{\varepsilon^\alpha} \right) - 1 \right) \right). \tag{3.12}$$

Proof: See Appendix A.

Remark 2. The guard region radius ε in the MI expression in (3.12) can be set by design or through measurements based on the SIC capability at the UE side. In particular, $\varepsilon = 0$ corresponds to the worst-case without SIC capability.

Theorem 2. The UL ergodic rates (in b/s/Hz) of the useful UE i in the FD and HD small-cell networks over two resource blocks are given by

$$C_i^{\mathrm{FD}} = \frac{4\pi\lambda_d}{\ln(2)} \int_0^{\infty} \int_0^{\infty} \frac{1}{1+\gamma} \cdot \left(\sum_{n=0}^{N_u-K_u} \left\{ \frac{(-s)^n}{n!} \frac{\mathrm{d}^n}{\mathrm{d}s^n} \exp\left(-s\sigma_i^2\right) \mathscr{L}_{I_i^{u,u}}[s] \mathscr{L}_{I_i^{d,u}}[s] \mathscr{L}_{I_i^{i}}[s] \right\}_{s=\frac{\gamma r^{\alpha}}{p_u}} \right) \cdot \mathrm{d}\gamma r \exp\left(-\pi\lambda_d r^2\right) \mathrm{d}r \tag{3.13}$$

and

$$C_i^{\mathrm{HD}} = \frac{2\pi\lambda_d}{\ln(2)} \int_0^{\infty} \int_0^{\infty} \frac{1}{1+\gamma} \left(\sum_{n=0}^{N_u-K_u} \left\{ \frac{(-s)^n}{n!} \frac{\mathrm{d}^n}{\mathrm{d}s^n} \exp\left(-s\sigma_i^2\right) \mathscr{L}_{I_i^{u,u}}[s] \right\}_{s=\frac{\gamma r^{\alpha}}{p_u}} \right) \cdot \mathrm{d}\gamma r \exp\left(-\pi\lambda_d r^2\right) \mathrm{d}r \tag{3.14}$$

where

$$\mathscr{L}_{I_i^{u,u}}[s] = \exp\left(-\pi K_u \lambda_d r^2 \left({}_2F_1\left(1, -\frac{2}{\alpha}; 1-\frac{2}{\alpha}; -\frac{s p_u}{r^{\alpha}}\right) - 1 \right) \right) \tag{3.15}$$

and

$$\mathscr{L}_{I_i^{d,u}}[s] = \exp\left(-\pi\lambda_d \left(s p_d\right)^{\frac{2}{\alpha}} \frac{\Gamma\left(1-\frac{2}{\alpha}\right)\Gamma\left(K_d+\frac{2}{\alpha}\right)}{\Gamma(K_d)} \right) \tag{3.16}$$

and

$$\mathscr{L}_{I_i^{i}}[s] = \left(1 + s p_d \theta\right)^{-\kappa}. \tag{3.17}$$

Proof: See Appendix B.

Remark 3. The Rician fading distribution parameters μ and ν in the residual SI expression in (3.17) can be tuned by design or measurements to capture the SI

cancellation capability at the BS side. For example, $\nu = 0$ and $\mu = 0$ correspond to perfect SI removal and non NLOS SI, respectively.

Remark 4. The derivatives of the interfering terms LT functions required for the calculation of the ergodic rates in the *Theorems 1-2*, which arise as a result of multi-antenna communications, can be readily computed through applying the Faà di Bruno's formula [113].

3.2.2 Passive Eavesdroppers

Next, we derive explicit expressions for the ergodic rates of the most malicious passive EDs in the DL and UL. Note that in this case the EDs act independently (do not exchange information).

Theorem 3. The DL ergodic rates (in b/s/Hz) of the most malicious passive ED v in the FD and HD small-cell networks over two resource blocks are given by

$$C_v^{\mathrm{FD}} = \frac{2}{\ln(2)} \int_0^{\infty} \frac{1}{1+\gamma} \times \left(1 - \exp\left(-2\pi\lambda_e \int_0^{\infty} \left[\exp\left(-s\sigma_v^2\right) \mathscr{L}_{I_v^{d,d}}[s] \mathscr{L}_{I_v^{u,d}}[s]\right]_{s=\frac{\gamma_r \alpha}{p_d}} r \, \mathrm{d}r\right)\right) \mathrm{d}\gamma \quad (3.18)$$

and

$$C_v^{\mathrm{HD}} = \frac{1}{\ln(2)} \int_0^{\infty} \frac{1}{1+\gamma} \left(1 - \exp\left(-2\pi\lambda_e \int_0^{\infty} \left[\exp\left(-s\sigma_v^2\right) \mathscr{L}_{I_v^{d,d}}[s]\right]_{s=\frac{\gamma_r \alpha}{p_d}} r \, \mathrm{d}r\right)\right) \mathrm{d}\gamma \quad (3.19)$$

where

$$\mathscr{L}_{I_v^{d,d}}[s] = \exp\left(-\pi\lambda_d \left(s p_d\right)^{\frac{2}{\alpha}} \frac{\Gamma\left(1-\frac{2}{\alpha}\right)\Gamma\left(K_d+\frac{2}{\alpha}\right)}{\Gamma(K_d)}\right) \quad (3.20)$$

and

$$\mathscr{L}_{I_v^{u,d}}[s] = \exp\left(-\pi K_u \lambda_d \left(s p_u\right)^{\frac{2}{\alpha}} \Gamma\left(1-\frac{2}{\alpha}\right)\Gamma\left(1+\frac{2}{\alpha}\right)\right). \quad (3.21)$$

Proof: See Appendix C.

Theorem 4. The UL ergodic rates (in b/s/Hz) of the most malicious passive ED c in the FD and HD small-cell networks over two resource blocks are given by

$$C_c^{\mathrm{FD}} = \frac{2}{\ln(2)} \int_0^{\infty} \frac{1}{1+\gamma} \times \left(1 - \exp\left(-2\pi\lambda_e \int_0^{\infty} \left\{ \exp\left(-s\sigma_c^2\right) \mathscr{L}_{I_c^{u,u}}[s] \mathscr{L}_{I_c^{d,u}}[s] \right\}_{s=\frac{\gamma_r \alpha}{p_u}} r \, \mathrm{d}r \right)\right) \mathrm{d}\gamma \tag{3.22}$$

and

$$C_c^{\mathrm{HD}} = \frac{1}{\ln(2)} \int_0^{\infty} \frac{1}{1+\gamma} \left(1 - \exp\left(-2\pi\lambda_e \int_0^{\infty} \left\{ \exp\left(-s\sigma_c^2\right) \mathscr{L}_{I_c^{u,u}}[s] \right\}_{s=\frac{\gamma_r \alpha}{p_u}} r \, \mathrm{d}r \right)\right) \mathrm{d}\gamma \tag{3.23}$$

where

$$\mathscr{L}_{I_c^{u,u}}[s] = \exp\left(-\pi K_u \lambda_d \left(s p_u\right)^{\frac{2}{\alpha}} \Gamma\left(1 - \frac{2}{\alpha}\right) \Gamma\left(1 + \frac{2}{\alpha}\right)\right) \tag{3.24}$$

and

$$\mathscr{L}_{I_c^{d,u}}[s] = \exp\left(-\pi \lambda_d \left(s p_d\right)^{\frac{2}{\alpha}} \frac{\Gamma\left(1 - \frac{2}{\alpha}\right) \Gamma\left(K_d + \frac{2}{\alpha}\right)}{\Gamma(K_d)}\right). \tag{3.25}$$

Proof: See Appendix D.

3.2.3 Colluding Eavesdroppers

The ergodic rates of the most malicious colluding EDs in the DL and UL are derived next. The cooperating EDs in this case form a distributed antenna system [108,109]. Note that most previous studies of randomly-located colluding EDs such as [66] are carried out for single-cell HD systems, where the EDs do not experience any interference. In the case of multi-cell FD systems with randomly-located colluding EDs, the analysis becomes significantly more challenging as one needs to account for the impact of MI in both the DL and the UL.

Theorem 5. The bounded DL ergodic rates (in b/s/Hz) of the most malicious

colluding ED v in the FD and HD small-cell networks over two resource blocks are given by

$$C_v^{\mathrm{FD}} \leq \frac{4\pi\lambda_e p_d}{\ln(2)\gamma(1+\gamma)} \int_0^{\infty} \int_{r_0}^{\infty} r^{1-\alpha} \int_0^{\infty} \exp\left(-s\sigma_v^2\right) \mathscr{L}_{I_v^{d,d}}[s] \mathscr{L}_{I_v^{u,d}}[s] \, \mathrm{d}s \, \mathrm{d}r \, \mathrm{d}\gamma \tag{3.26}$$

and

$$C_v^{\mathrm{HD}} \leq \frac{2\pi\lambda_e p_d}{\ln(2)\gamma(1+\gamma)} \int_0^{\infty} \int_{r_0}^{\infty} r^{1-\alpha} \int_0^{\infty} \exp\left(-s\sigma_v^2\right) \mathscr{L}_{I_v^{d,d}}[s] \, \mathrm{d}s \, \mathrm{d}r \, \mathrm{d}\gamma. \tag{3.27}$$

Proof: See Appendix E.

Theorem 6. The bounded UL ergodic rates (in b/s/Hz) of the most malicious colluding ED c in the FD and HD small-cell networks over two resource blocks are given by

$$C_c^{\mathrm{FD}} \leq \frac{4\pi\lambda_e p_u}{\ln(2)\gamma(1+\gamma)} \int_0^{\infty} \int_{r_0}^{\infty} r^{1-\alpha} \int_0^{\infty} \exp\left(-s\sigma_c^2\right) \mathscr{L}_{I_c^{u,u}}[s] \mathscr{L}_{I_c^{d,u}}[s] \, \mathrm{d}s \, \mathrm{d}r \, \mathrm{d}\gamma \tag{3.28}$$

and

$$C_c^{\mathrm{HD}} \leq \frac{2\pi\lambda_e p_u}{\ln(2)\gamma(1+\gamma)} \int_0^{\infty} \int_{r_0}^{\infty} r^{1-\alpha} \int_0^{\infty} \exp\left(-s\sigma_c^2\right) \mathscr{L}_{I_c^{u,u}}[s] \, \mathrm{d}s \, \mathrm{d}r \, \mathrm{d}\gamma. \tag{3.29}$$

Proof: The proof follows from a similar approach to that in Appendix E.

Remark 5. The parameter r_0 in the colluding EDs ergodic rate expressions from *Theorems 5-6* represents the guard region distance required to satisfy the secrecy non-outage condition.

The expressions developed in *Theorems 1-6* can be readily used to obtain the different SEs required in the calculation of the PHYLS performance via two-fold integral computations. This is in line with the state-of-the-art results on stochastic

geometry-based SE analysis of large-scale wireless networks in the literature [101]. Although there is no well-known method to simplify these SE expressions further, the proposed theoretical framework provides significant advantages in terms of computational complexity versus the MC simulations.

It should be noted that the results from chapter can be viewed as an extension of the previous chapter in that we have added MIMO capability and colluding scenarios in the analysis. By setting the number of BS antennas to one, the results would be the extension of the previous chapter covering both passive and colluding eavesdropping cases.

3.3 Numerical Results

In this part we investigate the PHYLS performance of FD and its HD counterpart in presence of both colluding and non-colluding EDs. The spatial density of the small-cell BSs is set to be $\lambda^{(d)} = \frac{4}{\pi}$ per km^2. The (per-user) BS and UE transmit powers are kept fixed at $p_d = 23$ dBm and $p_u = 20$ dBm, respectively. The noise spectral density at all receivers is -170 dBm/Hz and the total system bandwidth is $W = 10$ MHz. The MC simulations are obtained from 20 k trials in a circular region of radius 10 km.

The results are taken over two resource blocks. In the FD small-cell network, the DL and UL run simultaneously, whereas in the HD small-cell network, the DL and UL occur over different resource blocks. Furthermore, in the FD system, we take into account different interference cancellation schemes. In particular, in the DL, we consider the cases with and without SIC capability at the UE side. Moreover, in the UL, we capture the performance under different perfect SI cancellation and NLOS residual SI with a variance of -55 dB [5].

3.3.1 Impact of the Number of Base Station Antennas

3.3.1.1 Passive Eavesdroppers

We study the impact of the number of small-cell BS transmit and receive antennas on the small-cell network DL and UL PHYLS performance under a Poisson field of passive EDs in Fig. 3.1. It can be observed that in all cases, the ergodic secrecy

rate always increases in the number of antennas. This is due to the improved array gain from multi-antenna communications, and hence, stronger useful signal power, whilst the interference level remains the same. Furthermore, the FD over HD small-cell network PHYLS performance gain always increases in the number of antennas. In point of fact, even with SIC capability and perfect SI suppression, only negligible FD versus HD improvements in ergodic secrecy performance can be achieved when the small-cell BSs are equipped with a few antennas. This trend highlights the essential role of MIMO in harnessing the full potential of FD technology through enhancing the system robustness against the increased interference level versus that in the HD operation [114, 115].

The presence of significant residual SI (e.g., variance > -30 dB), would typically result in secrecy outage (even when the number of antennas is relatively large). The current SI cancellation capabilities can achieve orders of magnitude greater cancellation (e.g., in the range $60 - 100$ dB [12]), hence, the FD operation is certainly feasible. It is important to note that in such cases the impact of residual SI becomes negligible compared to the MI [17], [107]. It may be useful to note that to achieve higher FD versus HD PHYLS performance gains in the UL, the transmit power of the small-cell BSs should be reduced. It can be observed that the MC simulations confirm the validity of our theoretical findings in *Theorems 1-4*.

3.3.1.2 Colluding Eavesdroppers

Next, the impact of the number of small-cell BS transmit and receive antennas on the small-cell network DL and UL PHYLS performance under a Poisson field of colluding EDs is depicted in Fig. 3.2. Similar to the case of passive EDs, increasing the number of antennas always results in higher ergodic secrecy rates, as well as greater FD versus HD PHYLS performance gains. Furthermore, our findings indicate that the relative FD versus HD ergodic secrecy rate gain can be considerably higher in the case of colluding EDs. The reason is because each cooperative ED experiences added interference (i.e., MI) in the case of FD operation which in turn degrades the colluding EDs' combined SINR.

It is important to note that the case of collusion represents the absolute worst-

case scenario in terms of PHYLS performance. As a result, unless the EDs' spatial density is set to very small values (relative to the BS deployment density), the small-cell network experiences secrecy outage with high probability. It is important to note that the MC results from Fig. 3.2 confirm the validity of our theoretical findings in *Theorems 1-2* and *Theorems 5-6*.

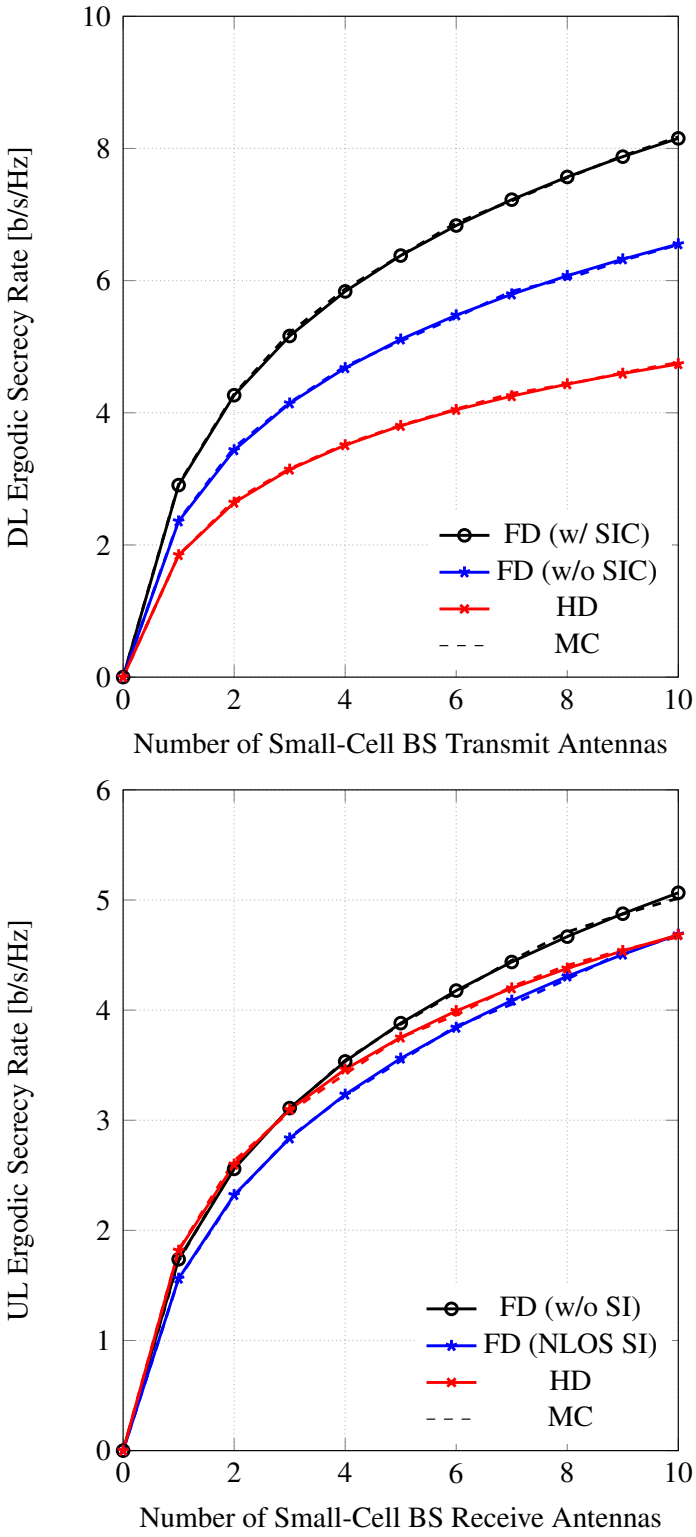

Figure 3.1: Impact of the number of BS transmit/receive antennas on the small-cell network PHY-layer security performance in the presence of a Poisson field of passive EDs. System parameters are: $\lambda_d = \frac{4}{\pi}$ km^{-2}, $\lambda_u = K_u \lambda_d$ km^{-2}, $\lambda_e = \frac{\lambda_d}{10}$ km^{-2}, $K_d = K_u = 1$, $p_d = 23$ dBm, $p_u = 20$ dBm, $W = 10$ MHz, $\sigma_o^2 = \sigma_v^2 = \sigma_i^2 = \sigma_c^2 = -170$ dBm/Hz, $\alpha = 4$.

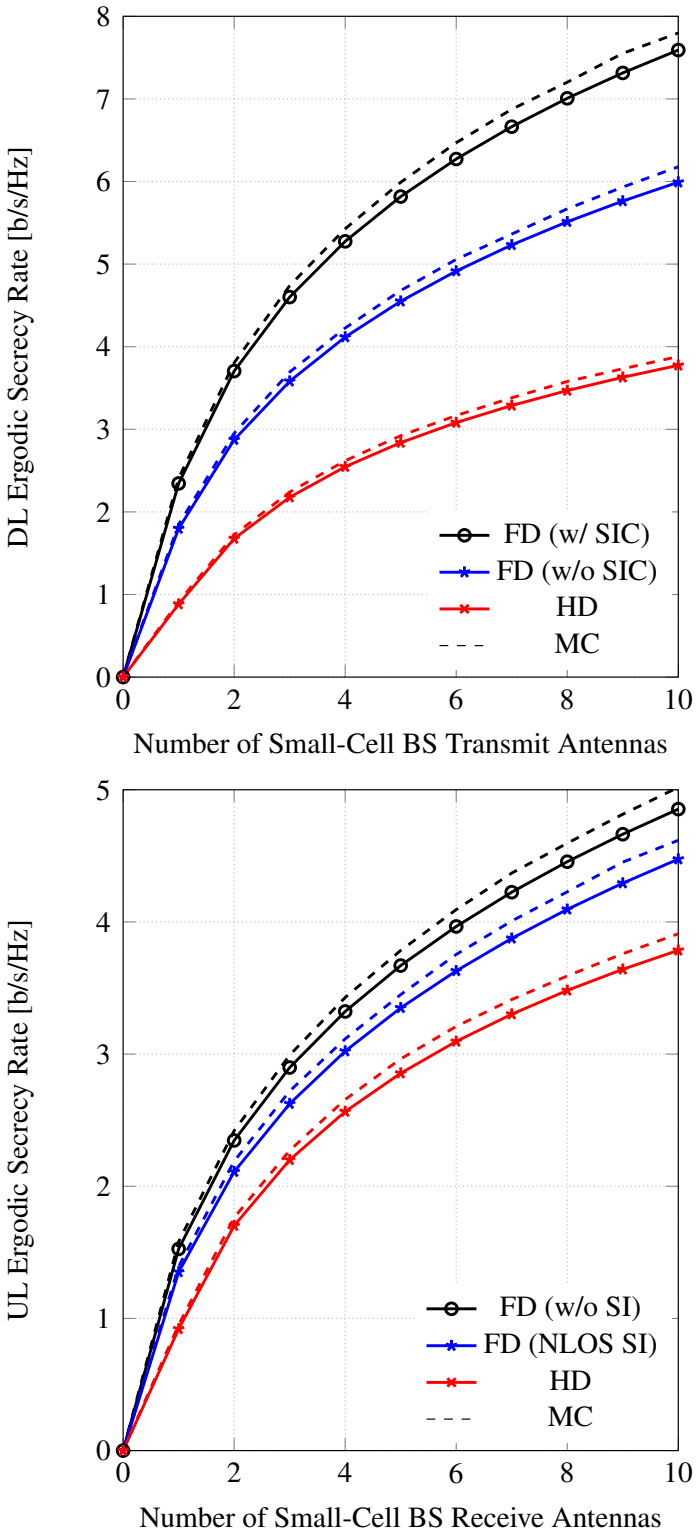

Figure 3.2: Impact of the number of BS transmit/receive antennas on the small-cell network PHY-layer security performance under a Poisson field of colluding EDs. System parameters are: $\lambda_d = \frac{4}{\pi}$ km^{-2}, $\lambda_u = K_u\lambda_d$ km^{-2}, $\lambda_e = \frac{\lambda_d}{200}$ km^{-2}, $r_0 = \frac{1}{2}$ km, $K_d = K_u = 1$, $p_d = 23$ dBm, $p_u = 20$ dBm, $W = 10$ MHz, $\sigma_o^2 = \sigma_v^2 = \sigma_i^2 = \sigma_c^2 = -170$ dBm/Hz, $\alpha = 4$.

3.3.2 Impact of the Number of Users

3.3.2.1 Passive Eavesdropping

We investigate the impact of the number of users served per resource block on the small-cell network DL and UL PHYLS performances under a Poisson field of passive EDs in Fig. 3.3. The results indicate that the per-user ergodic secrecy rate performance in all systems always decreases in the number of UEs served per cell. On the other hand, it should be noted that the corresponding ergodic area secrecy rate (e.g., $\lambda_d K_d S_o$ (b/s/Hz/km^2), in the DL) increases with higher number of users served per resource block. The reason is that with greater K_d and K_d, respectively, the DL and UL array gains are decreased due to the linear ZF beamforming. In addition, increasing K_d and K_u results in higher MI in the UL and DL, respectively. As a result, it can be inferred that the FD versus HD small-cell network PHYLS performance gain decreases as we increase the number of DL and UL UEs served per cell. Intuitively, if we keep K_u fixed, increasing K_d results in higher FD versus HD DL ergodic area secrecy rate (and vice versa). In addition, it should be noted that the importance of effective interference cancellation is heightened in the case of FD small-cell BSs serving more UEs, such to avoid secrecy outage scenarios.

3.3.2.2 Colluding Eavesdropping

In Fig. 3.4, we study the effect of the number of users served per resource block on the small-cell network DL and UL PHYLS performances under a Poisson field of colluding EDs. The trends previously highlighted in the case of passive PPP-based EDs also apply here. In particular, increasing the number of UEs served per cell deceases the per-user ergodic secrecy rate and increases the area ergodic secrecy rate, respectively. Also, in the case of large-scale ED collusion, the FD over HD small-cell network PHYLS performance gain decreases if we simultaneously increase the number of DL and UL UEs served per cell. On the other hand, for a given number of UL UEs in a cell, increasing the number of DL UEs served per resource block results in higher relative FD versus HD DL ergodic secrecy rate (and vice versa).

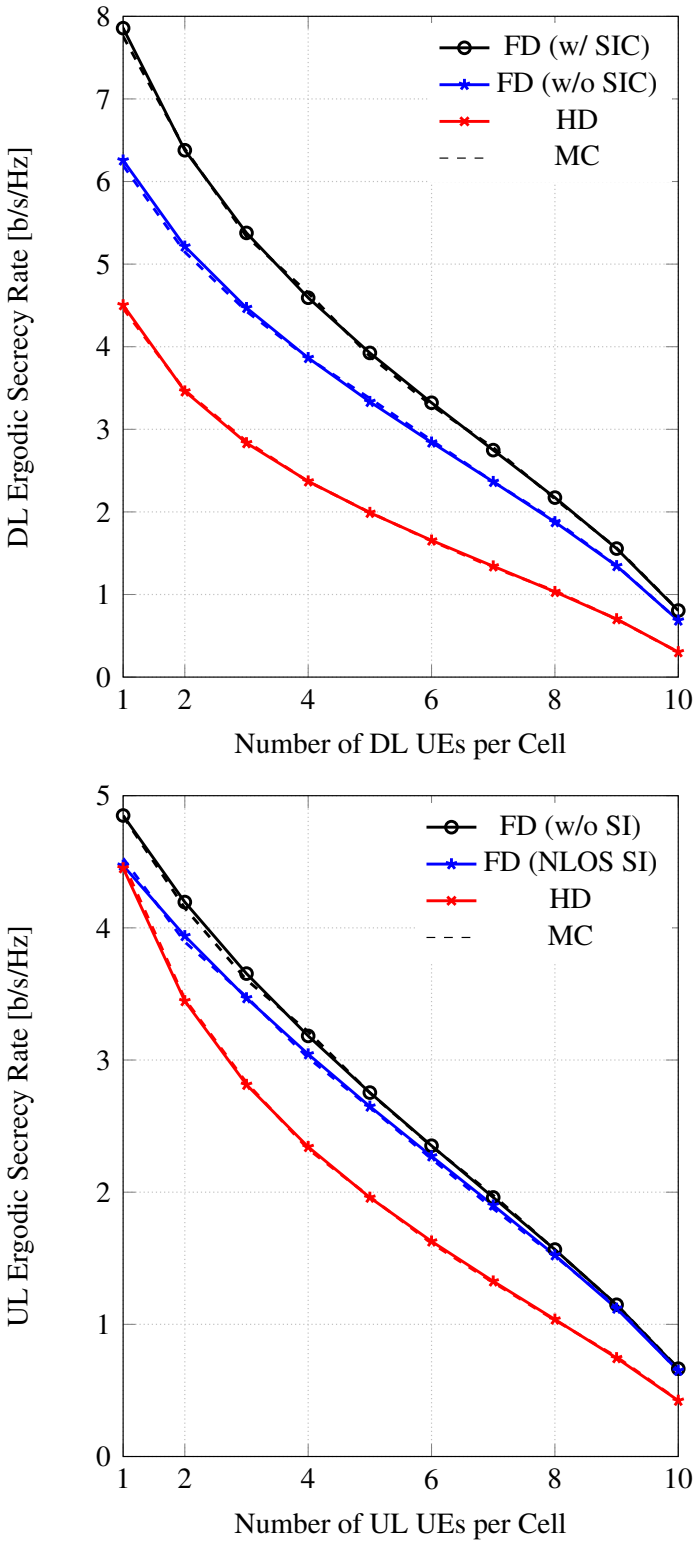

Figure 3.3: Impact of the number of UEs on the small-cell network PHY-layer security performance in the presence of a Poisson field of passive EDs. System parameters are: $\lambda_d = \frac{4}{\pi}$ km^{-2}, $\lambda_u = K_u\lambda_d$ km^{-2}, $\lambda_e = \frac{\lambda_d}{5}$ km^{-2}, $N_d = N_u = 10$, $p_d = 23$ dBm, $p_u = 20$ dBm, $W = 10$ MHz, $\sigma_o^2 = \sigma_v^2 = \sigma_i^2 = \sigma_c^2 = -170$ dBm/Hz, $\alpha = 4$.

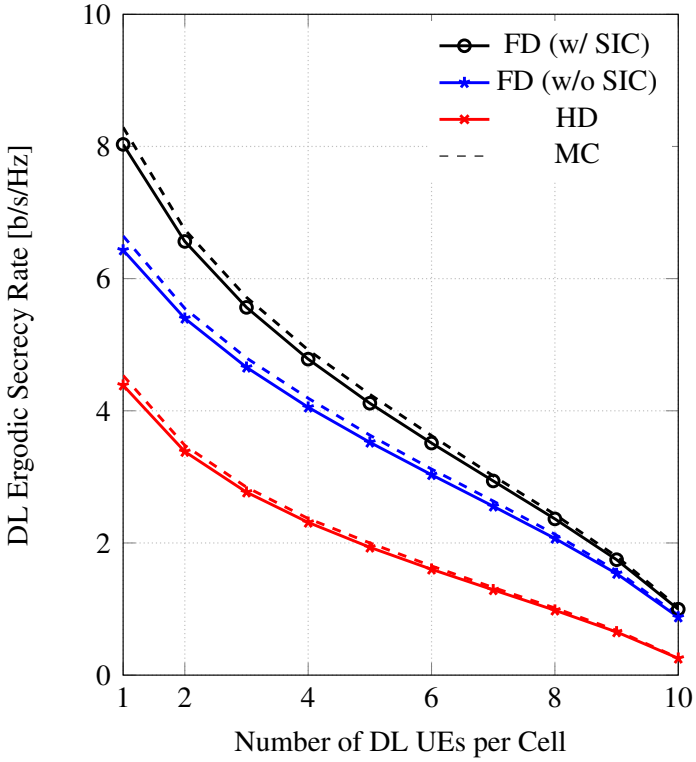

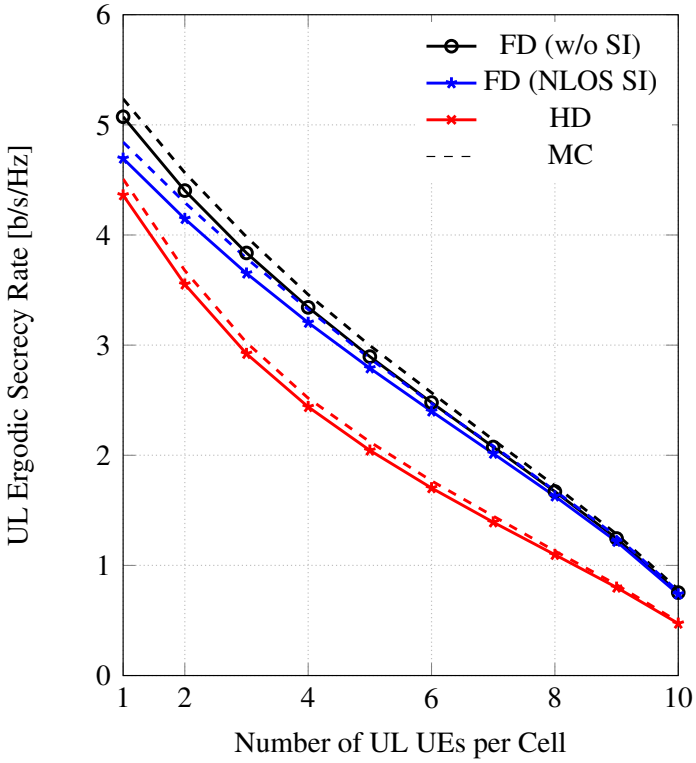

Figure 3.4: Impact of the number of UEs on the small-cell network PHY-layer security performance in the presence of a Poisson field of colluding EDs. System parameters are: $\lambda_d = \frac{4}{\pi}$ km^{-2}, $\lambda_u = K_u\lambda_d$ km^{-2}, $\lambda_e = \frac{\lambda_d}{400}$ km^{-2}, $r_0 = \frac{1}{2}$ km, $N_d = N_u = 10$, $p_d = 23$ dBm, $p_u = 20$ dBm, $W = 10$ MHz, $\sigma_o^2 = \sigma_v^2 = \sigma_i^2 = \sigma_c^2 = -170$ dBm/Hz, $\alpha = 4$.

3.3.3 Impact of the Eavesdroppers' Density

3.3.3.1 Passive Eavesdroppers

Next, we proceed by investigating the impact of the EDs' spatial density on the small-cell network DL and UL PHYLS performances under a PPP-based abstraction model of passive EDs in Fig. 3.5. As expected, it can be observed that the ergodic secrecy rate decreases in all cases in the ratio of ED over BS deployment densities. Moreover, increasing the spatial density of the EDs enhances the FD versus HD small-cell network PHYLS performance gain. This is because while the stronger ED channel capacity degrades the ergodic secrecy rate values, the respective rate of decrease in the PHYLS performance is higher in HD versus FD small-cell networks as a result of the extra interference experienced by the EDs in the latter system. As previously highlighted, the relative FD versus HD UL ergodic secrecy gain can be increased through reducing the transmit power of the small-cell BSs.

3.3.3.2 Colluding Eavesdroppers

Finally, the effect of EDs' spatial density on the small-cell network PHYLS performance in the presence of a Poisson field of colluding EDs is depicted in Fig. 3.6. We can observe similar trends to those highlighted in the case of passive EDs. In particular, the PHYLS performance benefits in all cases from smaller ED PPP-based deployment density. Moreover, the underlying FD versus HD gains in terms of ergodic secrecy rate increases with larger values of λ_e up to the point in which the system experiences secrecy outage. In addition, as previously highlighted, the UL PHYLS performance in the FD small-cell network is particularly susceptible to interference. Hence, enabling multi-antenna communications and interference cancellation capabilities is essential towards avoiding secrecy outage scenarios in the UL.

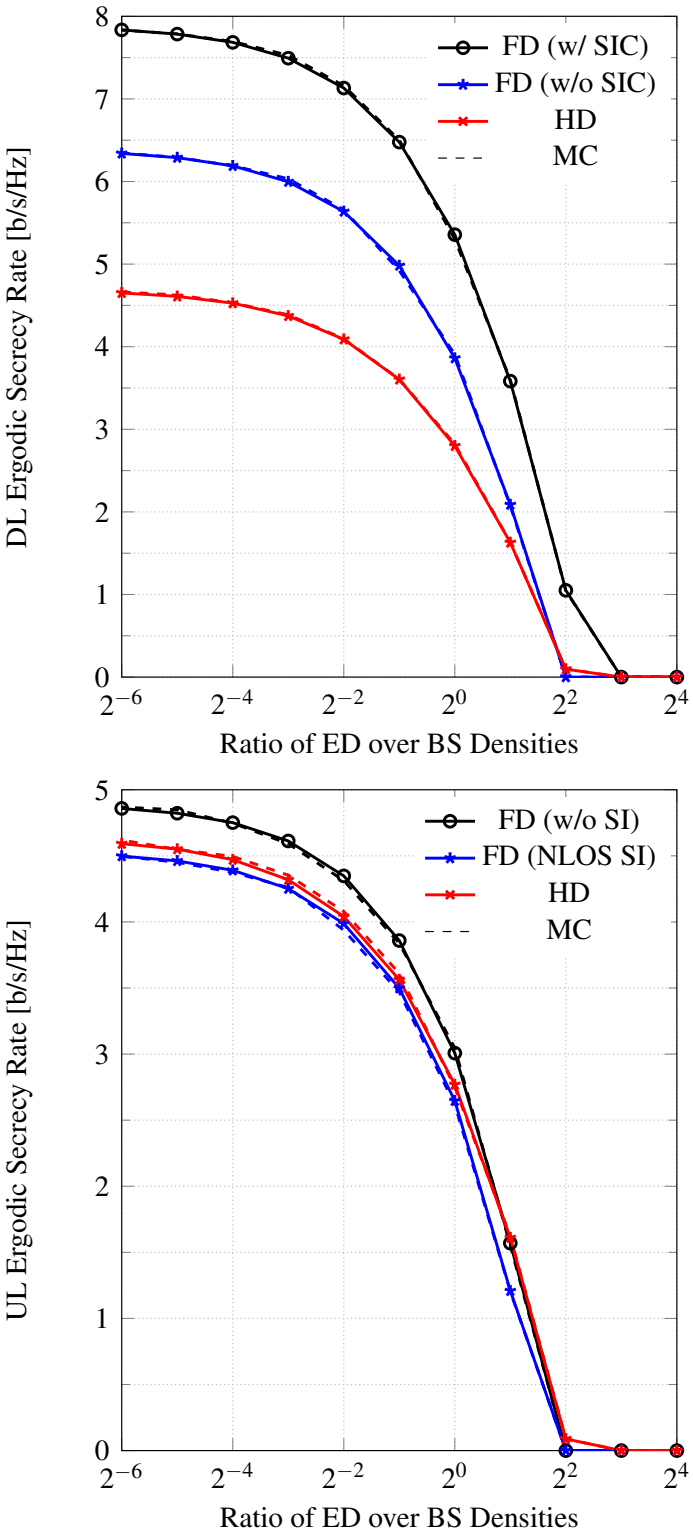

Figure 3.5: Impact of different passive EDs' spatial densities on the small-cell network PHY-layer security performance. System parameters are: $\lambda_d = \frac{4}{\pi}$ km^{-2}, $\lambda_u = K_u\lambda_d$ km^{-2}, $N_d = N_u = 8$, $K_d = K_u = 1$, $p_d = 23$ dBm, $p_u = 20$ dBm, $W = 10$ MHz, $\sigma_o^2 = \sigma_v^2 = \sigma_i^2 = \sigma_c^2 = -170$ dBm/Hz, $\alpha = 4$.

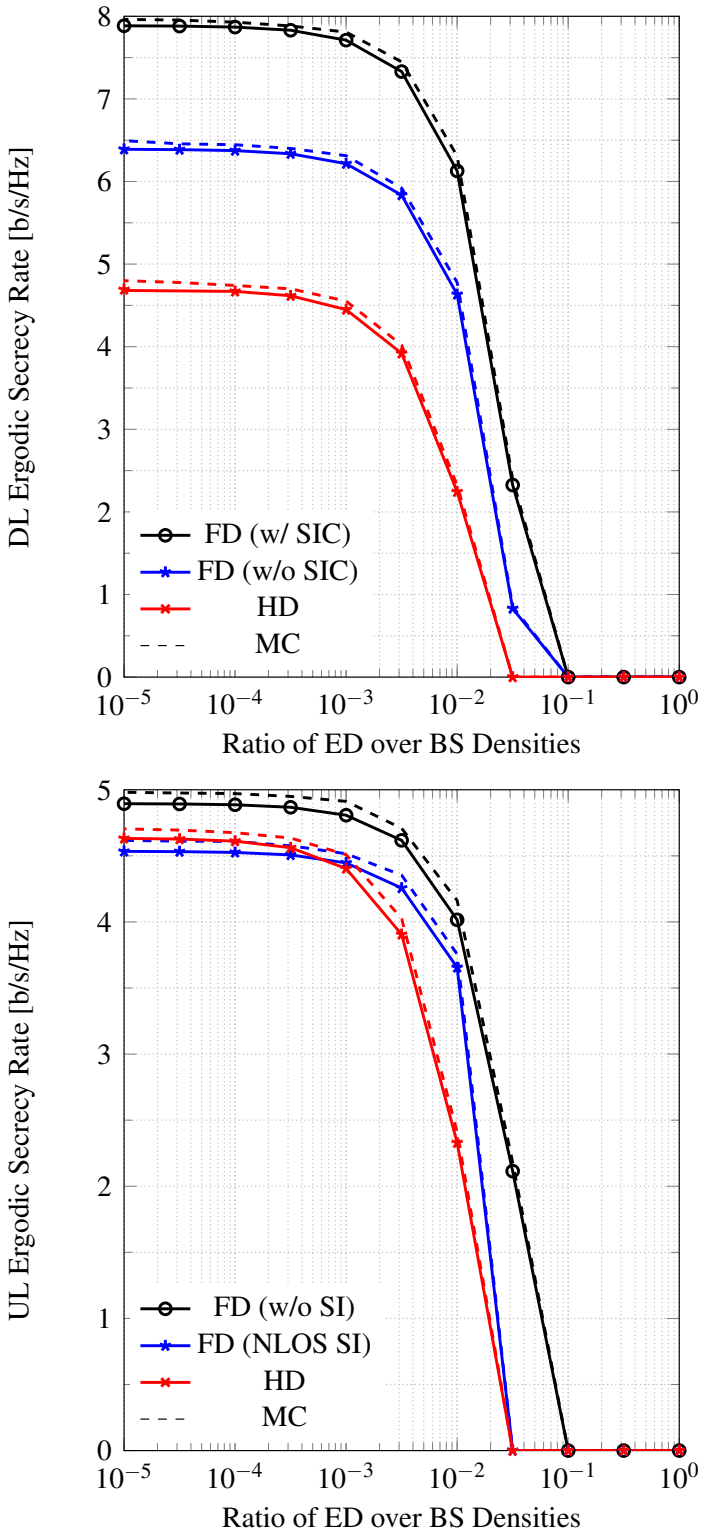

Figure 3.6: Impact of different colluding EDs' spatial densities on the small-cell network PHY-layer security performance. System parameters are: $\lambda_d = \frac{4}{\pi}$ km^{-2}, $\lambda_u = K_u \lambda_d$ km^{-2}, $r_0 = \frac{1}{2}$ km, $N_d = N_u = 8$, $K_d = K_u = 1$, $p_d = 23$ dBm, $p_u = 20$ dBm, $W = 10$ MHz, $\sigma_o^2 = \sigma_v^2 = \sigma_i^2 = \sigma_c^2 = -170$ dBm/Hz, $\alpha = 4$.

In Fig. 3.1 - Fig. 3.6, it is important note that in our defined system model, we consider the optimum scenario for EDs (the aggregation of all of their signals perfectly) which means the affect of colluding EDs on ergodic secrecy rate is much more significant than the case of passive EDs.

3.4 Conclusions

In this chapter we provided a stochastic geometry-based framework for the study of PHYLS performance in multi-cell FD small-cell networks. Similar to the previous chapter, the locations of the BSs, equipped with multiple antennas, and UEs were captured using the PPP-based abstraction model. The small-cell network was considered to be overlaid with a Poisson field of EDs, with both scenarios of independent as well as cooperative eavesdropping under consideration. By leveraging on the tools from applied probability theory, we derived explicit expressions for the ergodic secrecy rates with closed-form LT functions for the useful and interference signals statistics. With the aid of the proposed analytical model, and MC simulations, we drew network design insights concerning the ergodic secrecy rate performance. In particular, the findings highlighted that significant improvements in PHYLS performance can be attained by enabling FD functionality at the BS side, particularly, in conjunction with multi-antenna communications and interference cancellation schemes. In the next chapter by means of curve-fitting techniques, we derive closed-form expressions in certain cases of interest for special cases of interests.

The work presented in this chapter can be extended in a number of ways. One promising approach is to look at non-linear MIMO schemes beyond zero-forcing such to improve the ergodic secrecy rates of the full-duplex small-cell deployments. Power allocation and user selection are also interesting areas which can be looked at and exploited towards improving upon the results of this chapter.

Chapter 4

Explicit Expressions of Key Performance Indicators using Machine Learning

It can be readily observed that the expressions of the key performance indicators developed in the previous chapters do not admit closed-forms for general settings of system parameters. These semi-analytic expressions are fundamentally important for radio design and deployment as they make it possible to generate results and draw insights within a matter of minutes. Without these, one has to resort to the significantly more computationally-complex system-level simulations which depending on the choice of system parameters may require running times of several weeks or more. On the other hand, there is value in achieving explicit closed-form expressions for the sake of accessibility making it easier to generate results and identify the performance trends.

In what follows, we set out to generate explicit closed-form expressions of the key performance indicators using tools from machine learning. Specifically, we apply supervised learning-based non-linear curve-fitting techniques to large sets of (exact) theoretical data in order to obtain some explicit closed-form approximations for the different ergodic rates and ergodic secrecy rates under consideration. We accordingly provide goodness of fit measurements in terms of R-Squared (R^2) and estimated variance (Var). The validity of the developed closed-form formulas will

be assessed by direct comparison against the empirical data.

4.1 Special cases for BSs with MIMO

The following results are obtained for the special case where each multi-antenna small-cell BS serves a single UE per resource block in each DL/UL direction. This assumption is made for the sake of simplifying the non-linear curve-fitting operation. Towards the end of this chapter, we elaborate on the exact reasoning and challenges concerned with deriving similar results for the case of multi-user MIMO. However, it should be noted that the single-user MIMO transmission technology is widely employed for FD small-cell BS deployment in the literature [17]. In fact, most state-of-the-art massive MIMO panels in current 5G deployments provide single-user beamforming only. Further, the results are obtained for interference-limited environments, an assumption that closely captures the real-world propagation environments for small-cell deployments.

Corollary 1. Consider the special case with $N_d = N_u = N$, $K_d = K_u = 1$, $p_d = p_u$, $\alpha = 4$, $\sigma_d^2 = \sigma_u^2 = 0$. The DL ergodic rates (in b/s/Hz) of the useful UE o in the FD (with different SIC capabilities) and HD small-cell networks over two resource blocks are approximated by

$$C_o^{\mathrm{FD}} \approx 2.78\log(1+1.55N), \quad (\text{w/ SIC}, R^2 \approx 0.\dot{9}, \text{Var} \approx 2.00\times10^{-3}) \tag{4.1}$$

$$C_o^{\mathrm{FD}} \approx 2.33\log(1+1.3N), \quad (\text{w/o SIC}, R^2 \approx 0.\dot{9}, \text{Var} \approx 6.41\times10^{-3}) \tag{4.2}$$

$$C_o^{\mathrm{HD}} \approx 1.43\log(1+3.4N), \quad (R^2 \approx 0.\dot{9}, \text{Var} \approx 2.65\times10^{-4}). \tag{4.3}$$

Remark 1. The results from *Corollary 1* indicate that a significant gain in the FD DL ergodic rate can be achieved through reducing the MI level using SIC.

Corollary 2. Consider the special case with $N_d = N_u = N$, $K_d = K_u = 1$, $p_d = p_u$, $\alpha = 4$, $\sigma_d^2 = \sigma_u^2 = 0$. The UL ergodic rates (in b/s/Hz) of the useful UE i in the FD (with different residual SI) and HD small-cell networks over two resource blocks are approximated by

$$C_i^{\mathrm{FD}} \approx 2.33\log(1+1.3N), \quad (\text{w/o SI}, R^2 \approx 0.\dot{9}, \text{Var} \approx 6.41\times10^{-3}) \tag{4.4}$$

$$C_i^{\mathrm{FD}} \approx 2.31\log(1+1.3N), \quad (\text{w/ NLOS SI}, R^2 \approx 0.\dot{9}, \text{Var} \approx 6.59\times10^{-3}) \quad (4.5)$$

$$C_i^{\mathrm{HD}} \approx 1.43\log(1+3.4N), \quad (R^2 \approx 0.\dot{9}, \text{Var} \approx 2.65\times10^{-4}). \quad (4.6)$$

Remark 2. We observe based on the results from *Corollary 2* that the FD UL ergodic rate performance is largely limited by the MI as there is only a small difference in performance between the different perfect SI cancellation and NLOS SI cases.

Corollary 3. Consider the special case with $N_d = N_u = N$, $K_d = K_u = 1$, $p_d = p_u$, $\alpha = 4$, $\sigma_d^2 = \sigma_u^2 = 0$. The DL ergodic rates (in b/s/Hz) of the most malicious passive ED v and UL ergodic rates (in b/s/HZ) of the most malicious passive ED c in the FD and HD small-cell networks over two resource blocks are approximated by

$$C_v^{\mathrm{FD}} = C_c^{\mathrm{FD}} \approx 5\log(1+0.55\lambda_e), \quad (R^2 \approx 0.\dot{9},\ \text{variance} \approx 5.31\times10^{-5}) \quad (4.7)$$

$$C_v^{\mathrm{HD}} = C_c^{\mathrm{HD}} \approx 3\log(1+0.9\lambda_e), \quad (R^2 \approx 0.\dot{9},\ \text{variance} \approx 2.85\times10^{-5}). \quad (4.8)$$

Remark 3. The results from *Corollary 3* indicate that in the case of passive EDs, the ergodic rate of the most malicious ED increases only logarithmically in the EDs' spatial density.

Corollary 4. Consider the special case with $K_d = K_u = 1$, $p_d = p_u$, $\alpha = 4$, $\sigma_d^2 = \sigma_u^2 = 0$. The DL ergodic rates (in b/s/Hz) of the most malicious colluding ED v and the UL ergodic rates (in b/s/HZ) of the most malicious colluding ED c in the FD and HD small-cell networks over two resource blocks are approximated by

$$C_v^{\mathrm{FD}} = C_c^{\mathrm{FD}} \approx 42\frac{\lambda_e}{r_0^2}, \quad (R^2 \approx 0.\dot{9},\ \text{variance} \approx 7.40\times10^{-4}) \quad (4.9)$$

$$C_v^{\mathrm{HD}} = C_c^{\mathrm{HD}} \approx 84\frac{\lambda_e}{r_0^2}, \quad (R^2 \approx 0.\dot{9},\ \text{variance} \approx 2.70\times10^{-4}). \quad (4.10)$$

Remark 4. We observe based on the results from *Corollary 4.* that in the case of colluding EDs, the ergodic rate of the most malicious colluding ED increases linearly in the EDs' spatial density.

Note that the logarithmic versus linear behaviour of the most malicious ED ergodic rate in the EDs' spatial density under passive (Remark 3) and colluding (Remark 4) eavesdropping can be attributed to their corresponding SINR formulation (i.e., $\max(.)$ versus $\sum(.)$ functions).

Corollary 5. Consider the special case with $N_d = N_u = N$, $K_d = K_u = 1$, $p_d = p_u$, $\alpha = 4$, $\sigma_d^2 = \sigma_u^2 = 0$. The DL ergodic secrecy rate (in b/s/Hz) of the useful UE o with respect to the most malicious passive ED v in the FD (with different SIC capabilities) and HD small-cell networks over two resource blocks are approximated by

$$S_o^{\mathrm{FD}} = [2.55\log(1+2N) - 2.1\lambda_e]^+, \quad (\text{w/ SIC}, R^2 \approx 0.9\dot{9}, \text{Var} \approx 1.40\times 10^{-2}) \tag{4.11}$$

$$S_o^{\mathrm{FD}} = [2\log(1+2N) - 2.1\lambda_e]^+, \quad (\text{w/o SIC}, R^2 \approx 0.9\dot{9}, \text{Var} \approx 1.47\times 10^{-2}) \tag{4.12}$$

$$S_o^{\mathrm{HD}} = [1.4\log(1+3.6N) - 2.1\lambda_e]^+, \quad (R^2 \approx 0.9\dot{9}, \text{Var} \approx 1.16\times 10^{-2}). \tag{4.13}$$

Corollary 6. Consider the special case with $N_d = N_u = N$, $K_d = K_u = 1$, $p_d = p_u$, $\alpha = 4$, $\sigma_d^2 = \sigma_u^2 = 0$. The UL ergodic secrecy rate (in b/s/Hz) of the useful UE i with respect to the most malicious passive ED c in the FD (with different residual SI) and HD small-cell networks over two resource blocks are approximated by

$$S_i^{\mathrm{FD}} = [2\log(1+2N) - 2.1\lambda_e]^+, \quad (\text{w/o SI}, R^2 \approx 0.9\dot{9}, \text{Var} \approx 1.34\times 10^{-2}) \tag{4.14}$$

$$S_i^{\mathrm{FD}} = [1.94\log(1+2.2N) - 2.1\lambda_e]^+, (\text{w/ NLOS SI}, R^2 \approx 0.9\dot{9}, \text{Var} \approx 1.47\times 10^{-2}) \tag{4.15}$$

$$S_i^{\mathrm{HD}} = [1.4\log(1+3.6N) - 2.1\lambda_e]^+, \quad (R^2 \approx 0.9\dot{9}, \text{Var} \approx 1.16\times 10^{-2}). \tag{4.16}$$

Corollary 7. Consider the special case with $N_d = N_u = N$, $K_d = K_u = 1$, $p_d = p_u$, $\alpha = 4$, $\sigma_d^2 = \sigma_u^2 = 0$. The DL ergodic secrecy rate (in b/s/Hz) of the useful UE o with respect to the most malicious colluding ED v in the FD (with different SIC capabilities) and HD small-cell networks over two resource blocks are

approximated by

$$S_o^{\mathrm{FD}} = \left[2.5\log\left(1+2.2N\right) - 42\frac{\lambda_e}{r_0^2}\right]^+, \quad (\text{w/ SIC}, R^2 \approx 0.\dot{9}, \text{Var} \approx 6.40\times 10^{-2}) \tag{4.17}$$

$$S_o^{\mathrm{FD}} = \left[1.9\log\left(1+2.5N\right) - 42\frac{\lambda_e}{r_0^2}\right]^+, \quad (\text{w/o SIC}, R^2 \approx 0.\dot{9}, \text{Var} \approx 6.41\times 10^{-2}) \tag{4.18}$$

$$S_o^{\mathrm{HD}} = \left[1.4\log(1+3.6N) - 84\frac{\lambda_e}{r_0^2}\right]^+, \quad (R^2 \approx 0.\dot{9}, \text{Var} \approx 8.25\times 10^{-2}). \tag{4.19}$$

Corollary 8. Consider the special case with $N_d = N_u = N$, $K_d = K_u = 1$, $p_d = p_u$, $\alpha = 4$, $\sigma_d^2 = \sigma_u^2 = 0$. The UL ergodic secrecy rate (in b/s/Hz) of the useful UE i with respect to the most malicious colluding ED c in the FD (with different residual SI) and HD small-cell networks over two resource blocks are approximated by

$$S_i^{\mathrm{FD}} = \left[1.9\log\left(1+2.5N\right) - 42\frac{\lambda_e}{r_0^2}\right]^+, \quad (\text{w/o SI}, R^2 \approx 0.\dot{9}, \text{Var} \approx 6.41\times 10^{-2}) \tag{4.20}$$

$$S_i^{\mathrm{FD}} = \left[1.9\log\left(1+2.45N\right) - 42\frac{\lambda_e}{r_0^2}\right]^+, (\text{w/ NLOS SI}, R^2 \approx 0.\dot{9}, \text{Var} \approx 6.44\times 10^{-2}) \tag{4.21}$$

$$S_i^{\mathrm{HD}} = \left[1.4\log(1+3.6N) - 84\frac{\lambda_e}{r_0^2}\right]^+, \quad (R^2 \approx 0.\dot{9}, \text{Var} \approx 8.25\times 10^{-2}). \tag{4.22}$$

Remark 5. The results from *Corollaries 5-8* indicate that the DL and UL FD (w/o SI and w/ NLOS SI) over HD ergodic secrecy rate gains under both passive and colluding eavesdropping are always greater or equal to one (with $N \geq 1$ and $\lambda_e \geq 0$) - in other words, the FD operation always achieves an improved or equivalent PHYLS performance versus the HD counterpart. Whilst the system experiences secrecy non-outage, increasing the number of small-cell BS antennas ($N \to +\infty$) always enhances the DL and UL FD over HD ergodic secrecy rate gains. Further, the corresponding impact of the EDs' spatial density can be described as follows. As $\lambda_e \to 0$ (no eavesdropping), the DL and UL FD

over HD ergodic secrecy rate gains tend to the DL and UL FD over HD ergodic rate gains. Increasing λ_e from zero to λ_e^* continuously enhances the DL and UL FD over HD ergodic secrecy rate gains, where λ_e^* represents the critical point where the system experiences secrecy outage. With $\lambda_e \geq \lambda_e^*$, the DL and UL FD over HD ergodic secrecy rate gains tend to one. Note that the value of λ_e^* depends on the interference cancellation capabilities as well as the number of small-cell BS transmit/receive antennas.

In order to demonstrate the validity of the approximate expressions within *Corollaries 1-8* versus the (exact) theoretical data, we provide some numerical examples in Appendix F.

4.2 Numerical Results

In this section, we assess the validity of the proposed machine learning-based explicit closed-form expressions by comparing against empirical data. We will provide numerical results for all expressions developed in *Corollaries 1-8* capturing the different scenarios of interest under consideration. For sake of simplicity, the number of BS antennas in both UL and DL is equal $N_d = N_u = N$. The number of served UEs in the UL and DL also considered to be equal $K_d = K_u = 1$. Moreover the noise is assumed to be zero and path loss component $\alpha = 4$.

4.2.1 Impact of Number of Antennas on Ergodic Rate

In Fig. 4.1, we present the ergodic rate performance of the intended DL and UL UEs versus different number of small-cell BS antennas for the special case described in *Corollaries 1-2*. As expected, we can observe that in both cases of UL and DL, the ergodic rate at the receiver increases with number of antennas. Moreover, applying SIC scheme, significantly improves the ergodic rate in case of DL while SI cancellation in UL does not have a major effect. Furthermore, comparing the dotted line with the solid line, we can see that our closed-form approximations of the ergodic rate, almost overlap the empirical data in all cases.

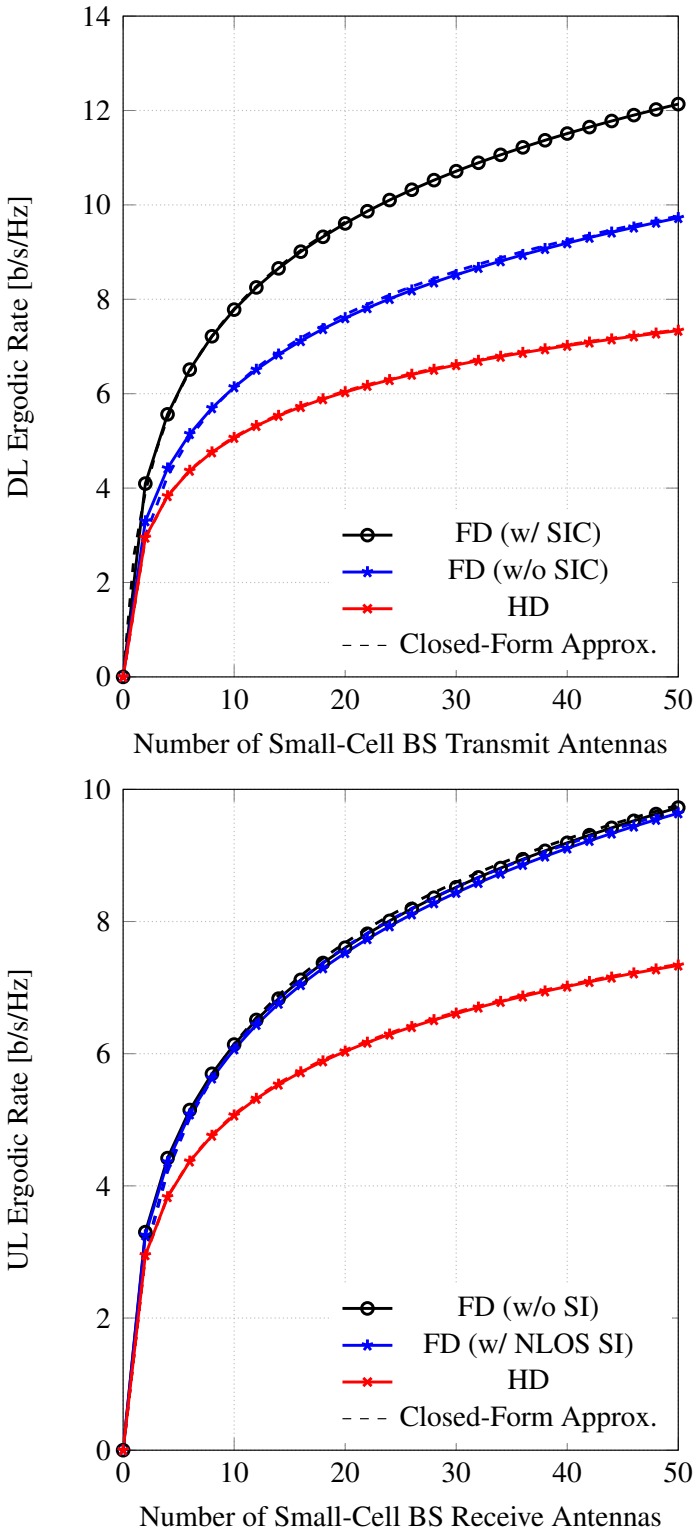

Figure 4.1: Ergodic rates of the intended DL and UL UEs versus the number of small-cell BS antennas. System parameters are: $K_d = K_u = 1$, $\sigma_o^2 = \sigma_i^2 = 0$, $\alpha = 4$.

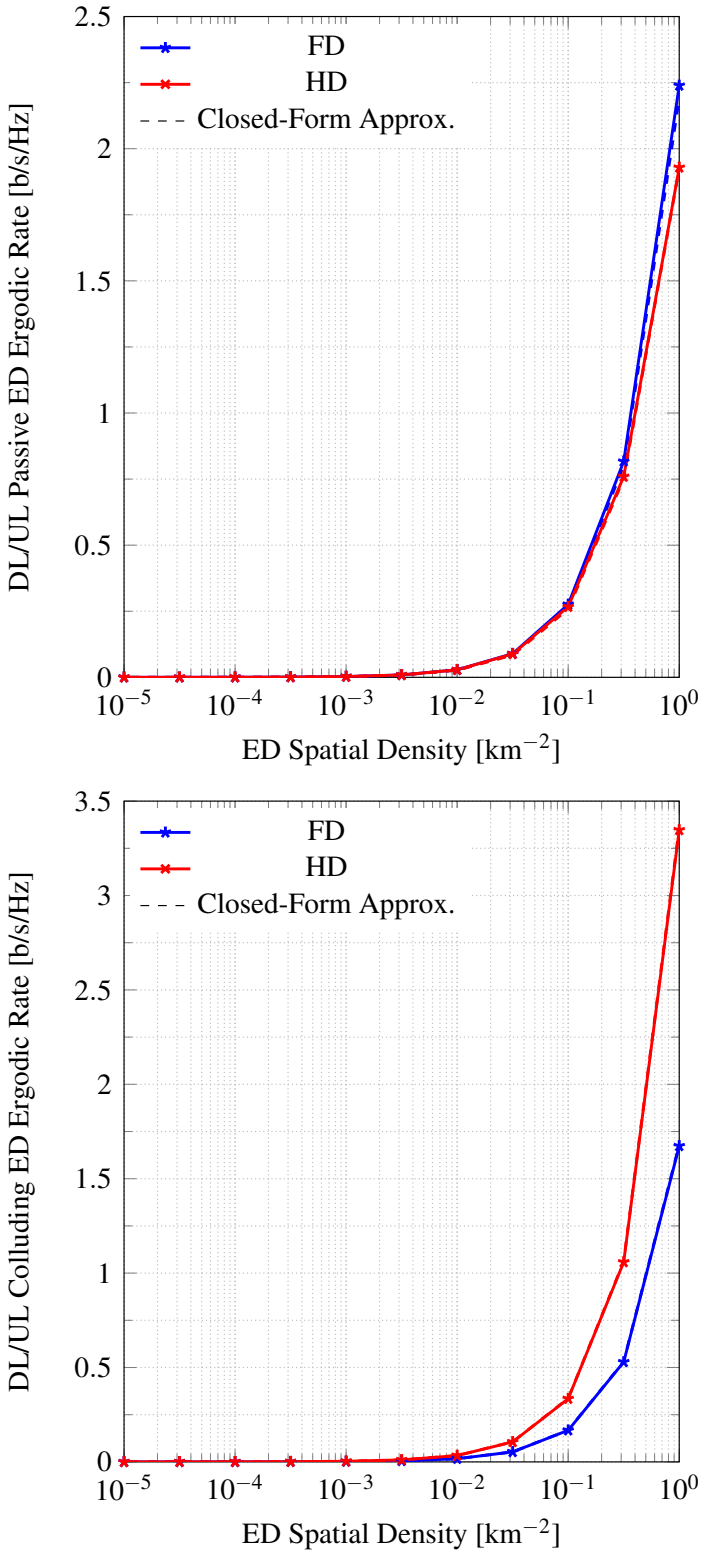

Figure 4.2: Ergodic rates of the most malicious DL and UL EDs versus the EDs' spatial densities. System parameters are: $r_0 = 5$ m (in case of collusion), $K_d = K_u = 1$, $\sigma_v^2 = \sigma_c^2 = 0$, $\alpha = 4$.

4.2.2 Impact of Density of EDs on EDs' Ergodic Rate

Thereafter, we look to depict the ergodic rate performance of the most malicious DL and UL EDs versus different EDs' spatial densities in Fig. 4.2. The results are obtained considering passive EDs as in *Corollary 3*, and colluding EDs as in *Corollary 4*, respectively.

As we expected, our results indicate that by increasing the density of EDs, the ergodic rate of EDs also improves. This trend is appeared to be much sharper in case of colluding EDs as there are more EDs collaborating for eavesdropping the channel. Similar to before, we can also observe from the graph that our approximation is closely overlapped with the empirical data.

4.2.3 Impact of Number of BS Antennas on Secrecy Rate

The DL and UL ergodic secrecy rates in the FD and HD small-cell networks in the presence of a Poisson field of passive EDs under the system parameters described in *Corollaries 5-6* are depicted in Fig. 4.3. Finally, the corresponding PHYLS performance in the presence of PPP-based colluding EDs for the special case described in *Corollaries 7-8* is shown in Fig. 4.4.

Considering the same parameters as before, in addition to a fixed density for EDs we can observe that in all cases, increasing the number of BS antennas improves the secrecy rate due to a better array gain at the receiver. Moreover, removing any interference at the eligible receivers also has a positive affect on the ergodic secrecy rate. As elaborated in the previous chapters, our results confirm that FD operation mode has a better performance than HD in terms of secrecy rate due to the EDs suffering from extra interference. Furthermore, all of our figures confirm the closeness of the derived closed-form approximations to the empirical data which leads to a great simplicity for generating results and drawing design insights.

The numerical examples provided in this Appendix confirm the validity of the approximate expressions in *Corollaries 1-8*. ■

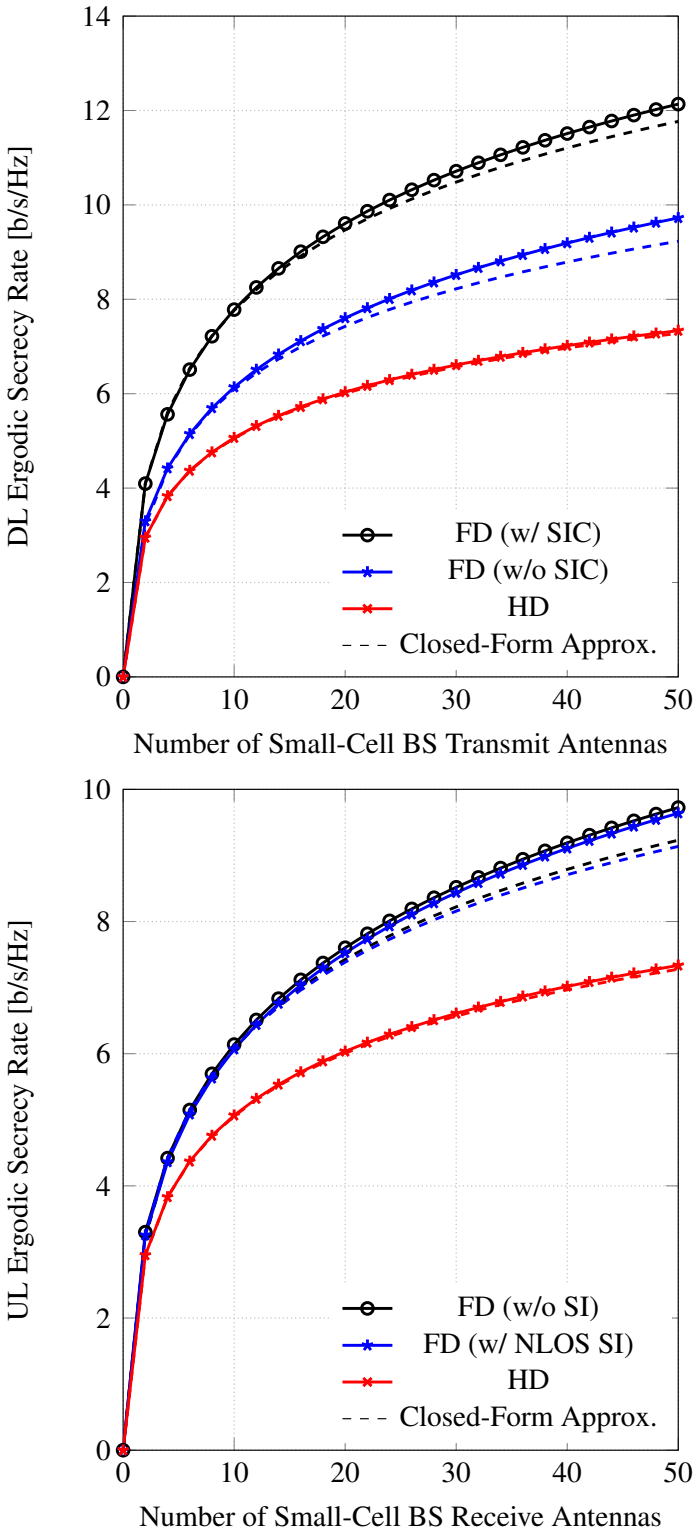

Figure 4.3: Ergodic secrecy rate in the presence of a Poisson field of passive EDs versus the number of small-cell BS antennas. System parameters are: $\lambda_e = 10^{-6}$ km^{-2}, $K_d = K_u = 1$, $\sigma_o^2 = \sigma_v^2 = \sigma_i^2 = \sigma_c^2 = 0$.

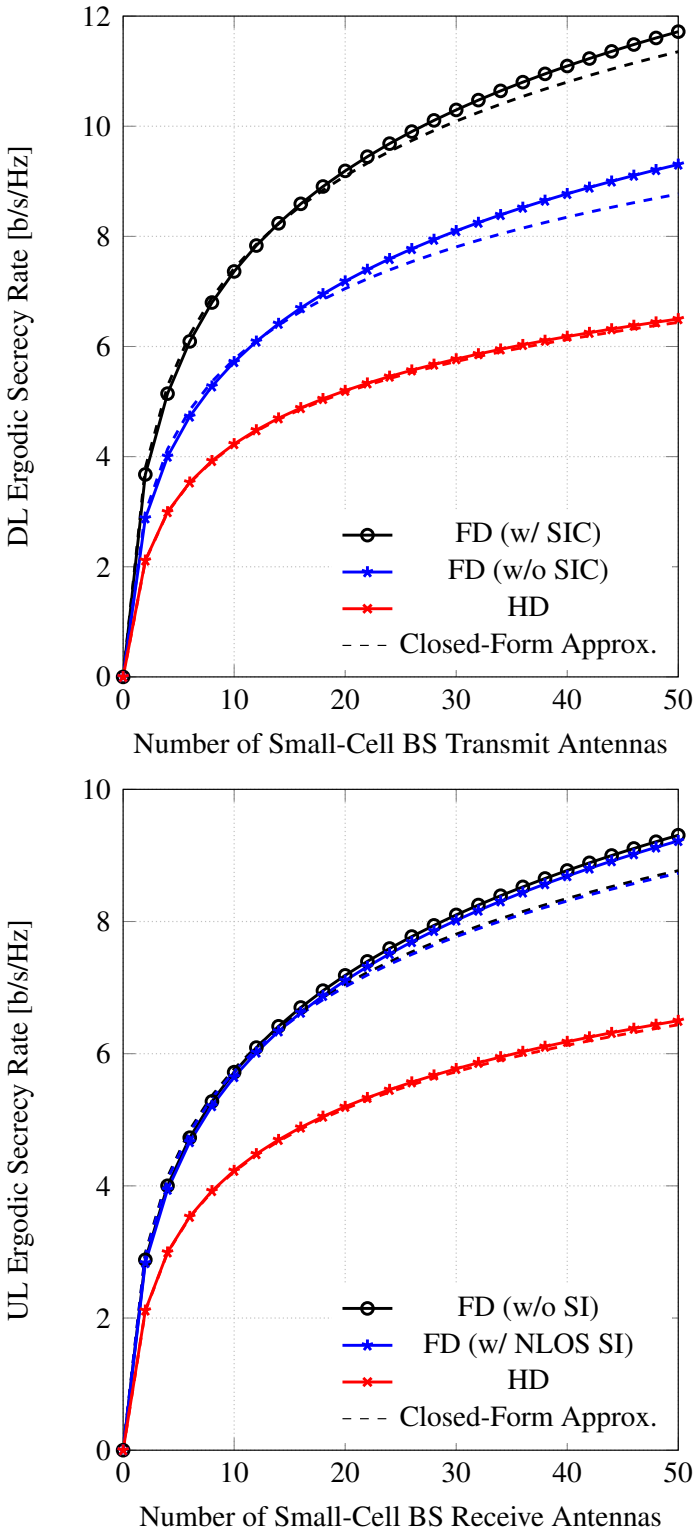

Figure 4.4: Ergodic secrecy rate in the presence of a Poisson field of colluding EDs versus the number of small-cell BS antennas. System parameters are: $\lambda_e = 10^{-4}$ km^{-2}, $r_0 = 0.1$ m, $K_d = K_u = 1$, $\sigma_o^2 = \sigma_v^2 = \sigma_i^2 = \sigma_c^2 = 0$.

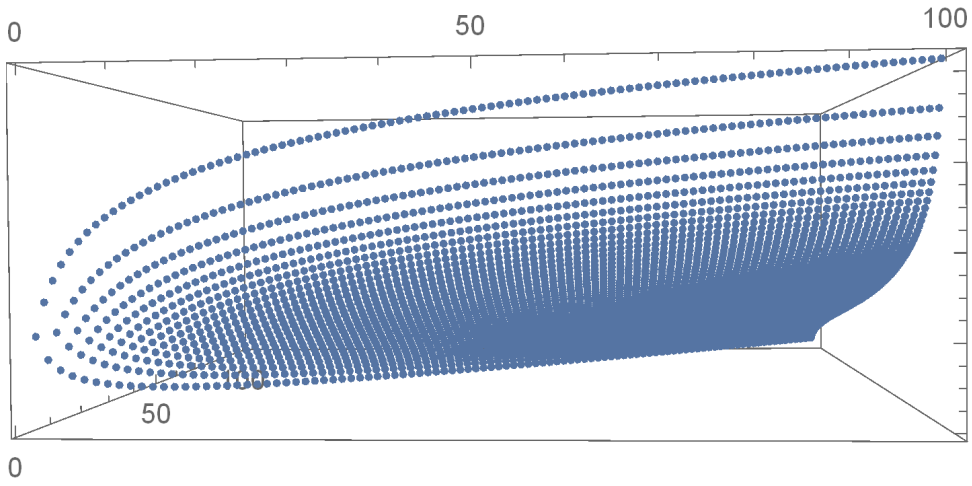

Figure 4.5: HD small-cell network DL SE performance with multi-user MIMO. Observe that the results are three-dimensional in the number of BS antennas (top axis), number of users served per resource block (bottom axis), and SE (left axis).

4.2.4 Non-Linear Curve-Fitting for Multi-User MIMO

The results from the previous chapters of this thesis were developed for the general case of multi-user MIMO. As highlighted in the beginning of this chapter, here, we have focused on the case of single-user MIMO for deriving closes-form expressions. In this section, we elaborate further on the exact reasoning and challenges concerned with deriving similar set of findings in the more general case of multi-user MIMO communications.

Consider the DL SE performance (left axis) of a HD small-cell network in Fig. 4.5, where the number of transmit antennas at the BS ranges from 1 to 100 (top axis), and the number of users served per resource block ranges from 1 up to the number of transmit antennas (bottom axis). In Fig. 4.6, we provide similar results, however, for the case where the number of users is fixed to one. When applying non-linear curve fitting techniques to the data in Fig. 4.6, we can obtain a highly accurate fit (given the data is a function of the number of antennas only). However, doing a similar task to the three-dimensional data in Fig. 4.5 is significantly more complicated. In spite of our best efforts, we could not obtain a general tractable

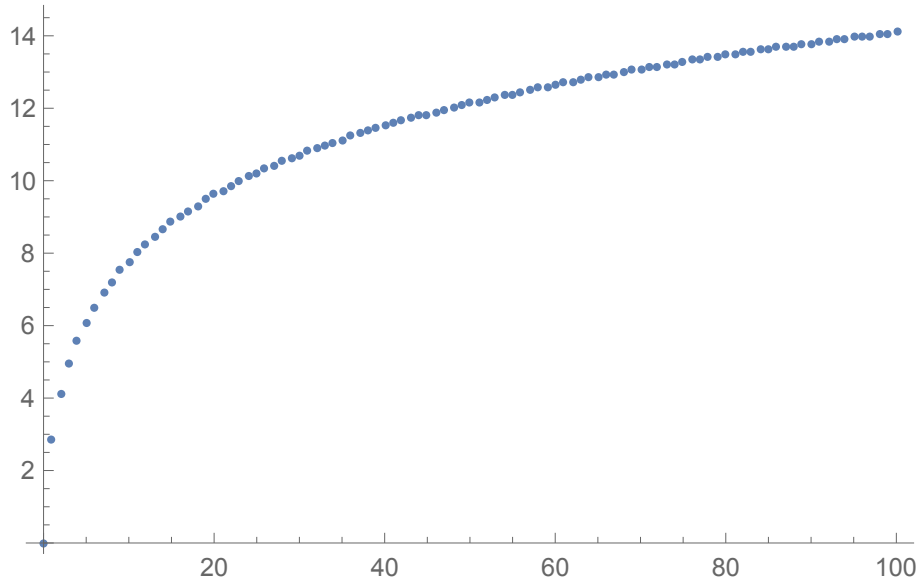

Figure 4.6: HD small-cell network DL SE performance with single-user MIMO. Observe that the results are two-dimensional in the number of BS antennas (bottom axis) and SE (left axis).

numerical fit with acceptable goodness of fit measures for the data in Fig. 4.5. As expected, the underlying variance between empirical versus fitted data was even worse for the case of FD small-cell network (e.g., with each FD MIMO small-cell BS serving multiple users in the DL and UL simultaneously).

4.3 Conclusions

In the previous chapters, we provided explicit semi-analytic expressions for secrecy rates capturing a wide-range of small-cell deployments with both full-duplex and half-duplex operations. These, albeit most useful for radio design and deployment, do not admit closed-forms for arbitrary system parameters. Therefore, in this chapter, we utilised tools from supervised machine learning in order to derive explicit closed-form approximations for the different key performance indicators. Specifically, we employed non-linear curve-fiting techniques on an extensive number of theoretical data points to achieve accurate closed-form approximations for the key performance indicators. Furthermore, in each case, we measured the goodness of fit of our model by two different parameters of R^2 and Var. To further assess the validity of the developed expressions, we provided numerical comparisons against

empirical data for all developed expressions and demonstrated the high accuracy of our results. The findings of this chapter greatly facilitate generating performance curves and identifying the bounds, trade-offs, and trends concerning the physical layer security of small-cell networks under both full-duplex and half-duplex modes of communications.

The work presented in this chapter can be extended in a number of ways. One immediate extension would be to extend the developed results for the case of multi-user MIMO. Also, other supervised learning techniques, in particular deep learning, can be used to derive more accurate expressions for the key performance indicators.

Chapter 5

Conclusions

With the rapid increase of data traffic, the role of small-cell networks and accordingly their vulnerability to attacks became significantly important. Previously, security was addressed in higher layers through various cryptographic approaches. However more recently, PHYLS is featured as an additional and inexpensive factor for enhancing security. On the other hand, in order to account for this traffic growth, various concepts such as FD (transmitting data at the same time and frequency) and MIMO (employing multiple antennas in the transceiver) are introduced. Inspired by above, this work was dedicated to investigate the performance of PHYLS in small-cell cellular networks that are operating in FD mode with both single and multiple antennas. We considered a field of BSs, UEs and (passive and colluding) EDs and mathematically modelled them with assist of Stochastic geometry tools which closely captures the real characteristics of the network. Furthermore, we applied MC simulation to confirm validity of our mathematical results.

Accordingly, we first investigated the PHYLS performance in a large-scale FD cellular network where both BSs and UEs operate in FD mode. The locations of the nodes were assumed to follow an independent stationary PPP where FD EDs are equipped with single-antennas and operate independently. We applied a cellular association strategy based on the strongest received SINR which is equivalent to the closest transmitter-receiver distance for a single-tier deployment. In our analysis all the channel gains including interferences, were assumed to follow Rayleigh distribution, apart from residual SI which is Rician with predefined parameters. Fol-

lowing these assumptions, we modelled the SINR in DL at the intended UE, and its associated BS in UL. The interference channels were defined and their LT functions are given in Appendices. Moreover, two other factors were introduced in order to compensate for the affect of interferences. In the SI case, the receiver was assumed to be enabled with SI cancellation capability. On the other hand, a guard region of a certain radius was considered to mitigate the coming interference from other cells and transmitting nodes. Next, considering the closest ED to the transmitter and using Shannon capacity theorem, the average secrecy rate in both UL and DL were derived by subtracting the received rate at ED from the eligible receiver. Accordingly, the impact of ED's density in compare with BS's density was analysed in both FD and HD mode. The affect of SI cancellation and SIC is also studied through tuning the defined guard region. Our findings illustrates that in a small-cell cellular network where each FD BS serves one UE per resource block, particularly in DL, has increasingly higher secrecy rate over its HD counterpart. Moreover, we showed that this trend is in fact very similar for FD and HD UEs.

The results from chapter 2 builds the fundamentals for the next part of our research which is explained in chapter 3. Here, considering the HD UEs in the DL, we extended our work to the scenario where BSs are equipped with multi-antennas and are able to communicate with several UEs simultaneously. The ZF beamforming is applied to surpass interference. Considering similar assumptions as chapter 2, we mathematically modelled SINR and derived expressions of average received rate in UL and DL. We have also taken into consideration both cases where EDs do not cooperate as well as the case where they optimally combine their information. Then we studied the influence of number of antennas in the BS, density of UEs, and density of EDs, in both scenarios of colluding and non-colluding EDs. Our findings show that in presence of passive EDs, the ergodic secrecy rate improves with the number of antennas in the BS particularly in the case of FD compared with its HD counterpart. In fact, by applying SIC and SI cancellation techniques, MIMO technology will significantly improves PHYLS performance which highlights the essential application of MIMO in cellular networks. This performance gain is even

higher in case of colluding EDs which is considered in its worst case, due to the extra interference that each ED experiences. On the other hand, we showed that the number of UEs that each BS serves in one resource block is negatively related to PHYLS performance. In other words, in both cases of UL and DL, increasing the number of simultaneously served UEs decreases the PHYLS. Moreover, similar to the previous chapter, the density of EDs in compare with BSs deployment, negatively impacts the performance of PHYLS in both cases of colluding and non-colluding EDs. Moreover, increasing density of EDs, enhances the FD over HD secrecy gain up to the point where secrecy outage occurs. This trend falls much sharper in case of colluding EDs. It is important to note that in all scenarios, application of SIC and SI cancellation improved PHYLS performance and in almost all cases, FD shows a better performance than HD in terms of PHYLS.

In spite of the valuable results that we derived in the previous chapters, it is not mathematically tractable to derive closed-form expressions for the key performance indicators for general settings of system parameters. Therefore, we dedicated the final chapter to derive closed-form approximate expressions for the key performance indicators in certain special cases of interest. We applied tools from machine learning, in particular non-linear curve-fitting techniques to a great set of theoretical data to achieve closed-form approximations for key performance indicators, including spectral efficiencies and secrecy rates, and we finally introduced two parameters to evaluate the fitness of our model: R-squared and estimated variance. We demonstrated the closeness of these developed closed-form expressions for all cases under consideration against empirical data.

The findings presented in this work can be extended and exploited in a number of ways. In terms of future research directions, there are many extensions, including looking at spectrum sharing and use of unlicensed bands. Naturally, operation of small-cells, in particular in full-duplex mode, requires close coordination for mitigating and managing interference. Machine learning and artificial intelligence will mostly likely play an important role towards facilitating dense deployments of small-cells and hence are promising areas for extension of this work. From a

practical perspective, in conjunction with continuing deployment of 5G networks worldwide, security is becoming an increasingly important aspect. Physical layer security has so far not received the attention that it deserves, particularly in terms of standardisation within 3GPP. This trend will surely change in the next releases of 5G, and to this end, development of proof-of-concepts and testbeds would greatly assist with understanding the fundamentals of physical layer security and its role in networks of the future.

Appendix A

Appendix A

A.1

The ergodic rate considering FD BSs and UEs for the user o in the DL per resource block can be calculated using

$$\begin{aligned} C_o^{\mathrm{FD}} &= \mathbb{E}\left[\log_2\left(1+\gamma_o^{\mathrm{FD}}\right)\right] \\ &= \frac{1}{\ln(2)}\int_0^{\infty}\int_0^{\infty}\frac{1-F^{\mathrm{FD}}_{\gamma_o|r_{b,o}=r}[\gamma]}{1+\gamma}\,\mathrm{d}\gamma\,\mathscr{P}_{r_{b,o}}[r]\,\mathrm{d}r \end{aligned} \tag{A.1}$$

where

$$\begin{aligned} F_{\gamma_o^{\mathrm{FD}}|r_{b,o}=r}[\gamma] &= \Pr\left[\gamma_o^{\mathrm{FD}} < \gamma \mid r_{b,o}=r\right] \\ &= 1-\Pr\left[g_{b,o} > \frac{\gamma r^{\alpha}}{p_d}\left(I_o^{d,d}+I_o^{u,d}+I_o^{o,o}+\sigma_o^2\right)\right] \\ &\overset{(i)}{=} 1-\left\{\exp\left(-s\sigma_o^2\right)\mathscr{L}_{I_o^{d,d}}[s]\mathscr{L}_{I_o^{u,d}}[s]\mathscr{L}_{I_o^{o,o}}[s]\right\}_{s=\frac{\gamma r^{\alpha}}{p_d}} \end{aligned} \tag{A.2}$$

with (i) follows from the fact that $g_{b,o} \sim exp(1)$. Hence, we arrive at (3.9).

The LT function of the inter-cell interference at the reference UE in the DL o is given by

$$
\begin{aligned}
\mathscr{L}_{I_o^{d,d}}(s) &= \mathbb{E}_{\phi_d, g_{l,o}}\left[\exp\left(-s\sum_{l\in\phi_d\setminus\{b\}} p_d g_{l,o} r_{l,o}^{-\alpha}\right)\right] \\
&\overset{(i)}{=} \mathbb{E}_{\phi_d}\left[\prod_{l\in\phi_d\setminus\{b\}} \mathbb{E}_{g_{l,o}}\left[\exp\left(-s p_d g_{l,o} r_{l,o}^{-\alpha}\right)\right]\right] \\
&\overset{(ii)}{=} \exp\left(-2\pi\lambda_d \int_r^{\infty}\left(1-\frac{1}{1+s p_d x^{-\alpha}}\right) x\,\mathrm{d}x\right) \\
&\overset{(iii)}{=} \exp\left(-\pi\lambda_d r^2\left({}_2F_1\left(1,-\frac{2}{\alpha};1-\frac{2}{\alpha};-\frac{s p_d}{r^{\alpha}}\right)-1\right)\right)
\end{aligned} \tag{A.3}
$$

where (i) follows independence property of PPP and uncorrelated channel conditions [80], (ii) is obtained by applying the probability generating functional (PGFL) of a PPP and converting from Cartesian to polar coordinates [116], and (iii) is written by applying the integral identity $\int_r^{+\infty}\left(1-\left(1+\beta x^{-\alpha}\right)^{-K}\right) x\,\mathrm{d}x = \frac{r^2}{2}\left({}_2F_1\left(-\frac{2}{\alpha},K;1-\frac{2}{\alpha};-\frac{\beta}{r^{\alpha}}\right)-1\right)$.

Using a similar approach to that in the above, the LT function of the MI at the reference UE in the DL o is given by

$$
\begin{aligned}
\mathscr{L}_{I_o^{u,d}}(s) &= \mathbb{E}_{\phi_u, g_{k,o}}\left[\exp\left(-s\sum_{k\in\phi_u} p_u g_{k,o} r_{k,o}^{-\alpha}\right)\right] \\
&= \exp\left(-2\pi\lambda_d \int_{\varepsilon}^{\infty}\left(1-\frac{1}{1+s p_u x^{-\alpha}}\right) x\,\mathrm{d}x\right) \\
&= \exp\left(-\pi\lambda_d \varepsilon^2\left({}_2F_1\left(1,-\frac{2}{\alpha};1-\frac{2}{\alpha};-\frac{s p_u}{\varepsilon^{\alpha}}\right)-1\right)\right)
\end{aligned} \tag{A.4}
$$

and

$$
\mathscr{L}_{I_i^{o,o}}(s) = \left(1+s p_u \theta\right)^{-\kappa}. \tag{A.5}
$$

where ε can be tuned by design or measurements to capture the SIC capability of the UEs. Hence, we arrive at *Theorem 1*. ■

A.2

Utilizing a similar approach to that in Appendix A, we can arrive at (3.13). Moreover, using a similar methodology, the LT functions of the different UL interfering UEs at the reference BS are given by

$$\begin{aligned}\mathscr{L}_{I_i^{u,u}}(s) &= \mathbb{E}_{\phi_u,h_{k,i}}\left[\exp\left(-s\sum_{k\in\hat{\phi}_u} p_u h_{k,i} r_{k,i}^{-\alpha}\right)\right] \\ &= \exp\left(-2\pi\lambda_d\int_r^{\infty}\left(1-\frac{1}{1+sp_u x^{-\alpha}}\right)x\,\mathrm{d}x\right) \\ &= \exp\left(-\pi\lambda_d r^2\left({}_2F_1\left(1,-\frac{2}{\alpha};1-\frac{2}{\alpha};-\frac{sp_u}{r^{\alpha}}\right)-1\right)\right) \end{aligned} \tag{A.6}$$

$$\begin{aligned}\mathscr{L}_{I_i^{d,u}}(s) &= \mathbb{E}_{\phi_d,h_{l,i}}\left[\exp\left(-s\sum_{l\in\phi_d} p_d h_{l,i} r_{l,i}^{-\alpha}\right)\right] \\ &= \exp\left(-2\pi\lambda_d\int_0^{\infty}\left(1-\frac{1}{(1+sp_d x^{-\alpha})^{K_d}}\right)x\,\mathrm{d}x\right) \\ &= \exp\left(-\pi\lambda_d\left(sp_d\right)^{\frac{2}{\alpha}}\frac{\Gamma\left(1-\frac{2}{\alpha}\right)\Gamma\left(1+\frac{2}{\alpha}\right)}{\Gamma(1)}\right) \end{aligned} \tag{A.7}$$

and

$$\mathscr{L}_{I_i^{b,b}}(s) = (1+sp_d\theta)^{-\kappa}. \tag{A.8}$$

Hence, we arrive at *Theorem 2*. ■

A.3

The ergodic rate of the most malicious passive ED in the DL v per resource block can be calculated using

$$C_v^{\mathrm{FD}} = \mathbb{E}\left[\log_2\left(1+\gamma_v^{\mathrm{FD}}\right)\right] = \frac{1}{\ln(2)}\int_0^{\infty}\frac{1-F_{\gamma_v}^{\mathrm{FD}}[\gamma]}{1+\gamma}\,\mathrm{d}\gamma \tag{A.9}$$

where

$$F_{\gamma_v^{\mathrm{FD}}}[\gamma] = \Pr[\gamma_v^{\mathrm{FD}} < \gamma] = \Pr\left[\max_{e\in\phi_e}\left(\frac{p_d g_{b,e} r_{b,e}^{-\alpha}}{I_e^{d,d} + I_e^{u,d} + \sigma_e^2}\right) < \gamma\right]$$
$$= \mathbb{E}_{\phi_e}\left[\prod_{e\in\phi_e} \Pr\left(\frac{p_d g_{b,e} r_{b,e}^{-\alpha}}{I_e^{d,d} + I_e^{u,d} + \sigma_e^2} < \gamma \mid \phi_e\right)\right] \overset{(i)}{=}$$
$$\exp\left(-2\pi\lambda_e \int_0^{\infty}\left(1 - \Pr\left[\frac{p_d g_{b,v} r^{-\alpha}}{I_v^{d,d} + I_v^{u,d} + \sigma_v^2} < \gamma\right]\right) r\,\mathrm{d}r\right) \tag{A.10}$$

with (i) obtained using the PGFL of a PPP and converting from Cartesian to polar coordinates. The probability from the above is given by

$$1 - \Pr\left[\frac{p_d g_{b,v} r^{-\alpha}}{I_v^{d,d} + I_v^{u,d} + \sigma_v^2} < \gamma\right]$$
$$= \Pr\left[g_{b,v} > \frac{\gamma r^{\alpha}}{p_d}\left(I_v^{d,d} + I_v^{u,d} + \sigma_v^2\right)\right]$$
$$= \left\{\exp\left(-s\sigma_v^2\right)\mathscr{L}_{I_v^{d,d}}(s)\mathscr{L}_{I_v^{u,d}}(s)\right\}_{s=\frac{\gamma r^{\alpha}}{p_d}}. \tag{A.11}$$

Hence, we arrive at (3.18).

The LT function of the inter-cell interference at the most malicious ED in the DL v is given by

$$\mathscr{L}_{I_v^{d,d}}(s) = \mathbb{E}_{\phi_d, g_{l,v}}\left[\exp\left(-s\sum_{l\in\phi_d} p_d g_{l,v} r_{l,v}^{-\alpha}\right)\right]$$
$$\overset{(i)}{=} \mathbb{E}_{\phi_d}\left[\prod_{l\in\phi_d} \mathbb{E}_{g_{l,v}}\left[\exp\left(-s p_d g_{l,v} r_{l,v}^{-\alpha}\right)\right]\right]$$
$$\overset{(ii)}{=} \exp\left(-2\pi\lambda_d \int_0^{\infty}\left(1 - \frac{1}{1 + s p_d x^{-\alpha}}\right) x\,\mathrm{d}x\right)$$
$$\overset{(iii)}{=} \exp\left(-\pi\lambda_d \left(s p_d\right)^{\frac{2}{\alpha}} \frac{\Gamma\left(1-\frac{2}{\alpha}\right)\Gamma\left(1+\frac{2}{\alpha}\right)}{\Gamma(1)}\right) \tag{A.12}$$

where (i) follows from the independence property of PPP and uncorrelated channel conditions, (ii) is obtained using the PGFL of a PPP and converting from Cartesian to polar coordinates, and (iii) is written using the integral identity $\int_0^{+\infty}\left(1-\left(1+\beta x^{-\alpha}\right)^{-K}\right) x\,\mathrm{d}x = \frac{\beta^{\frac{2}{\alpha}}\Gamma\left(1-\frac{2}{\alpha}\right)\Gamma\left(K+\frac{2}{\alpha}\right)}{2\Gamma(K)}$.

Using a similar approach to that in the above, the LT function of the MI at the most malicious ED in the DL v is given by

$$\begin{aligned}\mathscr{L}_{I_v^{u,d}}(s) &= \mathbb{E}_{\phi_u, g_{k,v}}\left[\exp\left(-s\sum_{k\in\phi_u} p_u g_{k,v} r_{k,v}^{-\alpha}\right)\right] \\ &= \exp\left(-2\pi\lambda_d \int_0^{\infty}\left(1-\frac{1}{1+sp_u x^{-\alpha}}\right) x\,\mathrm{d}x\right) \\ &= \exp\left(-\pi\lambda_d\,(sp_u)^{\frac{2}{\alpha}}\,\Gamma\left(1-\frac{2}{\alpha}\right)\Gamma\left(1+\frac{2}{\alpha}\right)\right). \end{aligned} \tag{A.13}$$

Hence, we arrive at *Theorem 3*. ■

Appendix B

Appendix B

B.1

The ergodic rate (considering FD BSs) for the user o in the DL per resource block can be calculated using

$$C_o^{\mathrm{FD}} = \mathbb{E}\left[\log_2\left(1+\gamma_o^{\mathrm{FD}}\right)\right] = \frac{1}{\ln(2)}\int_0^{\infty}\int_0^{\infty}\frac{1-F^{\mathrm{FD}}_{\gamma_o|r_{b,o}=r}[\gamma]}{1+\gamma}\,\mathrm{d}\gamma\,\mathscr{P}_{r_{b,o}}[r]\,\mathrm{d}r \quad \text{(B.1)}$$

where

$$\begin{aligned} F_{\gamma_o^{\mathrm{FD}}|r_{b,o}=r}[\gamma] &= \Pr\left[\gamma_o^{\mathrm{FD}} < \gamma \mid r_{b,o}=r\right] = 1-\Pr\left[G_{b,o} > \frac{\gamma r^{\alpha}}{p_d}\left(I_o^{d,d}+I_o^{u,d}+\sigma_o^2\right)\right] \\ &\overset{(i)}{=} 1-\sum_{n=0}^{N_d-K_d}\left\{\frac{(-s)^n}{n!}\frac{\mathrm{d}^n}{\mathrm{d}s^n}\exp\left(-s\sigma_o^2\right)\mathscr{L}_{I_o^{d,d}}[s]\mathscr{L}_{I_o^{u,d}}[s]\right\}_{s=\frac{\gamma r^{\alpha}}{p_d}} \end{aligned} \quad \text{(B.2)}$$

with (i) written using the identity $x^n f(x) \equiv (-1)^n \frac{\mathrm{d}^n}{\mathrm{d}s^n}\mathscr{L}_{f(x)}[s]$ (a property of LT function). Hence, we arrive at (3.9).

The LT function of the inter-cell interference at the reference UE in the DL o is given by

$$\begin{aligned} \mathscr{L}_{I_o^{d,d}}(s) &= \mathbb{E}_{\phi_d,G_{l,o}}\left[\exp\left(-s\sum_{l\in\phi_d\setminus\{b\}}p_d G_{l,o}r_{l,o}^{-\alpha}\right)\right] \\ &\overset{(i)}{=} \mathbb{E}_{\phi_d}\left[\prod_{l\in\phi_d\setminus\{b\}}\mathbb{E}_{G_{l,o}}\left[\exp\left(-sp_d G_{l,o}r_{l,o}^{-\alpha}\right)\right]\right] \end{aligned}$$

$$\overset{(ii)}{=} \exp\left(-2\pi\lambda_d \int_r^{\infty} \left(1 - \frac{1}{(1+sp_d x^{-\alpha})^{K_d}}\right) x \, \mathrm{d}x\right)$$
$$\overset{(iii)}{=} \exp\left(-\pi\lambda_d r^2 \left({}_2F_1\left(K_d, -\frac{2}{\alpha}; 1-\frac{2}{\alpha}; -\frac{sp_d}{r^{\alpha}}\right) - 1\right)\right) \tag{B.3}$$

where (i) follows independence property of PPP and uncorrelated channel conditions [80], (ii) is obtained by applying the probability generating functional (PGFL) of a PPP and converting from Cartesian to polar coordinates [116], and (iii) is written by applying the integral identity $\int_r^{+\infty} \left(1 - (1+\beta x^{-\alpha})^{-K}\right) x \, \mathrm{d}x = \frac{r^2}{2}\left({}_2F_1\left(-\frac{2}{\alpha}, K; 1-\frac{2}{\alpha}; -\frac{\beta}{r^{\alpha}}\right) - 1\right)$.

Using a similar approach to that in the above, the LT function of the MI at the reference UE in the DL o is given by

$$\begin{aligned}\mathscr{L}_{I_o^{u,d}}(s) &= \mathbb{E}_{\phi_u, G_{k,o}}\left[\exp\left(-s\sum_{k\in\phi_u} p_u G_{k,o} r_{k,o}^{-\alpha}\right)\right] \\ &= \exp\left(-2\pi K_u \lambda_d \int_{\varepsilon}^{\infty} \left(1 - \frac{1}{1+sp_u x^{-\alpha}}\right) x \, \mathrm{d}x\right) \\ &= \exp\left(-\pi K_u \lambda_d \varepsilon^2 \left({}_2F_1\left(1, -\frac{2}{\alpha}; 1-\frac{2}{\alpha}; -\frac{sp_u}{\varepsilon^{\alpha}}\right) - 1\right)\right)\end{aligned} \tag{B.4}$$

where ε can be tuned by design or measurements to capture the SIC capability of the UEs. Hence, we arrive at *Theorem 1*. ■

B.2

Utilizing a similar approach to that in Appendix A, we can arrive at (3.13). Moreover, using a similar methodology, the LT functions of the different UL interfering terms for the postcoding of the useful signal at the reference BS are given by

$$\begin{aligned}\mathscr{L}_{I_i^{u,u}}(s) &= \mathbb{E}_{\phi_u, H_{k,i}}\left[\exp\left(-s\sum_{k\in\hat{\phi}_u} p_u H_{k,i} r_{k,i}^{-\alpha}\right)\right] \\ &= \exp\left(-2\pi K_u \lambda_d \int_{r}^{\infty} \left(1 - \frac{1}{1+sp_u x^{-\alpha}}\right) x \, \mathrm{d}x\right) \\ &= \exp\left(-\pi K_u \lambda_d r^2 \left({}_2F_1\left(1, -\frac{2}{\alpha}; 1-\frac{2}{\alpha}; -\frac{sp_u}{r^{\alpha}}\right) - 1\right)\right)\end{aligned} \tag{B.5}$$

$$\begin{aligned}\mathscr{L}_{I_i^{d,u}}(s) &= \mathbb{E}_{\phi_d,H_{l,i}}\left[\exp\left(-s\sum_{l\in\phi_d} p_d H_{l,i} r_{l,i}^{-\alpha}\right)\right] \\ &= \exp\left(-2\pi\lambda_d\int_0^\infty\left(1-\frac{1}{(1+sp_d x^{-\alpha})^{K_d}}\right)x\,\mathrm{d}x\right) \\ &= \exp\left(-\pi\lambda_d\,(sp_d)^{\frac{2}{\alpha}}\,\frac{\Gamma\left(1-\frac{2}{\alpha}\right)\Gamma\left(K_d+\frac{2}{\alpha}\right)}{\Gamma(K_d)}\right)\end{aligned} \tag{B.6}$$

and

$$\mathscr{L}_{I_i^{b,b}}(s) = \mathbb{E}_{H_{l,i}}\left[\exp\left(-sp_d H_{i,i}\right)\right] = (1+sp_d\theta)^{-\kappa}. \tag{B.7}$$

Hence, we arrive at *Theorem 2*. ■

B.3

The ergodic rate (considering FD BSs) of the most malicious passive ED in the DL v per resource block can be calculated using

$$C_v^{\mathrm{FD}} = \mathbb{E}\left[\log_2\left(1+\gamma_v^{\mathrm{FD}}\right)\right] = \frac{1}{\ln(2)}\int_0^\infty \frac{1-F_{\gamma_v}^{\mathrm{FD}}[\gamma]}{1+\gamma}\,\mathrm{d}\gamma \tag{B.8}$$

where

$$\begin{aligned}F_{\gamma_v^{\mathrm{FD}}}[\gamma] &= \Pr[\gamma_v^{\mathrm{FD}}<\gamma] = \Pr\left[\max_{e\in\phi_e}\left(\frac{p_d G_{b,e} r_{b,e}^{-\alpha}}{I_e^{d,d}+I_e^{u,d}+\sigma_e^2}\right)<\gamma\right] \\ &= \mathbb{E}_{\phi_e}\left[\prod_{e\in\phi_e}\Pr\left(\frac{p_d G_{b,e} r_{b,e}^{-\alpha}}{I_e^{d,d}+I_e^{u,d}+\sigma_e^2}<\gamma \mid \phi_e\right)\right] \\ &\overset{(i)}{=} \exp\left(-2\pi\lambda_e\int_0^\infty\left(1-\Pr\left[\frac{p_d G_{b,v} r^{-\alpha}}{I_v^{d,d}+I_v^{u,d}+\sigma_v^2}<\gamma\right]\right)r\,\mathrm{d}r\right)\end{aligned} \tag{B.9}$$

with (i) obtained using the PGFL of a PPP and converting from Cartesian to polar coordinates. The probability from the above is given by

$$\begin{aligned}&1-\Pr\left[\frac{p_d G_{b,v} r^{-\alpha}}{I_v^{d,d}+I_v^{u,d}+\sigma_v^2}<\gamma\right] = \Pr\left[G_{b,v}>\frac{\gamma r^\alpha}{p_d}\left(I_v^{d,d}+I_v^{u,d}+\sigma_v^2\right)\right] \\ &= \left\{\exp\left(-s\sigma_v^2\right)\mathscr{L}_{I_v^{d,d}}(s)\mathscr{L}_{I_v^{u,d}}(s)\right\}_{s=\frac{\gamma r^\alpha}{p_d}}.\end{aligned} \tag{B.10}$$

Hence, we arrive at (3.18).

The LT function of the inter-cell interference at the most malicious ED in the DL v is given by

$$\begin{aligned}\mathscr{L}_{I_v^{d,d}}(s) &= \mathbb{E}_{\phi_d,G_{l,v}}\left[\exp\left(-s\sum_{l\in\phi_d} p_d G_{l,v} r_{l,v}^{-\alpha}\right)\right] \\ &\overset{(i)}{=} \mathbb{E}_{\phi_d}\left[\prod_{l\in\phi_d}\mathbb{E}_{G_{l,v}}\left[\exp\left(-sp_d G_{l,v} r_{l,v}^{-\alpha}\right)\right]\right] \\ &\overset{(ii)}{=} \exp\left(-2\pi\lambda_d\int_0^{\infty}\left(1-\frac{1}{(1+sp_d x^{-\alpha})^{K_d}}\right)x\,\mathrm{d}x\right) \\ &\overset{(iii)}{=} \exp\left(-\pi\lambda_d\left(sp_d\right)^{\frac{2}{\alpha}}\frac{\Gamma\left(1-\frac{2}{\alpha}\right)\Gamma\left(K_d+\frac{2}{\alpha}\right)}{\Gamma(K_d)}\right)\end{aligned} \tag{B.11}$$

where (i) follows from the independence property of PPP and uncorrelated channel conditions, (ii) is obtained using the PGFL of a PPP and converting from Cartesian to polar coordinates, and (iii) is written using the integral identity $\int_0^{+\infty}\left(1-(1+\beta x^{-\alpha})^{-K}\right)x\,\mathrm{d}x = \frac{\beta^{\frac{2}{\alpha}}\Gamma\left(1-\frac{2}{\alpha}\right)\Gamma\left(K+\frac{2}{\alpha}\right)}{2\Gamma(K)}$.

Using a similar approach to that in the above, the LT function of the MI at the most malicious ED in the DL v is given by

$$\begin{aligned}\mathscr{L}_{I_v^{u,d}}(s) &= \mathbb{E}_{\phi_u,G_{k,v}}\left[\exp\left(-s\sum_{k\in\phi_u} p_u G_{k,v} r_{k,v}^{-\alpha}\right)\right] \\ &= \exp\left(-2\pi K_u\lambda_d\int_0^{\infty}\left(1-\frac{1}{1+sp_u x^{-\alpha}}\right)x\,\mathrm{d}x\right) \\ &= \exp\left(-\pi K_u\lambda_d\left(sp_u\right)^{\frac{2}{\alpha}}\Gamma\left(1-\frac{2}{\alpha}\right)\Gamma\left(1+\frac{2}{\alpha}\right)\right).\end{aligned} \tag{B.12}$$

Hence, we arrive at *Theorem 3*. ■

B.4

Utilizing a similar approach to that in Appendix C, we can arrive at (3.22). Moreover, using a similar methodology, the LT functions of the different UL interfering

terms at the most malicious ED c are given by

$$\begin{aligned}\mathscr{L}_{I_c^{u,u}}(s) &= \mathbb{E}_{\phi_u,H_{k,c}}\left[\exp\left(-s\sum_{k\in\phi_u} p_u H_{k,c} r_{k,c}^{-\alpha}\right)\right] \\ &= \exp\left(-2\pi K_u \lambda_d \int_0^\infty \left(1-\frac{1}{1+sp_u x^{-\alpha}}\right) x\,\mathrm{d}x\right) \\ &= \exp\left(-\pi K_u \lambda_d (sp_u)^{\frac{2}{\alpha}} \Gamma\left(1-\frac{2}{\alpha}\right)\Gamma\left(1+\frac{2}{\alpha}\right)\right) \end{aligned} \tag{B.13}$$

and

$$\begin{aligned}\mathscr{L}_{I_c^{d,u}}(s) &= \mathbb{E}_{\phi_d,H_{l,c}}\left[\exp\left(-s\sum_{l\in\phi_d} p_d H_{l,c} r_{l,c}^{-\alpha}\right)\right] \\ &= \exp\left(-2\pi \lambda_d \int_0^\infty \left(1-\frac{1}{(1+sp_d x^{-\alpha})^{K_d}}\right) x\,\mathrm{d}x\right) \\ &= \exp\left(-\pi \lambda_d (sp_d)^{\frac{2}{\alpha}} \frac{\Gamma\left(1-\frac{2}{\alpha}\right)\Gamma\left(K_d+\frac{2}{\alpha}\right)}{\Gamma(K_d)}\right). \end{aligned} \tag{B.14}$$

Hence, we arrive at *Theorem 4*. ■

B.5

The ergodic rate (considering FD BSs) of the most malicious colluding ED in the DL v per resource block can be calculated using

$$C_v^{\mathrm{FD}} = \mathbb{E}\left[\log_2\left(1+\gamma_v^{\mathrm{FD}}\right)\right] = \frac{1}{\ln(2)}\int_0^\infty \frac{1-F_{\gamma_v}^{\mathrm{FD}}[\gamma]}{1+\gamma}\,\mathrm{d}\gamma \tag{B.15}$$

where

$$\begin{aligned} 1-F_{\gamma_v^{\mathrm{FD}}}[\gamma] &= \Pr[\gamma_v^{\mathrm{FD}} > \gamma] = \Pr\left[\sum_{e\in\phi_e}\left(\frac{p_d G_{b,e} r_{b,e}^{-\alpha}}{I_e^{d,d}+I_e^{u,d}+\sigma_e^2}\right) > \gamma\right] \\ &\overset{(i)}{\leq} \frac{1}{\gamma}\mathbb{E}\left[\sum_{e\in\phi_e}\left(\frac{p_d G_{b,e} r_{b,e}^{-\alpha}}{I_e^{d,d}+I_e^{u,d}+\sigma_e^2}\right)\right] \\ &\overset{(ii)}{=} \frac{2\pi\lambda_e}{\gamma}\int_{r_0}^\infty \mathbb{E}\left[\frac{p_d G_{b,e} r^{-\alpha}}{I_e^{d,d}+I_e^{u,d}+\sigma_e^2}\right] r\,\mathrm{d}r \\ &\overset{(iii)}{=} \frac{2\pi\lambda_e}{\gamma}\int_{r_0}^\infty \mathbb{E}\left[p_d G_{b,v} r^{-\alpha}\right]\int_0^\infty \exp\left(-s\sigma_v^2\right)\mathscr{L}_{I_e^{d,d}}[s]\mathscr{L}_{I_v^{u,d}}[s]\,\mathrm{d}s\, r\,\mathrm{d}r \end{aligned}$$

$$\overset{(iv)}{=} \frac{2\pi\lambda_e p_d}{\gamma} \int_{r_0}^{\infty} r^{1-\alpha} \int_0^{\infty} \exp\left(-s\sigma_v^2\right) \mathscr{L}_{I_e^{d,d}}[s] \mathscr{L}_{I_v^{u,d}}[s] \, \mathrm{d}s \, \mathrm{d}r \tag{B.16}$$

with (i) is written using the Markov inequality, (ii) follows from applying the Campbell's theorem to a sum over PPP and converting from Cartesian to polar coordinates [116], (iii) is obtained using the approach from [82] for calculating the moments of SINR, and (iv) is given by taking the average over the ED useful signal. Hence, we arrive at *Theorem 5*. ■

Bibliography

[1] Cisco Visual Networking Index Cisco. Global mobile data traffic forecast update, 2015–2020 white paper, 2016. *Online: https://www. cisco. com/c/dam/m/en_in/innovation/enterprise/assets/mobile-white-paper-c11-520862. pdf.*

[2] S. Chen, F. Qin, B. Hu, X. Li, and Z. Chen. User-centric ultra-dense networks for 5g: challenges, methodologies, and directions. *IEEE Wireless Communications*, 23(2):78–85, April 2016.

[3] C. X. Wang, F. Haider, X. Gao, X. H. You, Y. Yang, D. Yuan, H. M. Aggoune, H. Haas, S. Fletcher, and E. Hepsaydir. Cellular architecture and key technologies for 5g wireless communication networks. *IEEE Communications Magazine*, 52(2):122–130, February 2014.

[4] Vikram Chandrasekhar, Jeffrey G. Andrews, and Alan Gatherer. Femtocell networks: A survey. *CoRR*, abs/0803.0952, 2008.

[5] M. Duarte, C. Dick, and A. Sabharwal. Experiment-driven characterization of full-duplex wireless systems. *IEEE Trans. Wireless Commun.*, 11(12):4296–4307, Dec. 2012.

[6] Amir Keyvan Khandani. Methods for spatial multiplexing of wireless two-way channels, October 19 2010. US Patent 7,817,641.

[7] D. Nguyen, L. N. Tran, P. Pirinen, and M. Latva-aho. On the spectral efficiency of full-duplex small cell wireless systems. *IEEE Trans. Wireless Commun.*, 13(9):4896–4910, Sept. 2014.

[8] G. C. Alexandropoulos, M. Kountouris, and I. Atzeni. User scheduling and optimal power allocation for full-duplex cellular networks. In *2016 IEEE 17th International Workshop on Signal Processing Advances in Wireless Communications (SPAWC)*, pages 1–6, July 2016.

[9] S. Goyal, P. Liu, S. S. Panwar, R. A. Difazio, R. Yang, and E. Bala. Full duplex cellular systems: will doubling interference prevent doubling capacity? *IEEE Communications Magazine*, 53(5):121–127, May 2015.

[10] T. Riihonen, S. Werner, and R. Wichman. Mitigation of loopback self-interference in full-duplex MIMO relays. *IEEE Trans. Signal Process.*, 59(12):5983–5993, Dec. 2011.

[11] E. Everett, A. Sahai, and A. Sabharwal. Passive self-interference suppression for full-duplex infrastructure nodes. *IEEE Trans. Wireless Commun.*, 13(2):680–694, Feb. 2014.

[12] D. Kim, H. Lee, and D. Hong. A survey of in-band full-duplex transmission: From the perspective of PHY and MAC layers. *IEEE Commun. Surveys Tuts.*, 17(4):2017–2046, Fourth Quart. 2015.

[13] A. Sezgin, A. S. Avestimehr, M. A. Khajehnejad, and B. Hassibi. Divide-and-conquer: Approaching the capacity of the two-pair bidirectional Gaussian relay network. *IEEE Trans. Inf. Theory*, 58(4):2434–2454, Apr. 2012.

[14] C. Wang, H. Farhadi, and M. Skoglund. Achieving the degrees of freedom of wireless multi-user relay networks. *IEEE Trans. Commun.*, 60(9):2612–2622, Sept. 2012.

[15] Z. Tong and M. Haenggi. Throughput analysis for full-duplex wireless networks with imperfect self-interference cancellation. *IEEE Trans. Commun.*, 63(11):4490–4500, Nov. 2015.

[16] H. Tabassum, A. H. Sakr, and E. Hossain. Analysis of massive MIMO-enabled downlink wireless backhauling for full-duplex small cells. *IEEE Trans. Commun.*, 64(6):2354–2369, June 2016.

[17] I. Atzeni and M. Kountouris. Full-duplex MIMO small-cell networks with interference cancellation. *IEEE Trans. Wireless Commun.*, 16(12):8362–8376, Dec. 2017.

[18] A. Gupta and R. K. Jha. A survey of 5G network: Architecture and emerging technologies. *IEEE Access*, 3:1206–1232, July 2015.

[19] I. Atzeni and M. Kountouris. Full-duplex mimo small-cell networks with interference cancellation. *IEEE Transactions on Wireless Communications*, 16(12):8362–8376, Dec 2017.

[20] W. Keusgen. On limits of wireless communications when using multiple dual-polarized antennas. In *10th International Conference on Telecommunications, 2003. ICT 2003.*, volume 1, pages 204–210 vol.1, Feb 2003.

[21] N. Chiurtu, B. Rimoldi, and E. Telatar. On the capacity of multi-antenna gaussian channels. In *Proceedings. 2001 IEEE International Symposium on Information Theory (IEEE Cat. No.01CH37252)*, pages 53–, June 2001.

[22] J. G. Andrews, S. Buzzi, W. Choi, S. V. Hanly, A. Lozano, A. C. K. Soong, and J. C. Zhang. What will 5g be? *IEEE Journal on Selected Areas in Communications*, 32(6):1065–1082, June 2014.

[23] H. Q. Ngo, E. G. Larsson, and T. L. Marzetta. Energy and spectral efficiency of very large multiuser mimo systems. *IEEE Transactions on Communications*, 61(4):1436–1449, April 2013.

[24] G. Caire, N. Jindal, M. Kobayashi, and N. Ravindran. Multiuser mimo achievable rates with downlink training and channel state feedback. *IEEE Transactions on Information Theory*, 56(6):2845–2866, June 2010.

[25] F. Rusek, D. Persson, B. K. Lau, E. G. Larsson, T. L. Marzetta, O. Edfors, and F. Tufvesson. Scaling up mimo: Opportunities and challenges with very large arrays. *IEEE Signal Processing Magazine*, 30(1):40–60, Jan 2013.

[26] S. Shafiee and S. Ulukus. Achievable rates in gaussian miso channels with secrecy constraints. In *2007 IEEE International Symposium on Information Theory*, pages 2466–2470, June 2007.

[27] A. Khisti and G. W. Wornell. Secure transmission with multiple antennas—part ii: The mimome wiretap channel. *IEEE Transactions on Information Theory*, 56(11):5515–5532, Nov 2010.

[28] Frédérique Oggier and Babak Hassibi. The secrecy capacity of the mimo wiretap channel. In *Information Theory, 2008. ISIT 2008. IEEE International Symposium on*, pages 524–528. IEEE, 2008.

[29] A. Mukherjee and A. L. Swindlehurst. Robust beamforming for security in mimo wiretap channels with imperfect csi. *IEEE Transactions on Signal Processing*, 59(1):351–361, Jan 2011.

[30] N. Romero-Zurita, M. Ghogho, and D. McLernon. Outage probability based power distribution between data and artificial noise for physical layer security. *IEEE Signal Processing Letters*, 19(2):71–74, Feb 2012.

[31] G. Geraci, M. Egan, J. Yuan, A. Razi, and I. B. Collings. Secrecy sum-rates for multi-user mimo regularized channel inversion precoding. *IEEE Transactions on Communications*, 60(11):3472–3482, November 2012.

[32] M. Bloch, J. Barros, M. R. D. Rodrigues, and S. W. McLaughlin. Wireless information-theoretic security. *IEEE Trans. Inf. Theory*, 54(6):2515–2534, June 2008.

[33] F. He, H. Man, and W. Wang. Maximal ratio diversity combining enhanced security. *IEEE Communications Letters*, 15(5):509–511, May 2011.

[34] M. Z. I. Sarkar and T. Ratnarajah. On the secrecy mutual information of nakagami-m fading simo channel. In *2010 IEEE International Conference on Communications*, pages 1–5, May 2010.

[35] H. Suzuki. A statistical model for urban radio propogation. *IEEE Transactions on Communications*, 25(7):673–680, Jul 1977.

[36] Jonathan Katz, Alfred J Menezes, Paul C Van Oorschot, and Scott A Vanstone. *Handbook of applied cryptography*. CRC press, 1996.

[37] W. Wang, K. C. Teh, and K. H. Li. Artificial noise aided physical layer security in multi-antenna small-cell networks. *IEEE Transactions on Information Forensics and Security*, 12(6):1470–1482, June 2017.

[38] L. Wang, N. Yang, M. Elkashlan, P. L. Yeoh, and J. Yuan. Physical layer security of maximal ratio combining in two-wave with diffuse power fading channels. *IEEE Transactions on Information Forensics and Security*, 9(2):247–258, Feb 2014.

[39] A. Mukherjee, S. A. A. Fakoorian, J. Huang, and A. L. Swindlehurst. Principles of physical layer security in multiuser wireless networks: A survey. *IEEE Commun. Surveys Tuts.*, 16(3):1550–1573, Third Quart. 2014.

[40] Aaron D Wyner. The wire-tap channel. *Bell Labs Technical Journal*, 54(8):1355–1387, 1975.

[41] L. Dong, Z. Han, A. P. Petropulu, and H. V. Poor. Improving wireless physical layer security via cooperating relays. *IEEE Trans. Signal Process.*, 58(3):1875–1888, Mar. 2010.

[42] G. Zheng, L. C. Choo, and K. K. Wong. Optimal cooperative jamming to enhance physical layer security using relays. *IEEE Trans. Signal Process.*, 59(3):1317–1322, Mar. 2011.

[43] J. Li, A. P. Petropulu, and S. Weber. On cooperative relaying schemes for wireless physical layer security. *IEEE Trans. Signal Process.*, 59(10):4985–4997, Oct. 2011.

[44] Y. Zou, X. Wang, and W. Shen. Physical-layer security with multiuser scheduling in cognitive radio networks. *IEEE Trans. Commun.*, 61(12):5103–5113, Dec. 2013.

[45] M. Elkashlan, L. Wang, T. Q. Duong, G. K. Karagiannidis, and A. Nallanathan. On the security of cognitive radio networks. *IEEE Trans. Veh. Technol.*, 64(8):3790–3795, Aug. 2015.

[46] T. Lv, H. Gao, and S. Yang. Secrecy transmit beamforming for heterogeneous networks. *IEEE J. Sel. Areas Commun.*, 33(6):1154–1170, June 2015.

[47] D. W. K. Ng, E. S. Lo, and R. Schober. Robust beamforming for secure communication in systems with wireless information and power transfer. *IEEE Trans. Wireless Commun.*, 13(8):4599–4615, Aug. 2014.

[48] L. Wang, K. K. Wong, M. Elkashlan, A. Nallanathan, and S. Lambotharan. Secrecy and energy efficiency in massive MIMO aided heterogeneous C-RAN: A new look at interference. *IEEE J. Sel. Topics Signal Process.*, 10(8):1375–1389, Dec. 2016.

[49] Giovanni Geraci, Harpreet S. Dhillon, Jeffrey G. Andrews, Jinhong Yuan, and Iain B. Collings. Physical layer security in downlink multi-antenna cellular networks. *CoRR*, abs/1307.7211, 2013.

[50] H. Wang, X. Zhou, and M. C. Reed. Physical layer security in cellular networks: A stochastic geometry approach. *IEEE Transactions on Wireless Communications*, 12(6):2776–2787, June 2013.

[51] H. Zhang, T. Wang, L. Song, and Z. Han. Radio resource allocation for physical-layer security in d2d underlay communications. In *2014 IEEE In-*

ternational Conference on Communications (ICC), pages 2319–2324, June 2014.

[52] C. Ma, J. Liu, X. Tian, H. Yu, Y. Cui, and X. Wang. Interference exploitation in d2d-enabled cellular networks: A secrecy perspective. *IEEE Transactions on Communications*, 63(1):229–242, Jan 2015.

[53] Sudarshan Vasudevan, Dennis Goeckel, and Donald F. Towsley. Security-capacity trade-off in large wireless networks using keyless secrecy. In *Proceedings of the Eleventh ACM International Symposium on Mobile Ad Hoc Networking and Computing*, MobiHoc '10, pages 21–30, New York, NY, USA, 2010. ACM.

[54] O. O. Koyluoglu, C. E. Koksal, and H. E. Gamal. On secrecy capacity scaling in wireless networks. *IEEE Transactions on Information Theory*, 58(5):3000–3015, May 2012.

[55] A. Sarkar and M. Haenggi. Secrecy coverage. In *2010 Conference Record of the Forty Fourth Asilomar Conference on Signals, Systems and Computers*, pages 42–46, Nov 2010.

[56] Martin Haenggi. The secrecy graph and some of its properties. In *Information Theory, 2008. ISIT 2008. IEEE International Symposium on*, pages 539–543. IEEE, 2008.

[57] X. Zhou, R. K. Ganti, and J. G. Andrews. Secure wireless network connectivity with multi-antenna transmission. *IEEE Transactions on Wireless Communications*, 10(2):425–430, February 2011.

[58] P. C. Pinto and M. Z. Win. Continuum percolation in the intrinsically secure communications graph. In *2010 International Symposium On Information Theory Its Applications*, pages 349–354, Oct 2010.

[59] Amites Sarkar and Martin Haenggi. Percolation in the secrecy graph: Bounds on the critical probability and impact of power constraints. In *Information Theory Workshop (ITW), 2011 IEEE*, pages 673–677. IEEE, 2011.

[60] Y. Liang, H. V. Poor, and L. Ying. Secrecy throughput of manets under passive and active attacks. *IEEE Transactions on Information Theory*, 57(10):6692–6702, Oct 2011.

[61] Xiangyun Zhou, Meixia Tao, and Rodney A. Kennedy. Cooperative jamming for secrecy in decentralized wireless networks. *2012 IEEE International Conference on Communications (ICC)*, pages 2339–2344, 2012.

[62] X. Zhou, R. K. Ganti, J. G. Andrews, and A. Hjørungnes. On the throughput cost of physical layer security in decentralized wireless networks. *IEEE Trans. Wireless Commun.*, 10(8):2764–2775, Aug. 2011.

[63] T. X. Zheng, H. M. Wang, and Q. Yin. On transmission secrecy outage of a multi-antenna system with randomly located eavesdroppers. *IEEE Commun. Lett.*, 18(8):1299–1302, Aug. 2014.

[64] T. X. Zheng, H. M. Wang, J. Yuan, D. Towsley, and M. H. Lee. Multi-antenna transmission with artificial noise against randomly distributed eavesdroppers. *IEEE Trans. Commun.*, 63(11):4347–4362, Nov. 2015.

[65] G. Chen and J. P. Coon. Secrecy outage analysis in random wireless networks with antenna selection and user ordering. *IEEE Wireless Commun. Lett.*, 6(3):334–337, June 2017.

[66] G. Chen, J. P. Coon, and M. Di Renzo. Secrecy outage analysis for downlink transmissions in the presence of randomly located eavesdroppers. *IEEE Trans. Inf. Forensics Security*, 12(5):1195–1206, May 2017.

[67] S. Goel and R. Negi. Guaranteeing secrecy using artificial noise. *IEEE Transactions on Wireless Communications*, 7(6):2180–2189, June 2008.

[68] A. Khisti, G. Wornell, A. Wiesel, and Y. Eldar. On the gaussian mimo wiretap channel. In *2007 IEEE International Symposium on Information Theory*, pages 2471–2475, June 2007.

[69] J. Zhu, R. Schober, and V. K. Bhargava. Secure transmission in multicell massive mimo systems. *IEEE Transactions on Wireless Communications*, 13(9):4766–4781, Sept 2014.

[70] Onur Ozan Koyluoglu, Hesham El Gamal, Lifeng Lai, and H. Vincent Poor. Interference alignment for secrecy. *CoRR*, abs/0810.1187, 2008.

[71] L. Lai and H. El Gamal. The relay–eavesdropper channel: Cooperation for secrecy. *IEEE Trans. Inf. Theory*, 54(9):4005–4019, Sept. 2008.

[72] A. D. Wyner. The wire-tap channel. *The Bell System Technical Journal*, 54(8):1355–1387, Oct 1975.

[73] J. Sun, X. Li, M. Huang, Y. Ding, J. Jin, and G. Pan. Performance analysis of physical layer security over shadowed fading channels. *IET Communications*, 12(8):970–975, 2018.

[74] F. Oggier and B. Hassibi. The secrecy capacity of the mimo wiretap channel. *IEEE Transactions on Information Theory*, 57(8):4961–4972, Aug 2011.

[75] H. ElSawy, E. Hossain, and M. Haenggi. Stochastic geometry for modeling, analysis, and design of multi-tier and cognitive cellular wireless networks: A survey. *IEEE Commun. Surveys Tuts.*, 15(3):996–1019, Third Quart. 2013.

[76] Edward N Gilbert. Random plane networks. *Journal of the Society for Industrial and Applied Mathematics*, 9(4):533–543, 1961.

[77] H. S. Dhillon, R. K. Ganti, F. Baccelli, and J. G. Andrews. Modeling and analysis of k-tier downlink heterogeneous cellular networks. *IEEE Journal on Selected Areas in Communications*, 30(3):550–560, April 2012.

[78] H. S. Jo, Y. J. Sang, P. Xia, and J. G. Andrews. Heterogeneous cellular networks with flexible cell association: A comprehensive downlink sinr analysis. *IEEE Transactions on Wireless Communications*, 11(10):3484–3495, October 2012.

[79] J. G. Andrews. Seven ways that hetnets are a cellular paradigm shift. *IEEE Communications Magazine*, 51(3):136–144, March 2013.

[80] M. Haenggi, J. G. Andrews, F. Baccelli, O. Dousse, and M. Franceschetti. Stochastic geometry and random graphs for the analysis and design of wireless networks. *IEEE J. Sel. Areas Commun.*, 27(7):1029–1046, Sept. 2009.

[81] François Baccelli and Bartlomiej Blaszczyszyn. *Stochastic Geometry and Wireless Networks, Volume I - Theory*, volume 1 of *Foundations and Trends in Networking Vol. 3: No 3-4, pp 249-449*. NoW Publishers, 2009. Stochastic Geometry and Wireless Networks, Volume II - Applications; see http://hal.inria.fr/inria-00403040.

[82] A. Shojaeifard, K. A. Hamdi, E. Alsusa, D. K. C. So, and J. Tang. Exact SINR statistics in the presence of heterogeneous interferers. *IEEE Trans. Inf. Theory*, 61(12):6759–6773, Dec. 2015.

[83] A. H. Sakr and E. Hossain. On user association in multi-tier full-duplex cellular networks. *IEEE Trans. Commun.*, 65(9):4080–4095, Sept. 2017.

[84] C. Mukasa, V. A. Aalo, and G. Efthymoglou. Performance analysis of a mobile receiver in a field of poisson interferers. In *2017 IEEE 38th Sarnoff Symposium*, pages 1–6, Sept 2017.

[85] Dietrich Stoyan. *Stochastic Geometry and Its Applications*. Wiley, Chichester New York, 1995.

[86] J. G. Andrews, F. Baccelli, and R. K. Ganti. A tractable approach to coverage and rate in cellular networks. *IEEE Trans. Commun.*, 59(11):3122–3134, Nov. 2011.

[87] Martin Haenggi and Radha Krishna Ganti. Interference in large wireless networks. *Found. Trends Netw.*, 3(2):127–248, February 2009.

[88] J. E. Moyal. The general theory of stochastic population processes. *Acta Math.*, 108:1–31, 1962.

[89] I. Kachalsky, I. Zakirzyanov, and V. Ulyantsev. Applying reinforcement learning and supervised learning techniques to play hearthstone. In *2017 16th IEEE International Conference on Machine Learning and Applications (ICMLA)*, pages 1145–1148, Dec 2017.

[90] X. Zhou and M. R. McKay. Secure transmission with artificial noise over fading channels: Achievable rate and optimal power allocation. *IEEE Trans. Veh. Technol.*, 59(8):3831–3842, Oct. 2010.

[91] X. Zhang, X. Zhou, and M. R. McKay. Enhancing secrecy with multi-antenna transmission in wireless ad hoc networks. *IEEE Trans. Inf. Forensics Security*, 8(11):1802–1814, Nov. 2013.

[92] P. C. Pinto, J. Barros, and M. Z. Win. Secure communication in stochastic wireless networks part I: Connectivity. *IEEE Trans. Inf. Forensics Security*, 7(1):125–138, Feb. 2012.

[93] P. C. Pinto, J. Barros, and M. Z. Win. Secure communication in stochastic wireless networks part II: maximum rate and collusion. *IEEE Trans. Inf. Forensics Security*, 7(1):139–147, Feb. 2012.

[94] D. Nguyen, L. N. Tran, P. Pirinen, and M. Latva-aho. Precoding for full duplex multiuser MIMO systems: Spectral and energy efficiency maximization. *IEEE Trans. Sig. Process.*, 61(16):4038–4050, Aug. 2013.

[95] C. Capar, D. Goeckel, B. Liu, and D. Towsley. Secret communication in large wireless networks without eavesdropper location information. In *IEEE INFOCOM*, pages 1152–1160, Mar. 2012.

[96] Q. Ye, B. Rong, Y. Chen, M. Al-Shalash, C. Caramanis, and J. G. Andrews. User association for load balancing in heterogeneous cellular networks. *IEEE Trans. Wireless Commun.*, 12(6):2706–2716, June 2013.

[97] H. ElSawy and E. Hossain. On stochastic geometry modeling of cellular uplink transmission with truncated channel inversion power control. *IEEE Trans. Wireless Commun.*, 13(8):4454–4469, Aug. 2014.

[98] T. D. Novlan, H. S. Dhillon, and J. G. Andrews. Analytical modeling of uplink cellular networks. *IEEE Trans. Wireless Commun.*, 12(6):2669–2679, June 2013.

[99] M. Di Renzo and P. Guan. Stochastic geometry modeling and system-level analysis of uplink heterogeneous cellular networks with multi-antenna base stations. *IEEE Trans. Commun.*, 64(6):2453–2476, June 2016.

[100] A. Shojaeifard, K. K. Wong, M. Di Renzo, G. Zheng, K. A. Hamdi, and J. Tang. Self-interference in full-duplex multi-user MIMO channels. *IEEE Commun. Lett.*, 21(4):841–844, Apr. 2017.

[101] G. Geraci, H. S. Dhillon, J. G. Andrews, J. Yuan, and I. B. Collings. Physical layer security in downlink multi-antenna cellular networks. *IEEE Trans. Commun.*, 62(6):2006–2021, June 2014.

[102] A. Shojaeifard, K.-K. Wong, W. Yu, G. Zheng, and J. Tang. Full-duplex cloud radio access network: Stochastic design and analysis. *arXiv:1711.02026*, 2017.

[103] G. Liu, F. R. Yu, H. Ji, V. C. M. Leung, and X. Li. In-band full-duplex relaying: A survey, research issues and challenges. *IEEE Commun. Surveys Tuts.*, 17(2):500–524, Second Quart. 2015.

[104] G. Zheng, I. Krikidis, J. Li, A. P. Petropulu, and B. Ottersten. Improving physical layer secrecy using full-duplex jamming receivers. *IEEE Trans. Signal Process.*, 61(20):4962–4974, Oct. 2013.

[105] A. El Shafie, A. Sultan, and N. Al-Dhahir. Physical-layer security of a buffer-aided full-duplex relaying system. *IEEE Commun. Lett.*, 20(9):1856–1859, Sept. 2016.

[106] R. Li, Y. Chen, G. Y. Li, and G. Liu. Full-duplex cellular networks. *IEEE Commun. Mag.*, 55(4):184–191, Apr. 2017.

[107] A. Shojaeifard, K. K. Wong, M. D. Renzo, G. Zheng, K. A. Hamdi, and J. Tang. Massive MIMO-enabled full-duplex cellular networks. *IEEE Trans. Commun.*, 65(11):4734–4750, Nov. 2017.

[108] S. Vuppala and G. Abreu. Asymptotic secrecy analysis of random networks with colluding eavesdroppers. *IEEE Syst. J.*, accepted 2016.

[109] S. Jia, J. Zhang, H. Zhao, and R. Zhang. Relay selection for improved security in cognitive relay networks with jamming. *IEEE Wireless Commun. Lett.*, 6(5):662–665, Oct. 2017.

[110] A. M. Hunter, J. G. Andrews, and S. Weber. Transmission capacity of ad hoc networks with spatial diversity. *IEEE Trans. Wireless Commun.*, 7(12):5058–5071, Dec. 2008.

[111] V. Chandrasekhar, M. Kountouris, and J. G. Andrews. Coverage in multi-antenna two-tier networks. *IEEE Trans. Wireless Commun.*, 8(10):5314–5327, Oct. 2009.

[112] A. Shojaeifard, K. A. Hamdi, E. Alsusa, D. K. C. So, J. Tang, and K. K. Wong. Design, modeling, and performance analysis of multi-antenna heterogeneous cellular networks. *IEEE Trans. Commun.*, 64(7):3104–3118, July 2016.

[113] Francesco Faá di Bruno. Théorie des formes binaires. *Librairie Breno, Turin.*, 1876.

[114] S. Akbar, Y. Deng, A. Nallanathan, M. Elkashlan, and G. K. Karagiannidi. Massive multiuser MIMO in heterogeneous cellular networks with full duplex small cells. *IEEE Trans. Commun.*, 65(11):4704–4719, Nov. 2017.

[115] J. Bai and A. Sabharwal. Asymptotic analysis of MIMO multi-cell full-duplex networks. *IEEE Trans. Wireless Commun.*, 16(4):2168–2180, Apr. 2017.

[116] Martin Haenggi. *Stochastic geometry for wireless networks*. Cambridge University Press, 2012.